

Geophysical Field Report:  
High Resolution Resistivity and Induced Polarization Survey

WHITE GOLD Project  
Resistivity/IP Survey: Phase II

Dawson Mining District  
NTS: 115O/03; 115O/04

Work Performed On: August 14<sup>th</sup> – September 1<sup>st</sup>, 2017 and  
September 10<sup>th</sup> – September 28<sup>th</sup>, 2017

FOR:

White Gold Corp.  
100 University Avenue, 8th Floor  
Toronto, Ontario, Canada M5J2Y1  
(800) 564 6253

BY:

Jen Hanlon, M.Sc., GIT  
GroundTruth Exploration Inc.  
BOX 70, Dawson City, YT.

Date: November 24<sup>th</sup>, 2017  
Table of Contents

1.0 Introduction	6
2.0 Survey Theory	7
2.1 Field Survey Operating Procedure	8
2.2 Data Processing	8
3.0 Survey Personnel and Program Dates	9
3.1 Survey Personnel	9
3.2 Program Dates	9
4.0 Golden Saddle	10
4.1 Survey Summary	10
4.2 Survey Results	11
4.3 Interpretation	23
5.0 Arc	24
5.1 Survey Summary	24
5.2 Survey Results	25
5.3 Interpretation	29
6.0 Ulli Ridge	30
6.1 Survey Summary	30
6.2 Survey Results	32
6.3 Interpretation	37
7.0 McKinnon	38
7.1 Survey Summary	38
7.2 Survey Results	40
7.3 Interpretation	47
Appendix A: Description of Files and File Structure	49
Appendix B: SuperSting R8/IP Technical Specification	50
Appendix C: Extended dipole-dipole array	52
Appendix D: Data Misfit Crossplots	53

## Table of Figures

Figure 1: Overview map of White Gold 2017 RES/IP grids.	7
Figure 2: 2017 completed RES/IP grid on the Golden Saddle zone.	11
Figure 3: WHTIP17-01 sections.	12
Figure 4: WHTIP17-02 sections.	12
Figure 5: WHTIP17-03 sections.	13
Figure 6: WHTIP17-04 sections.	14
Figure 7: WHTIP17-05 sections.	15
Figure 8: WHTIP17-06 sections.	16
Figure 9: WHTIP17-07 sections.	16
Figure 10: WHTIP17-08 sections.	17
Figure 11: WHTIP17-09 sections.	18
Figure 12: WHTIP17-10 sections.	19
Figure 13: WHTIP17-11 sections.	20
Figure 14: WHTIP17-12 sections.	21
Figure 15: WHTIP17-13 sections.	22
Figure 16: WHTIP17-14 sections.	22
Figure 17: 2017 completed RES/IP grid on the Arc zone.	25
Figure 18: ARCIP17-01 sections.	26
Figure 19: ARCIP17-02 sections.	26
Figure 20: ARCIP17-03 sections.	27
Figure 21: ARCIP17-04 sections.	27
Figure 22: ARCIP17-05 sections.	28
Figure 23: ARCIP17-06 sections.	28
Figure 24: ARCIP17-07 sections.	29
Figure 25: 2017 completed RES/IP northern grid on the Ulli Ridge zone.	31
Figure 26: 2017 completed RES/IP southern grid on the Ulli Ridge zone.	32
Figure 27: ULRIP17-01 sections.	33
Figure 28: ULRIP17-02 sections.	33
Figure 29: ULRIP17-03 sections.	34
Figure 30: ULRIP17-04 sections.	34
Figure 31: ULRIP17-05 sections.	35
Figure 32: ULRIP17-06 sections.	35
Figure 33: ULRIP17-07 sections.	36
Figure 34: ULRIP17-08 sections.	36
Figure 35: ULRIP17-09 sections.	37
Figure 36: 2017 completed RES/IP grid on the McKinnon zone.	39
Figure 37: MCKIP17-01 sections.	40
Figure 38: MCKIP17-02 sections.	41

Figure 39: MCKIP17-03 sections.	41
Figure 40: MCKIP17-04 sections.	42
Figure 41: MCKIP17-05 sections.	43
Figure 42: MCKIP17-06 sections.	44
Figure 43: MCKIP17-07 sections.	45
Figure 44: MCKIP17-08 sections.	45
Figure 45: MCKIP17-09 sections.	46
Figure 46: MCKIP17-10 sections.	46
Figure 47: MCKIP17-11 sections.	47

## Table of Appendix Figures

Figure D-1: WHTIP17-01 data misfit crossplots.	53
Figure D-2: WHTIP17-02 data misfit crossplots.	54

Figure D-3: WHTIP17-03 data misfit crossplots.	54
Figure D-4: WHTIP17-04 data misfit crossplots.	55
Figure D-5: WHTIP17-05 data misfit crossplots.	55
Figure D-6: WHTIP17-06 data misfit crossplots.	56
Figure D-7: WHTIP17-07 data misfit crossplots.	56
Figure D-8: WHTIP17-08 data misfit crossplots.	57
Figure D-9: WHTIP17-09 data misfit crossplots.	57
Figure D-10: WHTIP17-10 data misfit crossplots.	58
Figure D-11: WHTIP17-01 data misfit crossplots.	58
Figure D-12: WHTLIP17-12 data misfit crossplots.	59
Figure D-13: WHTIP17-13 data misfit crossplots.	59
Figure D-14: WHTIP17-14 data misfit crossplots.	60
Figure D-15: ARCIP17-01 data misfit crossplots.	60
Figure D-16: ARCIP17-02 data misfit crossplots.	61
Figure D-17: ARCIP17-03 data misfit crossplots.	61
Figure D-18: ARCIP17-04 data misfit crossplots.	62
Figure D-19: ARCIP17-05 data misfit crossplot.	62
Figure D-20: ARCIP17-06 data misfit crossplots.	63
Figure D-21: ARCIP17-07 data misfit crossplot.	63
Figure D-22: ULRIP17-01 data misfit crossplots.	64
Figure D-23: ULRIP17-02 data misfit crossplot.	64
Figure D-24: ULRIP17-03 data misfit crossplot.	65
Figure D-25: ULRIP17-04 data misfit crossplots.	65
Figure D-26: ULRIP17-05 data misfit crossplots.	66
Figure D-27: ULRIP17-06 data misfit crossplots.	66
Figure D-28: ULRIP17-07 data misfit crossplots.	67
Figure D-29: ULRIP17-08 data misfit crossplots.	67
Figure D-30: ULRIP17-09 data misfit crossplots.	68
Figure D-31: MCKIP17-01 data misfit crossplots.	68
Figure D-32: MCKIP17-02 data misfit crossplots.	69
Figure D-33: MCKIP17-03 data misfit crossplots.	69
Figure D-34: MCKIP17-04 data misfit crossplots.	70
Figure D-35: MCKIP17-05 data misfit crossplots.	70
Figure D-36: MCKIP17-06 data misfit crossplots.	71
Figure D-37: MCKIP17-07 data misfit crossplots.	71
Figure D-38: MCKIP17-08 data misfit crossplots.	72
Figure D-39: MCKIP17-09 data misfit crossplots.	72
Figure D-40: MCKIP17-10 data misfit crossplots.	73

Figure D-41: MCKIP17-11 data misfit crossplots.

73

## 1.0 Introduction

White Gold Corporation (WGO) headquartered in Toronto, ON commissioned GroundTruth Exploration Inc. (GroundTruth) headquartered in Dawson City, YT to complete high resolution resistivity and induced polarization (RES/IP) surveys on four

subproperties on the White Gold (WHT) property during the 2017 field season. These properties are the Golden Saddle, Arc, Ulli Ridge, and McKinnon.

The purpose of the RES/IP survey is to identify geological structure and delineate extent of mineralized zones that are indicated by soil anomalies. This report details the results of the RES/IP surveys. Additional surveying and interpretation is left to WGO's discretion.

Figure 1 shows an overview of the four subproperty locations within the White Gold property. Note that there are 14 lines at the Golden Saddle, 7 lines at the Arc, 9 lines at Ulli Ridge (split between two grids), and 11 lines at McKinnon (split between two grids). Note that the larger McKinnon grid (the most south-east grid in Figure 1) utilizes a few pre-existing cut lines so the resulting grid lines are not evenly spaced. Maps of the completed grids are shown in Figures 2, 17, 27, 28, and 40, respectively.

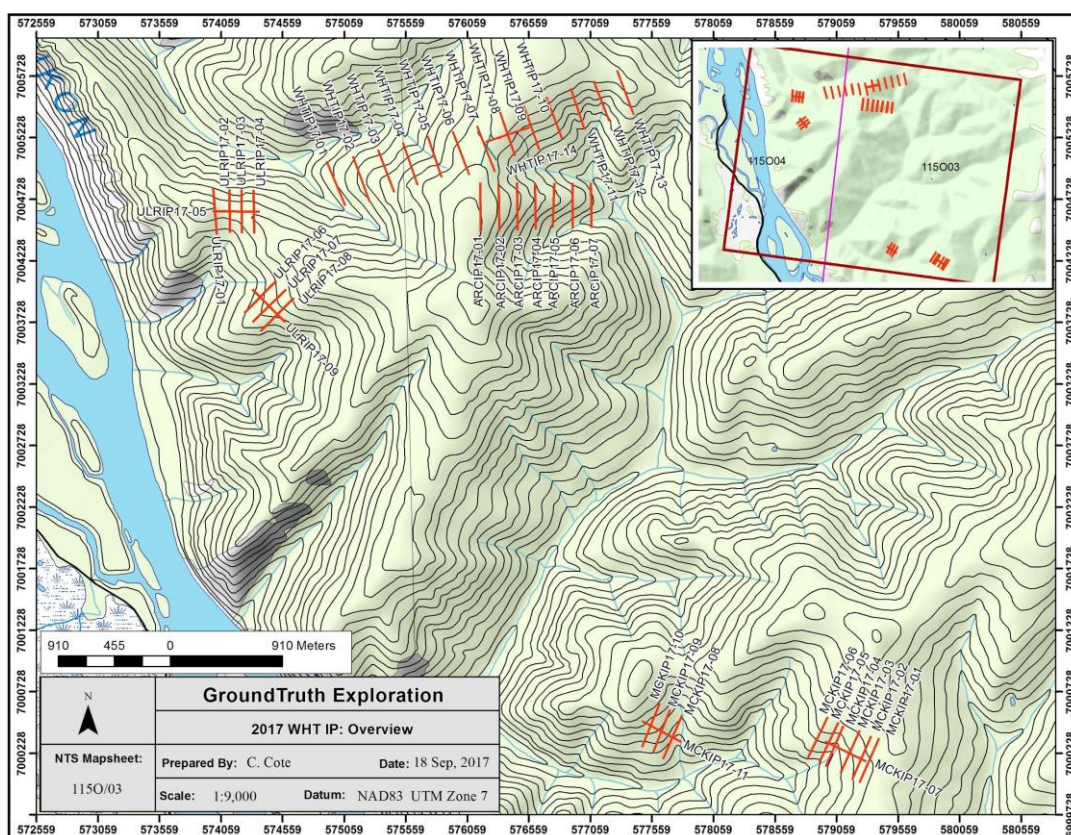




Figure 1: Overview map of White Gold 2017 RES/IP grids. Note that lines denoted with WHT are on the Golden Saddle, ARC are on the Arc, ULR are on Ulli Ridge, and MCK are on the McKinnon.

## 2.0 Survey Theory

Resistivity and Induced Polarization surveys are an appropriate approach to lode-source gold exploration in Yukon Territories because of the resistivity contrasts inherent to the mineralization and geological structures that are associated with gold deposits. The non-invasive nature of RES/IP combined with its cost efficiency make it a valuable contribution to exploration efforts.

RES/IP surveys involve current injection from the ground surface to induce an electric field that is a function of the conductivity distribution in the subsurface. A current injection typically uses one sink electrode and one source electrode. A measurement of potential field is then acquired across two electrodes that are different from the current electrodes. Hundreds of potential field measurements are made at intervals along the RES/IP traverse for successive current injections to generate the final raw profile of apparent subsurface resistivity.

There are a wide number of array types used to perform RES/IP surveys, each involving a different configuration of current and potential electrodes. Different arrays have strengths and weaknesses in regards to the time necessary to complete the survey and the measurement sensitivity to vertical or horizontal subsurface features. GroundTruth utilizes an extended dipole-dipole array for the WHT project to adequately image the target zones. Details on the extended dipole-dipole array can be found in Appendix C.

### 2.1 Field Survey Operating Procedure

A crew of 5 GroundTruth personnel sets up and operates each survey. Brief operating procedures are as follows:

1. The midpoint of a traverse is located and the length of the line is sighted using a compass and GPS.
2. Minimal brush is cut along the line to place pickets and set up equipment.
3. 84 electrodes are diligently inserted into the ground, equivalently spaced along the line at 5m and hammered to a depth of 50cm (10% of electrode spacing).
4. Calcium Chloride (CaCl<sub>2</sub>, 25% solution) is added to the base of all electrodes.
5. Cables are laid and connected to the electrodes.
6. Contact resistance test is conducted.



7. Extra electrodes and CaCl solution is added to each electrode with CR >2,000 Ohms. CR test is repeated.
8. Continue to add electrodes and CaCl until satisfactory CR values are achieved.
9. Operator initializes survey.
10. Operator uses DGPS and data collection software to document survey line parameters incl. electrode locations, topography, and notable geological/cultural features if present. Pickets are placed along the line every 50m.
11. Crew cuts and prepares the next survey line.

## 2.2 Data Processing

Immediately after each survey is completed in the field, the data measurements are downloaded and reviewed for integrity. Any field errors are thus addressed before moving the equipment. RES/IP datasets are processed daily by the lead operator using EarthImager2D software provided by Advanced Geosciences Inc. Outlier/noisy data are removed and the cleaned dataset is inverted. Terrain correction to the inversion mesh is applied from topographic measurements collected in the field using a differential GPS. All raw data from the DGPS and SuperSting are archived for future consultation.

## 3.0 Survey Personnel and Program Dates

### 3.1 Survey Personnel

The following table summarizes the GroundTruth personnel involved in completing the survey lines on each of the four White Gold subproperties. Note that on the Arc the GroundTruth team started with five personnel, but the last few survey lines were completed with three.

Personnel	Position	Golden Saddle	Arc	Ulli Ridge	McKinnon
Jen Hanlon	Lead Geophysical Operator and Crew Chief	✓	✓	✓	✓
Hector Barrientos	Secondary Lead	✓	✓	✓	✓
Andrew Truax	Geo Technician	✓		✓	✓

Pawel Kapa	Geo Technician	✓	✓ -partial	✓	✓
Julian Moore	Geo Technician	✓	✓ -partial		✓
Braeden Burnett	Geo Technician		✓	✓	

Table 1: Summary of GroundTruth personnel involved in the RES/IP data acquisition on the White Gold subproperties (Golden Saddle, Arc, Ulli Ridge, and McKinnon).

### 3.2 Program Dates

#### Golden Saddle:

Mobilize August 13<sup>th</sup>  
Field Surveys August 14<sup>th</sup> - August 25<sup>th</sup>

#### Arc:

Mobilize August 22<sup>nd</sup>  
Field Surveys August 26<sup>th</sup> – September 1<sup>th</sup> (excluding August 29<sup>th</sup>)  
Demobilize to Dawson September 2<sup>nd</sup>

#### Ulli Ridge:

Mobilize September 10<sup>th</sup>  
Field Surveys September 11<sup>th</sup> – September 18<sup>th</sup>

#### McKinnon:

Mobilize September 19<sup>th</sup>  
Field Surveys September 20<sup>th</sup> – September 28<sup>st</sup>

## 4.0 Golden Saddle

### 4.1 Survey Summary

An overview of the RES/IP grid on the Golden Saddle is shown in Figure 2. Brief specifications about the survey lines are outlined below.

---

Lines:	WHTIP17-01 – WHTIP17-14
Number of Electrodes	84
Electrode Spacing	5m
Line Length	415m
Array	Extended dipole-dipole

Ground cover on the Golden Saddle is a mixture of black spruce, wet or frozen moss, dry and pebble-rich, and aspen covered rich soil. The center of the grid crosses over the saddle where there is a cleared area for an exploration camp. This is where the ground is driest and most rocky. The east end of the grid saddles a steep south-facing slope covered in deadfall, aspen trees and rich soil with localized rocky areas. The west side of the grid traverses a north-facing slope that terminates near the confluence of two small creeks. The terrain on this side becomes more covered by black spruce and wet moss further down into the valley. This range of terrain types lead to different zones of electrode contact resistance (CR). The east side of the grid ranged in CR between 600–3,400 Ohms, sometimes getting as high as 5,400 Ohms in boulder-rich spots. In the center of the grid (over the saddle), CR values ranged between 1,100–4,000 Ohms, and more commonly reached upwards of 6,000 Ohms. On the west side of the grid, CR values ranged between 500–3,000 Ohms, with outlier values around 5,700 Ohms. In situations where one side of the traverse had better contacts than the other, the array measurement direction was chosen to read from low to high CR.

As the survey profiles were read in the field (traverses were read from east to west), increasing cable noise was noticed in the RES/IP data. This was addressed as soon as possible to reduce noise in the remaining surveys.

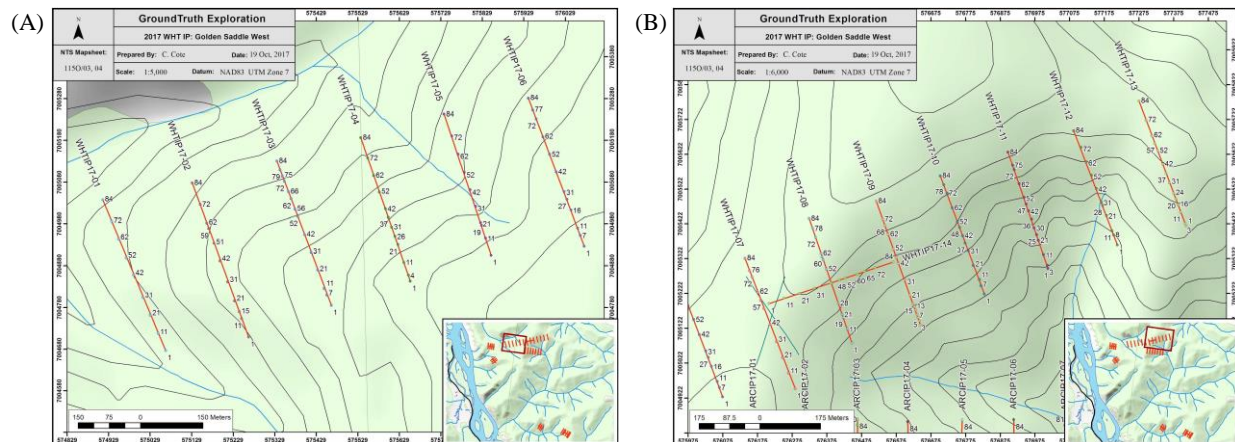


Figure 2: 2017 completed RES/IP grid on the Golden Saddle. Note that WHTIP17-14 is a crossline. (A) West side of grid (WHTIP17-01 - WHTIP17-06), and (B) East side of grid (WHTIP17-07 - WHTIP17-14).

## 4.2 Survey Results

The following figures display the inverted resistivity and induced polarization results along each traverse in the Golden Saddle zone. Note that the depth of penetration of the IP results is generally less than the resistivity results.

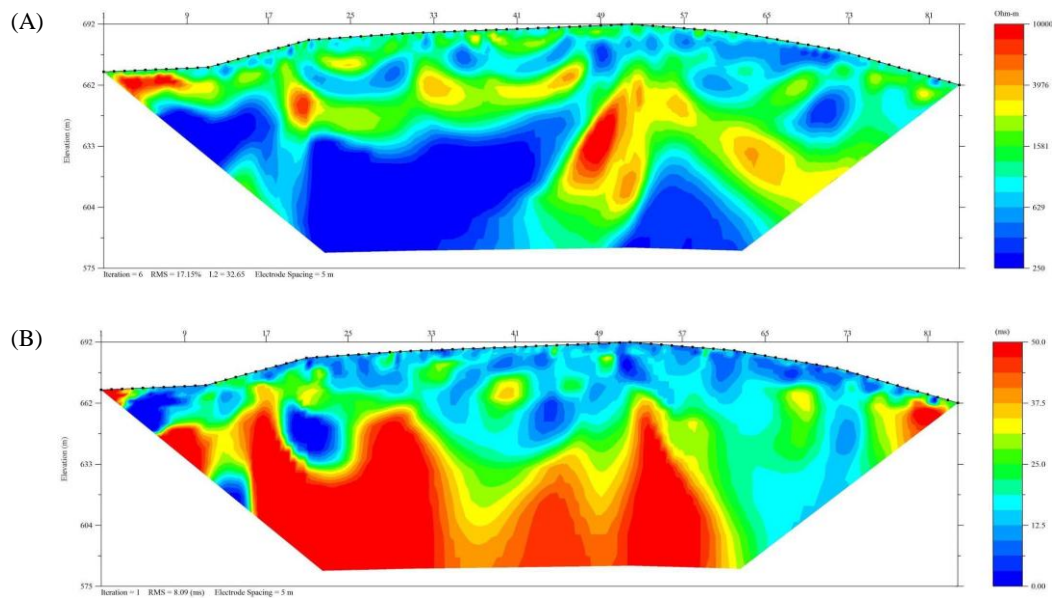
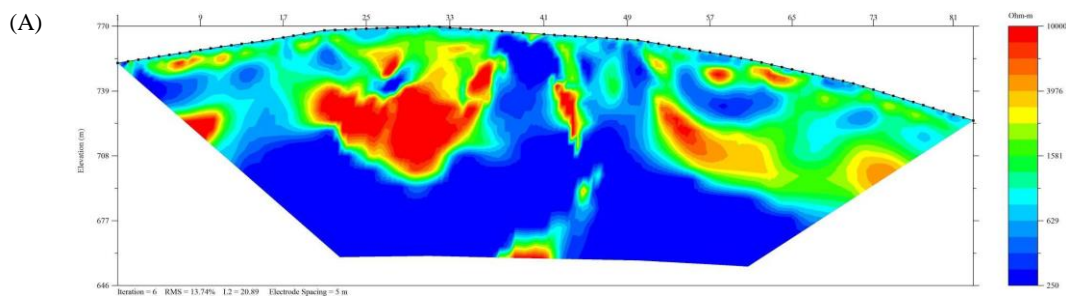


Figure 3: WHTIP17-01 sections. (A) Inverted resistivity (scale 250-10,000 Ohm-m). (B) Inverted IP (scale 0-50 ms).



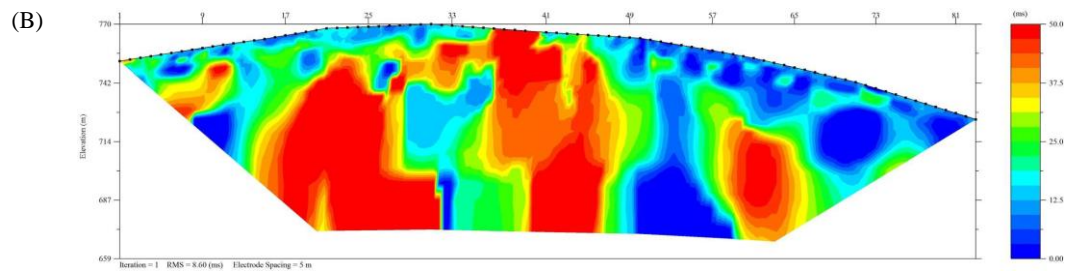


Figure 4: WHTIP17-02 sections. (A) Inverted resistivity (scale 250-10,000 Ohm-m). (B) Inverted IP (scale 0-50 ms).

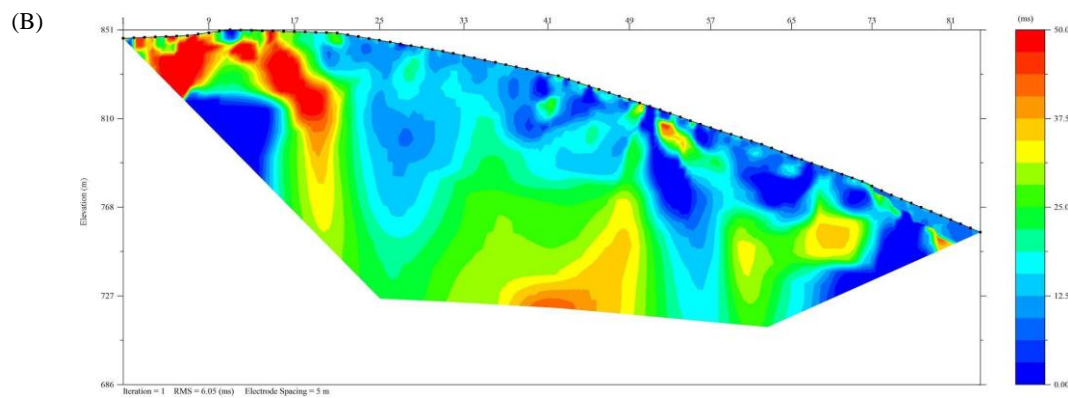
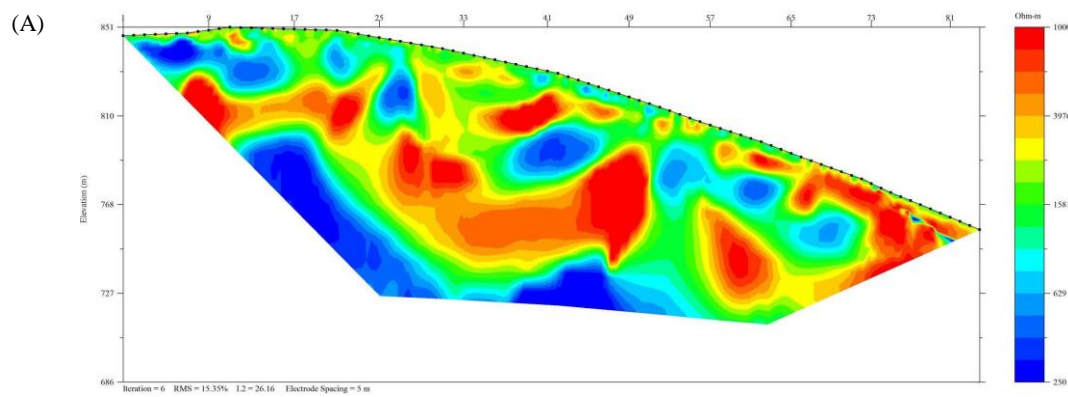


Figure 5: WHTIP17-03 sections. (A) Inverted resistivity (scale 250-10,000 Ohm-m). (B) Inverted IP (scale 0-50 ms).



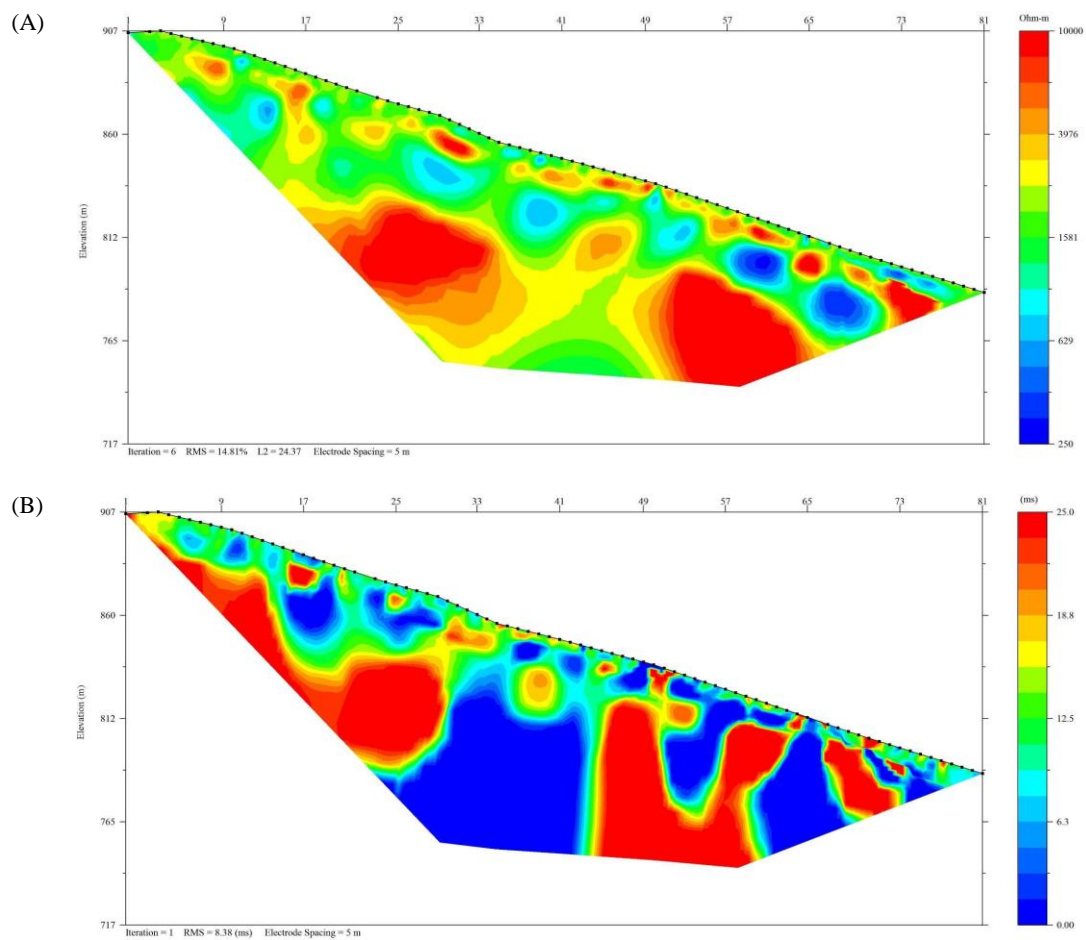


Figure 6: WHTIP17-04 sections. (A) Inverted resistivity (scale 250-10,000 Ohm-m). (B) Inverted IP (scale 0-25 ms).



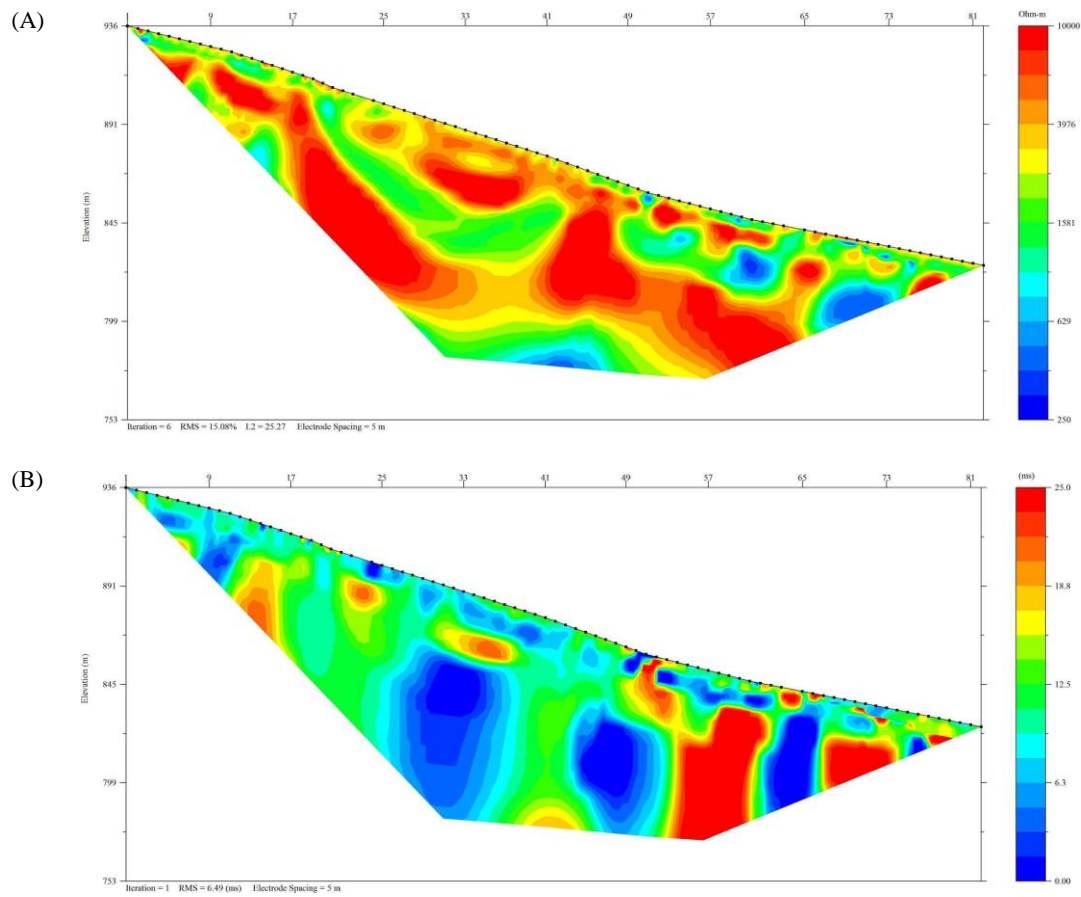


Figure 7: WHTIP17-05 sections. (A) Inverted resistivity (scale 250-10,000 Ohm-m). (B) Inverted IP (scale 0-25 ms).

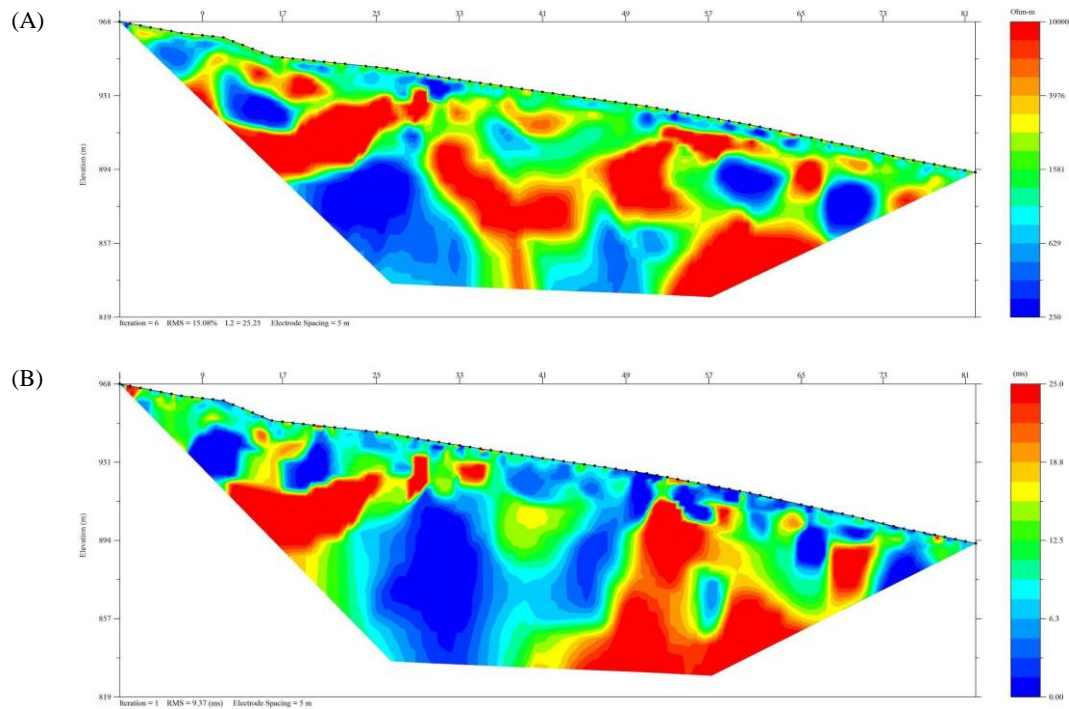


Figure 8: WHTIP17-06 sections. (A) Inverted resistivity (scale 250-10,000 Ohm-m). (B) Inverted IP (scale 0-25 ms).

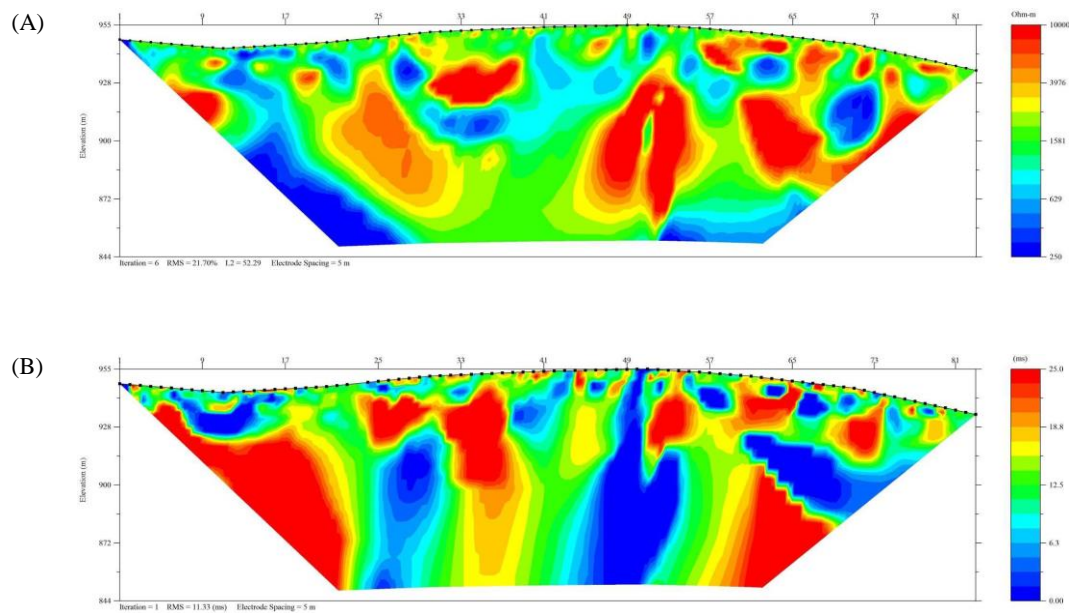


Figure 9: WHTIP17-07 sections. (A) Inverted resistivity (scale 250-10,000 Ohm-m). (B) Inverted IP (scale 0-25 ms).

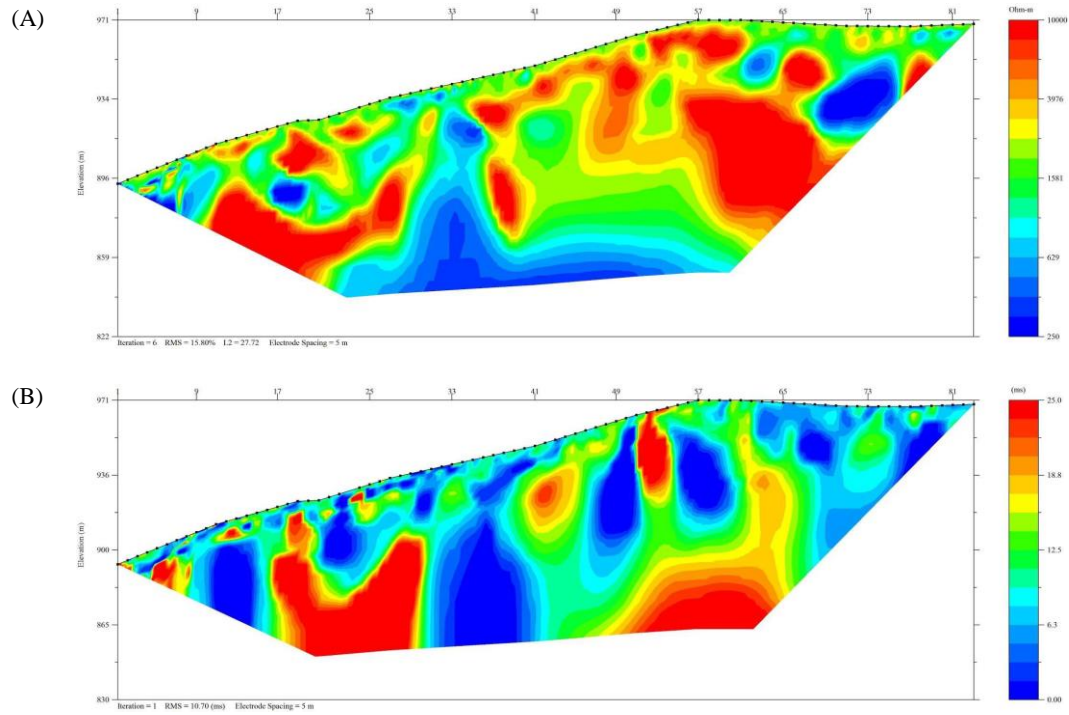


Figure 10: WHTIP17-08 sections. (A) Inverted resistivity (scale 250-10,000 Ohm-m). (B) Inverted IP (scale 0-25 ms).



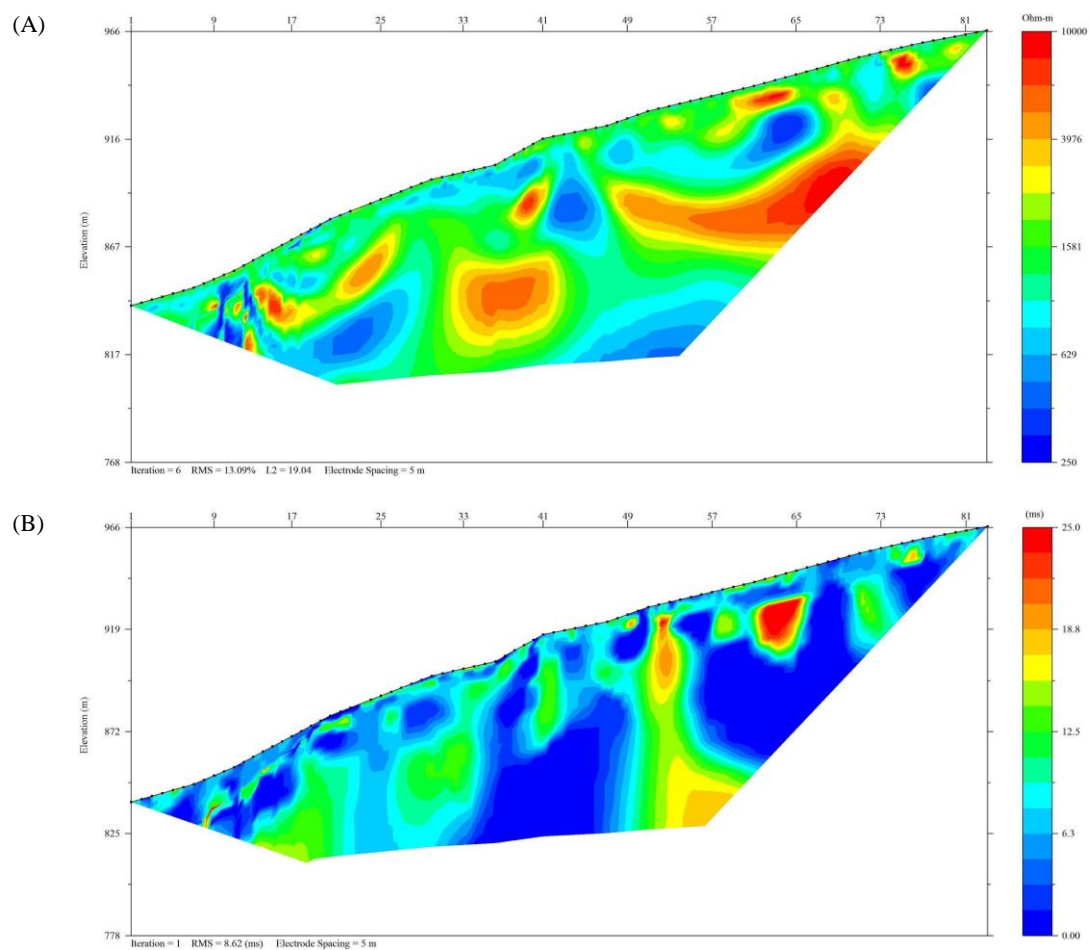


Figure 12: WHTIP17-10 sections. (A) Inverted resistivity (scale 250-10,000 Ohm-m). (B) Inverted IP (scale 0-25 ms).

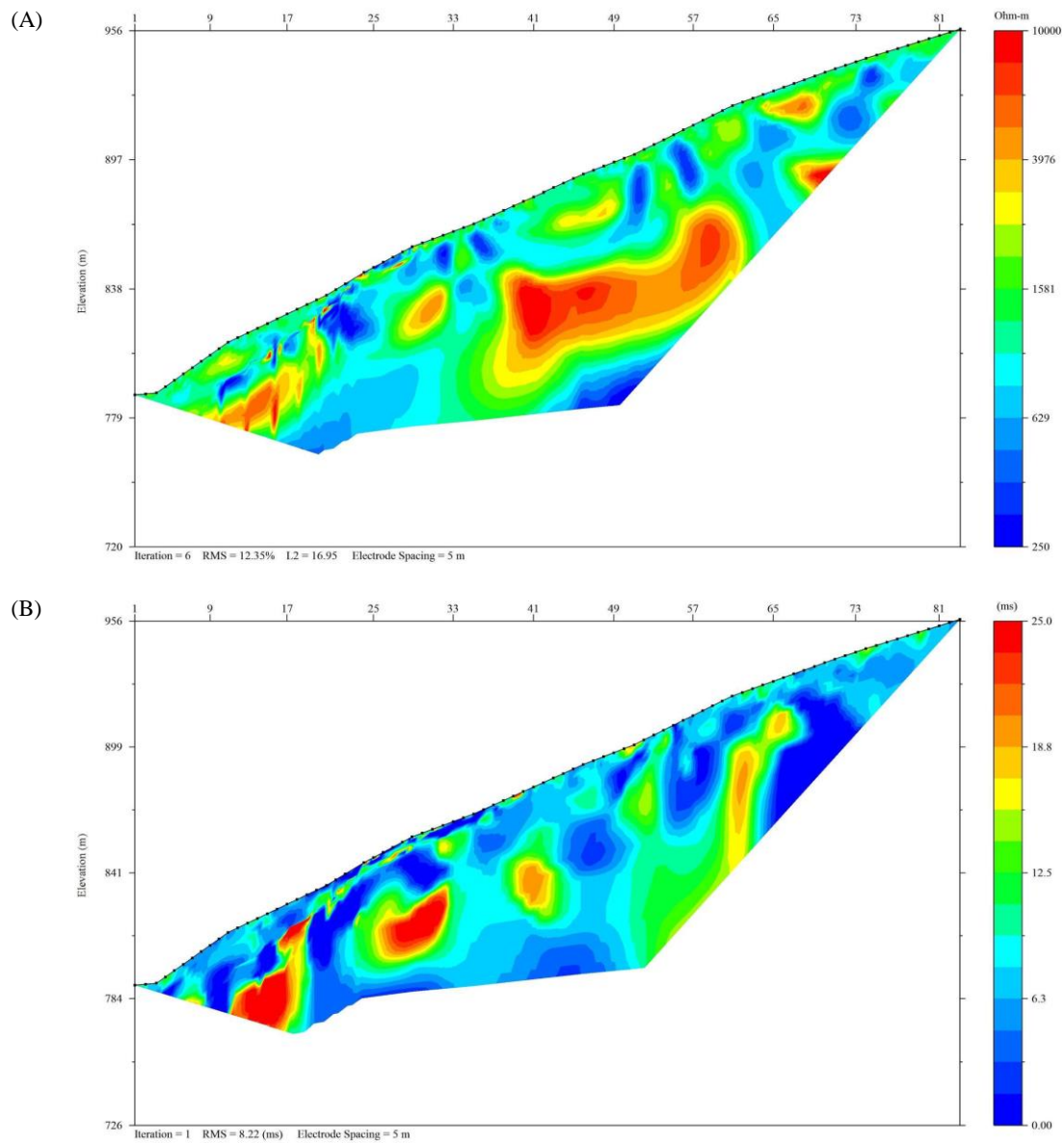


Figure 13: WHTIP17-11 sections. (A) Inverted resistivity (scale 250-10,000 Ohm-m). (B) Inverted IP (scale 0-25 ms).



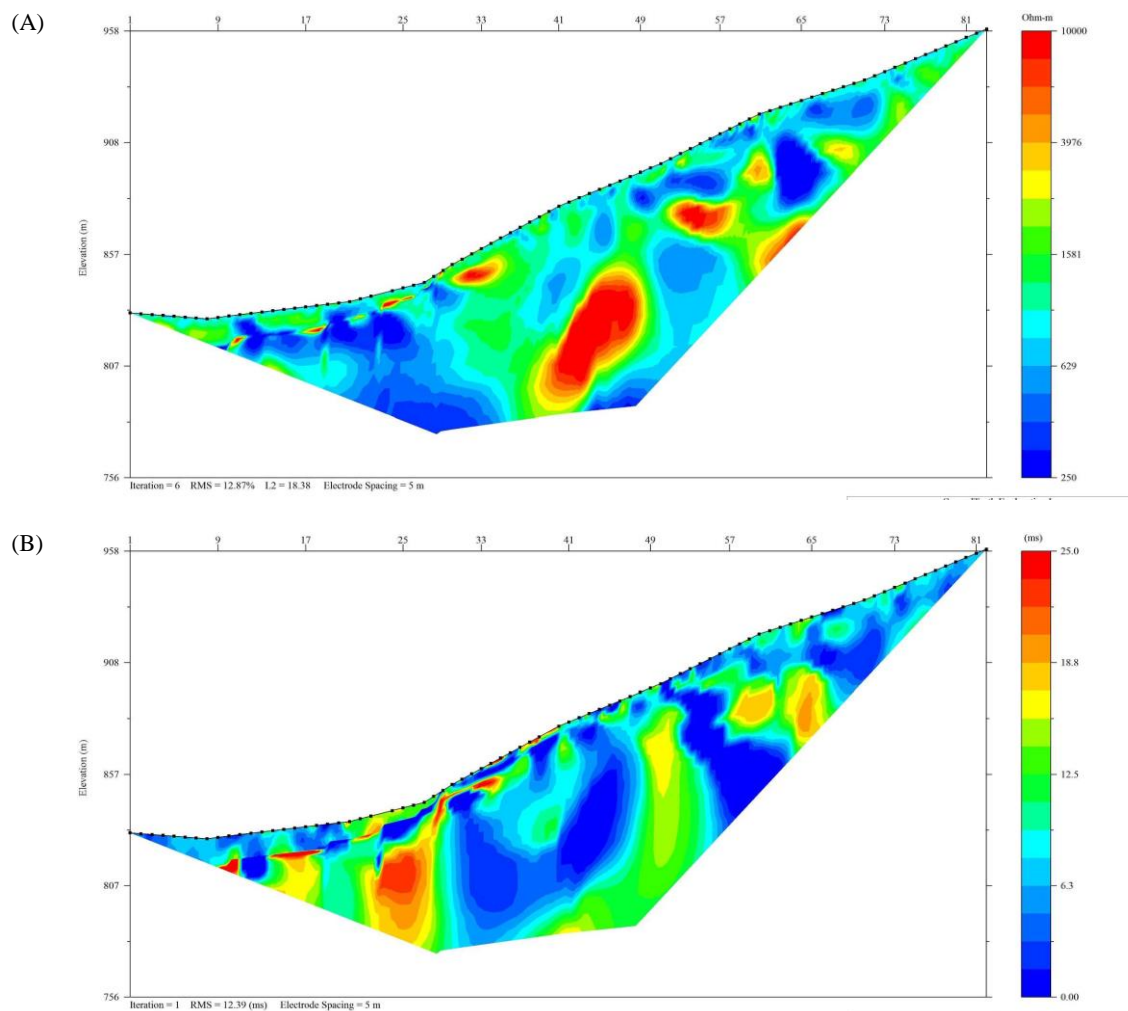


Figure 14: WHTIP17-12 sections. (A) Inverted resistivity (scale 250-10,000 Ohm-m). (B) Inverted IP (scale 0-25 ms).



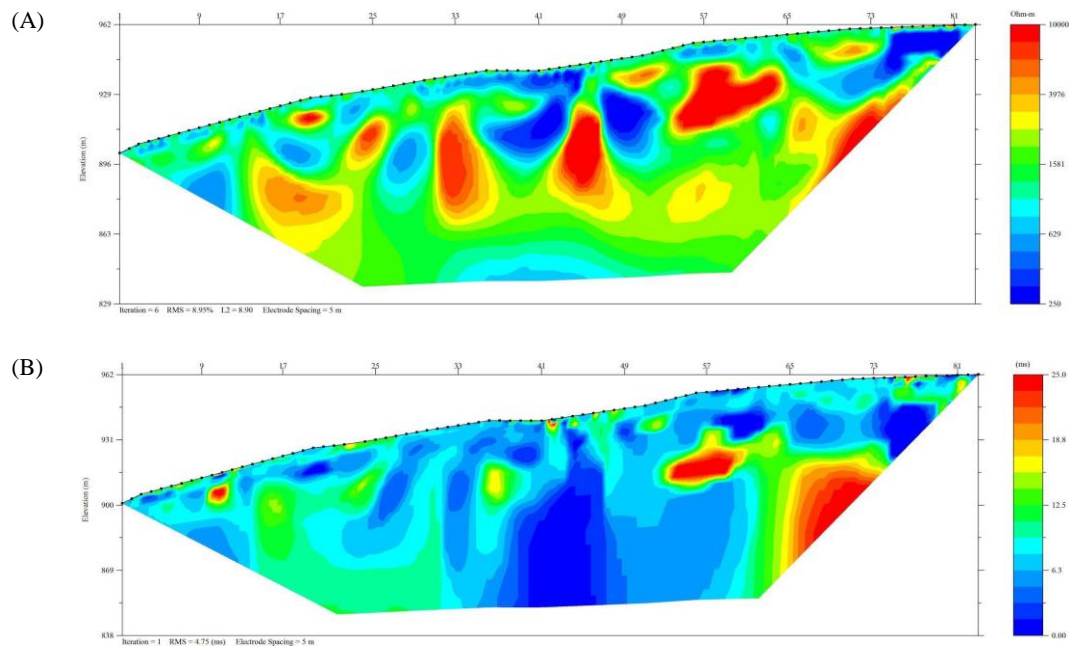


Figure 15: WHTIP17-13 sections. (A) Inverted resistivity (scale 250-10,000 Ohm-m). (B) Inverted IP (scale 0-25 ms).

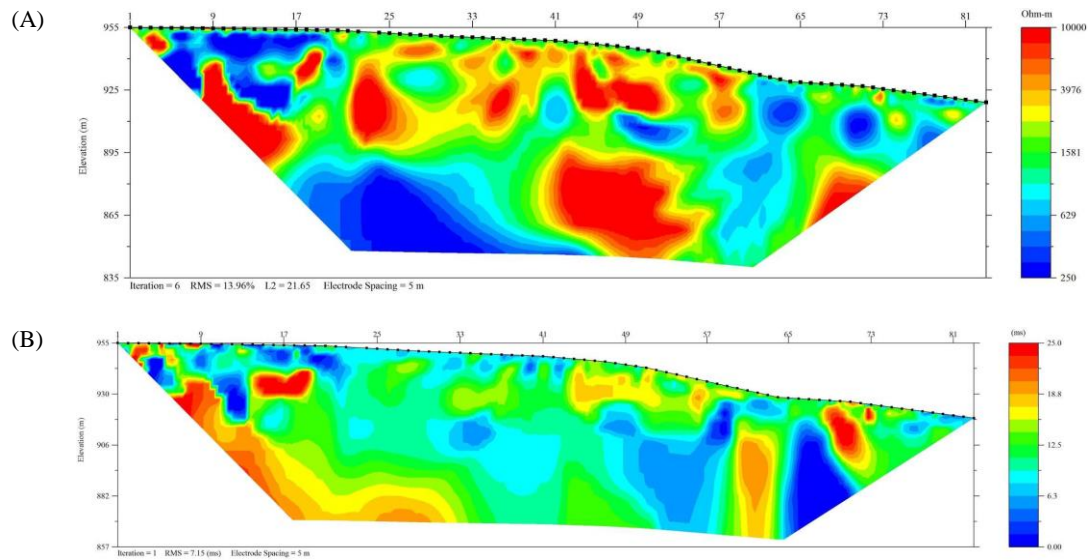


Figure 16: WHTIP17-14 sections. (A) Inverted resistivity (scale 250-10,000 Ohm-m). (B) Inverted IP (scale 0-25 ms).

#### 4.3 Interpretation

Interpretation of 2-D resistivity and induced polarization surveys first requires identifying anomalous zones that are caused by real subsurface electrical boundaries versus those that are artefacts formed during the inversion process. Real anomalous zones will trend between adjacent RES/IP lines and show correlation with crossline data. This section provides a brief qualitative description of the electrical conductivity and chargeability anomalies that trend between the RES/IP sections presented in section 4.2.

The resistivity sections show a subvertical disruption that runs approximately northeast-southwest through the grid. It appears to dip towards the southeast. This lineament is accompanied by a chargeability low in the IP sections. Overall, the gridded area is most resistive near the middle (lines WHTIP17-03–WHTIP17-08 and WHTIP17-14). A deeper conductive structure appears in lines WHTIP17-01– WHTIP17-03. There is another (but smaller magnitude) conductive structure that trends on the southern end of lines WHTIP17-10–WHTIP17-12. There is good correlation with resistivity and chargeability results between the crossline WHTIP17-14 and intersecting lines WHTIP17-07– WHTIP17-09.

Similarities between the conductive and resistive units throughout the Golden Saddle RES/IP survey lines inflicts confidence that these anomalies define real subsurface electrical boundaries. To further constrain this interpretation, it is recommended that known geological and geochemical information is incorporated. This will aid the interpreter to gain a better understanding of these anomalies and potentially aid them to find the geological structures and mineralized zones inherent to gold deposits.

## 5.0 Arc

### 5.1 Survey Summary

An overview of the RES/IP grid on the Arc zone is shown in Figure 18. Brief specifications about the survey lines are outlined below.

Lines	ARCIP17-01 – ARCIP17-07
Number of Electrodes	84
Electrode Spacing	5m
Line Length	415m
Array	Extended dipole-dipole

As seen in Figure 18, the Arc grid is located roughly over a ridge that is oriented east-west. Elevation profile of the ridge is highest to the west and comes close to a small creek confluence to the east. Terrain covering the Arc zone is mostly dense aspen trees, brush and low-lying shrubs near the center of the ridge. Ground cover is a mixture of grass, rock, bare soil, and moss. This lead to a range of electrode contact resistance values. The south side of the ridge typically had lower CR that ranged between 800–2,800 Ohms and the north side of the ridge had higher CR that ranged between 3,500–9,200 Ohms. The total range of CR values across a single survey traverse was smaller along lines on the west side of the grid, and larger closer to the valley. In situations where one side of the traverse had better contacts than the other, the array measurement direction was chosen to read from low to high CR.

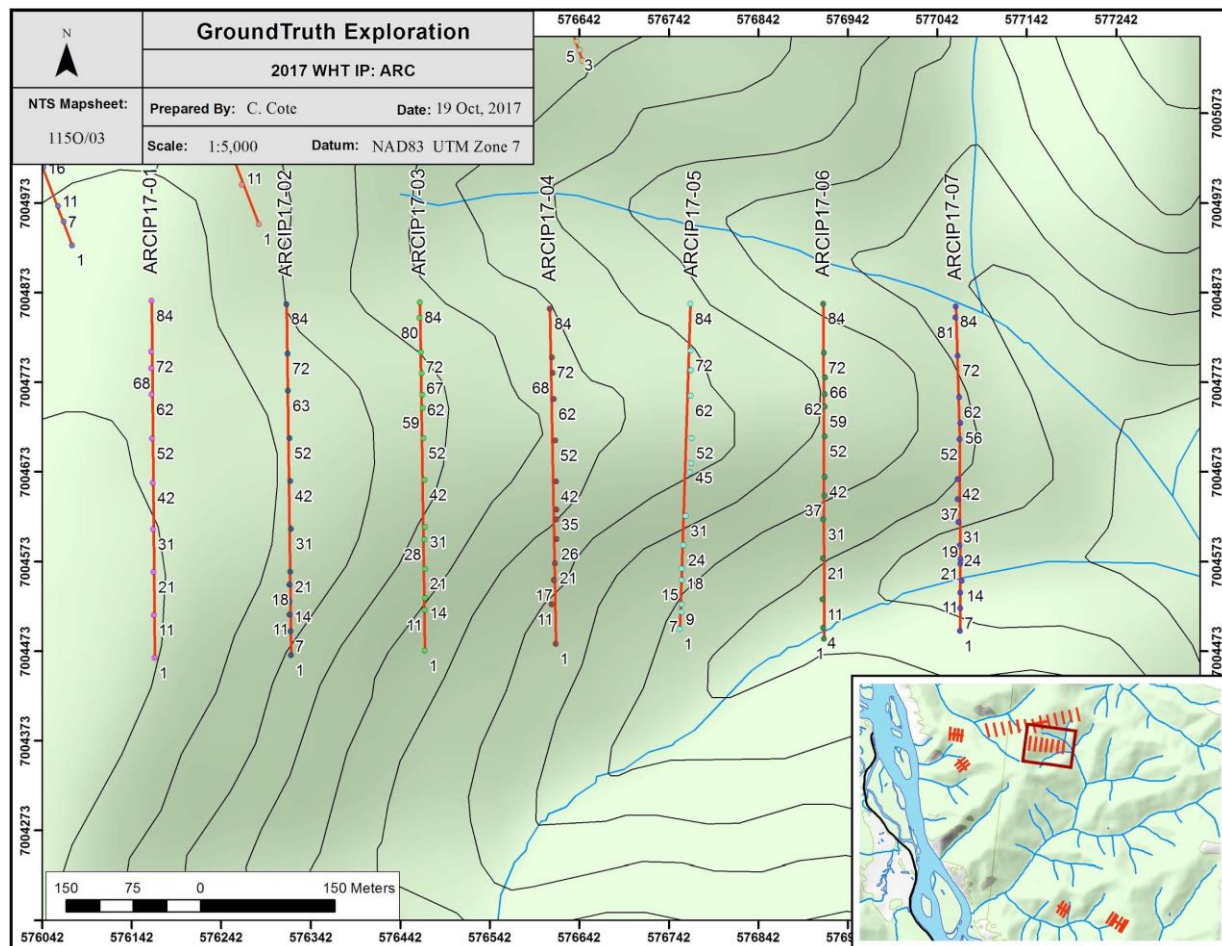


Figure 17: 2017 completed RES/IP grid on the Arc zone.

## 5.2 Survey Results

The following figures display the inverted resistivity and induced polarization sections along each traverse in the Arc zone. Note that the depth of penetration of the IP results is generally less than the resistivity results.

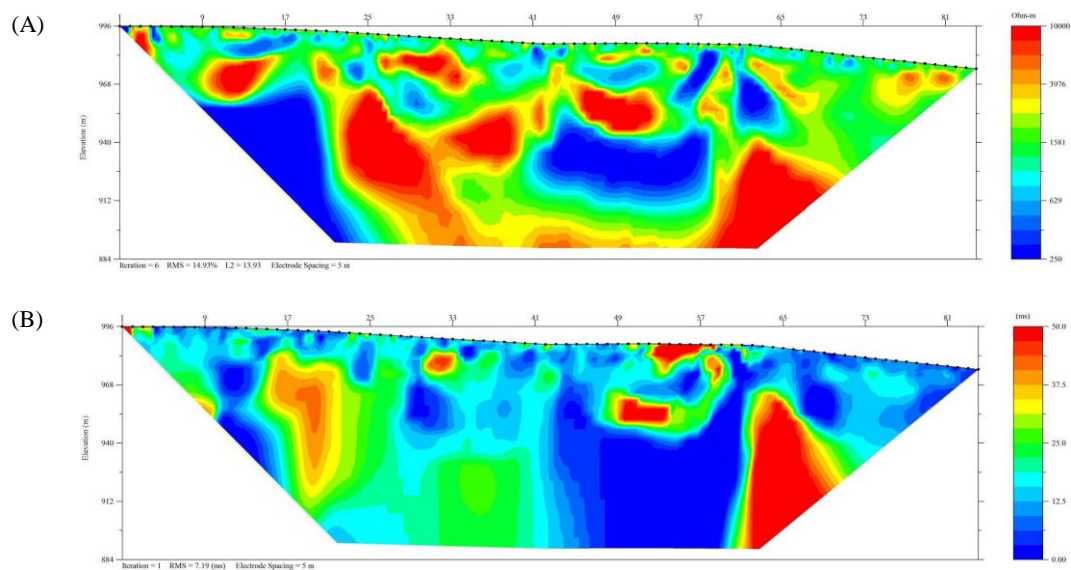


Figure 18: ARCI17-01 sections. (A) Inverted resistivity (scale 250-10,000 Ohm-m). (B) Inverted IP (scale 0-50 ms).

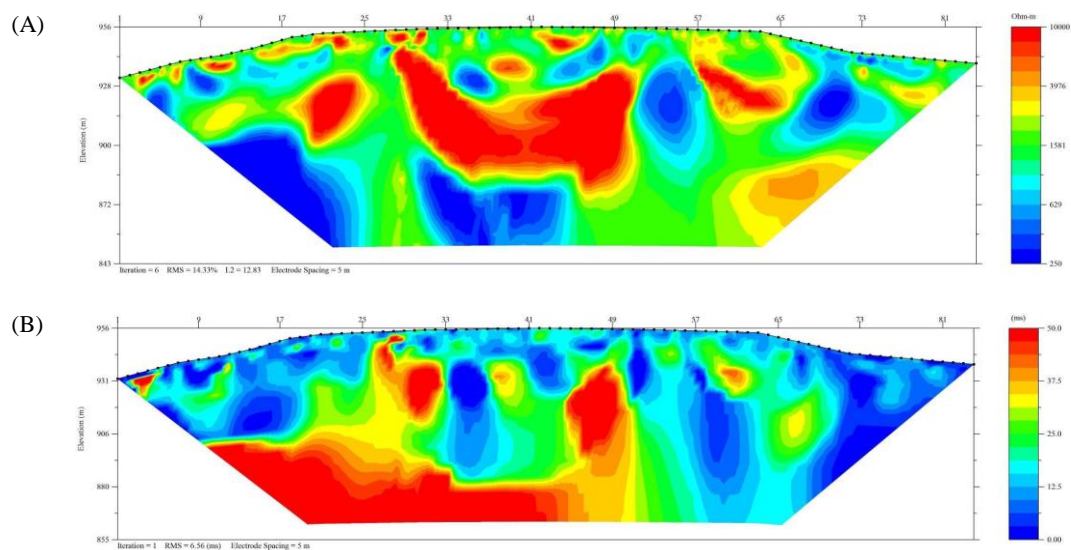


Figure 19: ARCI17-02 sections. (A) Inverted resistivity (scale 250-10,000 Ohm-m). (B) Inverted IP (scale 0-50 ms).



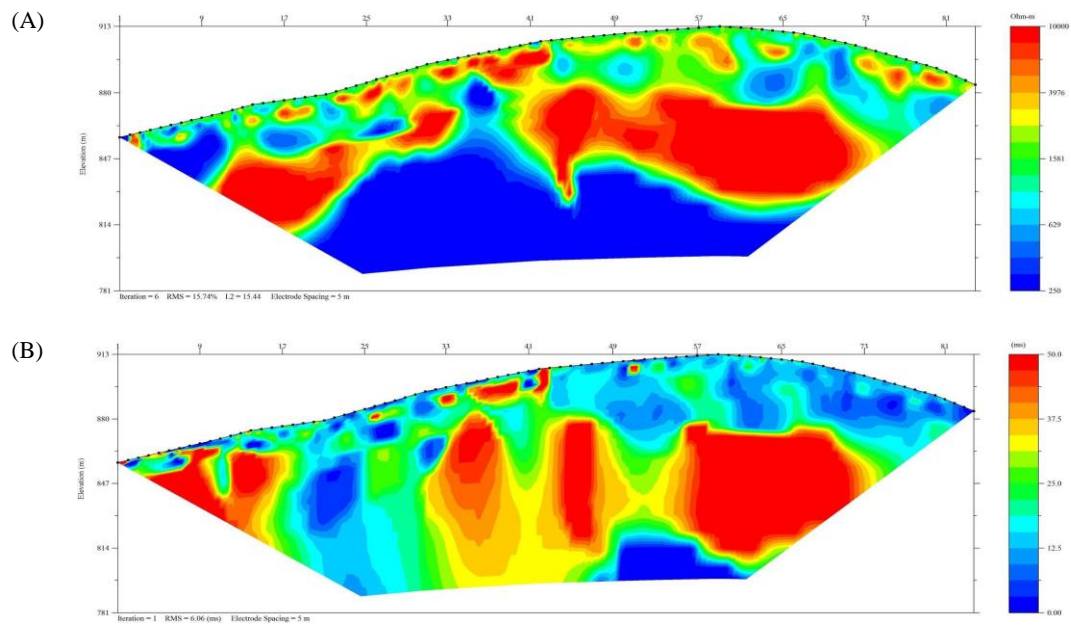


Figure 20: ARCIP17-03 sections. (A) Inverted resistivity (scale 250-10,000 Ohm-m). (B) Inverted IP (scale 0-75 ms).

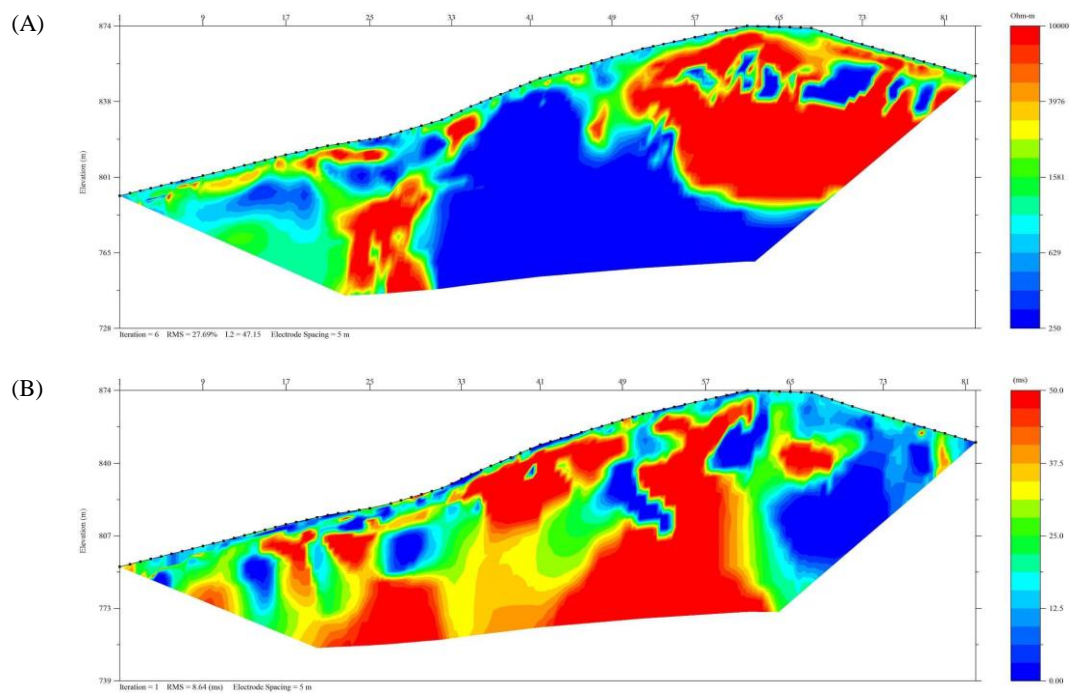


Figure 21: ARCIP17-04 sections. (A) Inverted resistivity (scale 250-10,000 Ohm-m). (B) Inverted IP (scale 0-50 ms).

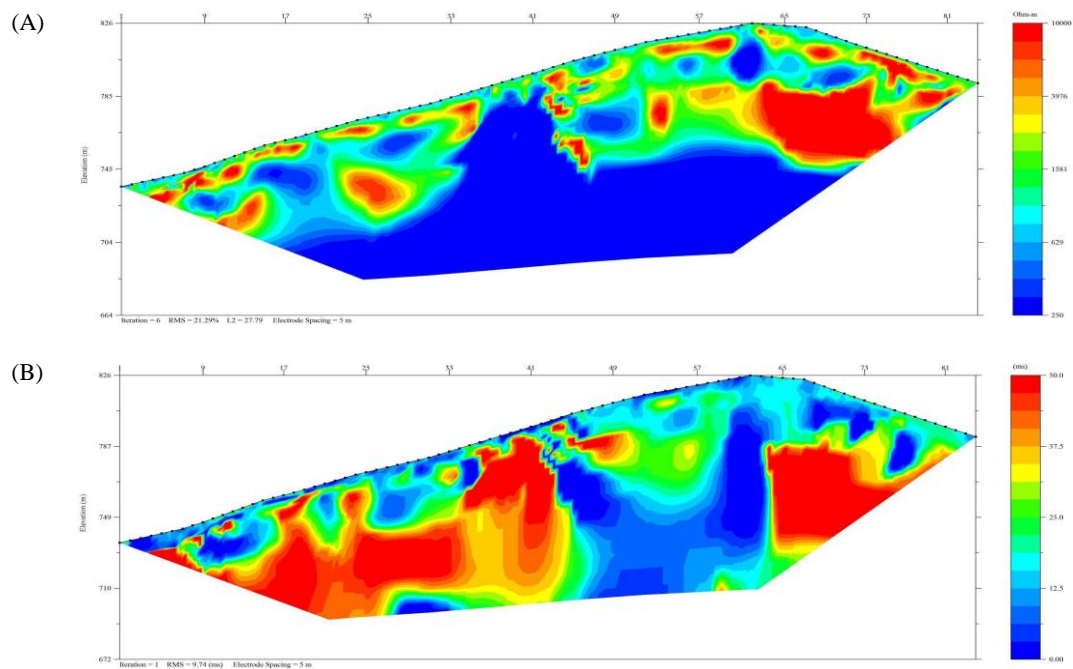
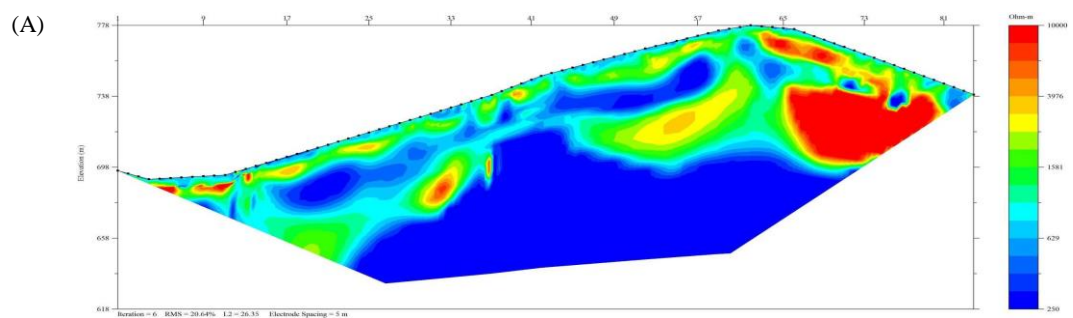


Figure 22: ARCIP17-05 sections. (A) Inverted resistivity (scale 250-10,000 Ohm-m). (B) Inverted IP (scale 0-50 ms).





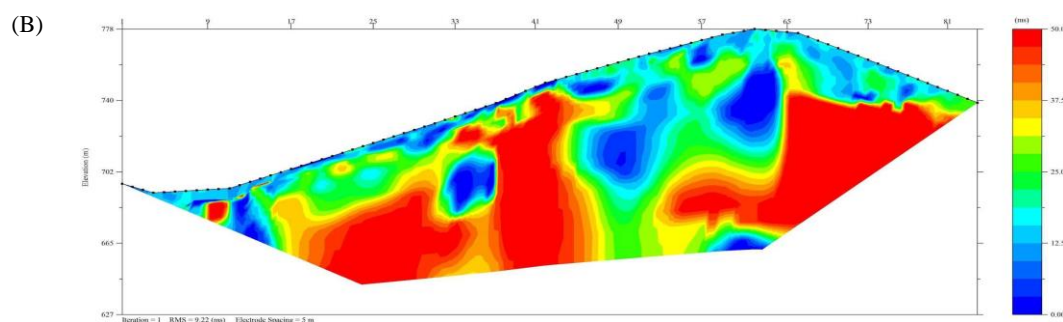


Figure 23: ARCIP17-06 sections. (A) Inverted resistivity (scale 250-10,000 Ohm-m). (B) Inverted IP (scale 0-50 ms).

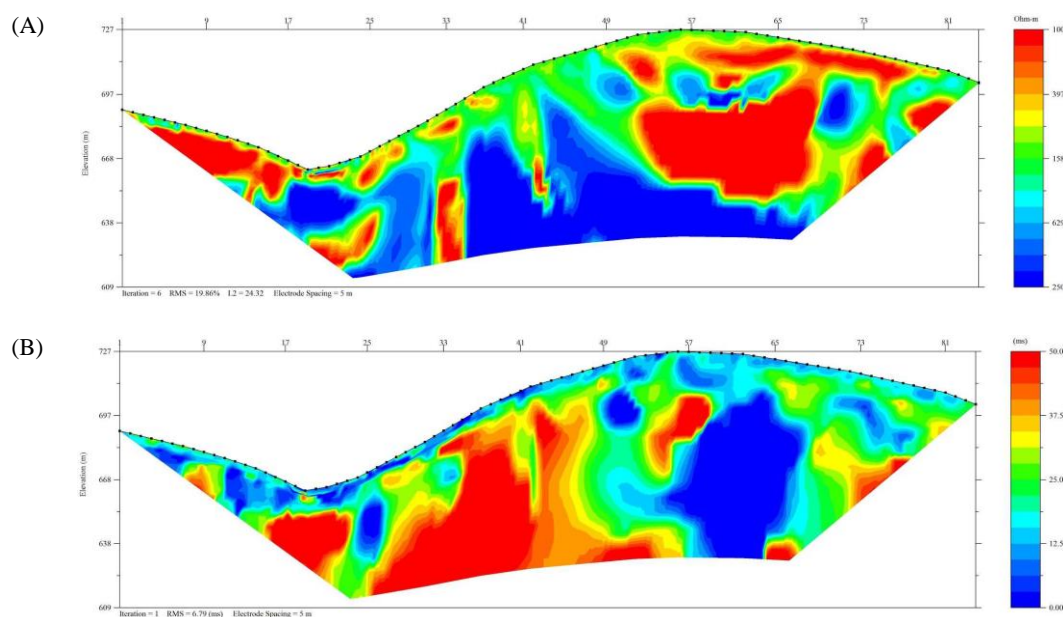


Figure 24: ARCIP17-07 sections. (A) Inverted resistivity (scale 250-10,000 Ohm-m). (B) Inverted IP (scale 0-50 ms).

### 5.3 Interpretation

Qualitatively, the 2-D RES/IP surveys acquired in the Arc zone show trending zones of resistivity and chargeability between the profiles. Notably, the resistivity surveys show a conductive zone at depth near the center of the profiles that appears in lines ARCIP17-03–ARCIP17-07. This conductive feature is overlain by a resistive unit to the north and a less resistive unit to the south. The IP profiles show correlations between chargeability high zones (i.e. the southern parts of lines ARCIP17-02–ARCIP17-07) and a

chargeability low zone near the top of the ridge in lines ARCIP17-05–ARCIP17-07). To further constrain this interpretation, it is recommended that known geological and geochemical information is incorporated about the site. This will aid the interpreter to gain a better understanding of these anomalies and potentially aid them to identify geological structures and mineralized zones inherent to gold deposits.

## 6.0 Ulli Ridge

### 6.1 Survey Summary

An overview of the two 2017 RES/IP grids on the Ulli Ridge zone is shown in Figures 27 and 28. Brief specifications about the survey lines are outlined below.

Lines	ULRIP17-01 – ULRIP17-09
Number of Electrodes	84
Electrode Spacing	5m
Line Length	415m
Array	Extended dipole-dipole

Survey lines in the Ulli Ridge zone are separated into two different grids: one to the north composed of five lines located over a subtle saddle, and the other to the south composed of four lines located over a ridge. Placement of the survey lines maximize coverage of gold-in-soil anomalies and geological structures. Two crosslines (ULRIP17-05 and ULRIP17-09) are utilized to gain sufficient spatial insight to the distribution of subsurface structures.

The gridded areas are covered by a combination of deadfall, thick and small poplar trees, conifers, and low-lying ground cover. Soil is clay-rich and sand-rich and there are localized rock areas. These ground conditions lead to electrode contact resistances that generally ranged between 500–3,000 Ohms. Sometimes the best achievable contact

resistance was as high as 7,000 Ohms, but this was rare. In situations where one side of the traverse had better contacts than the other, the array measurement direction was chosen to read from low to high CR.

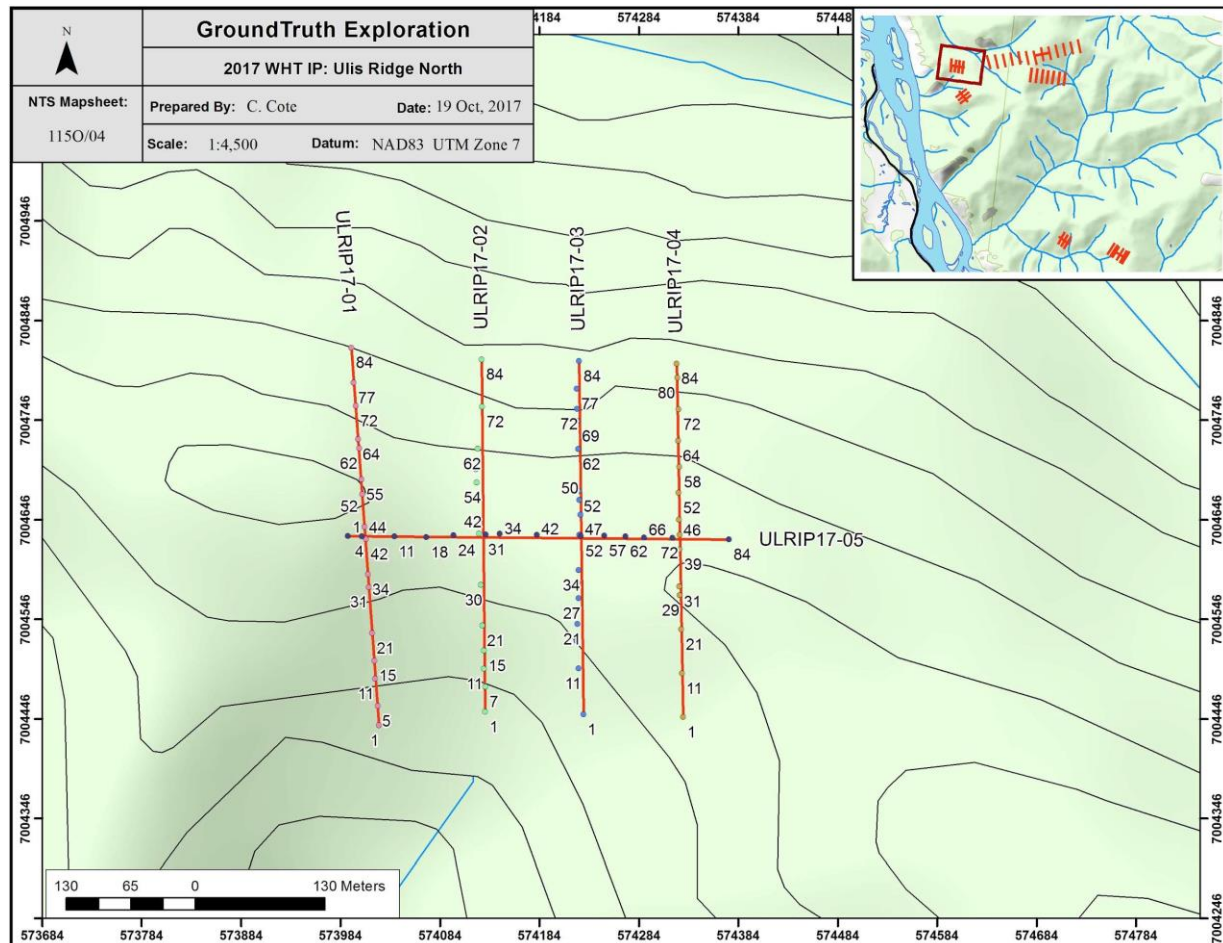


Figure 25: 2017 completed RES/IP northern grid on the Ulli Ridge zone.

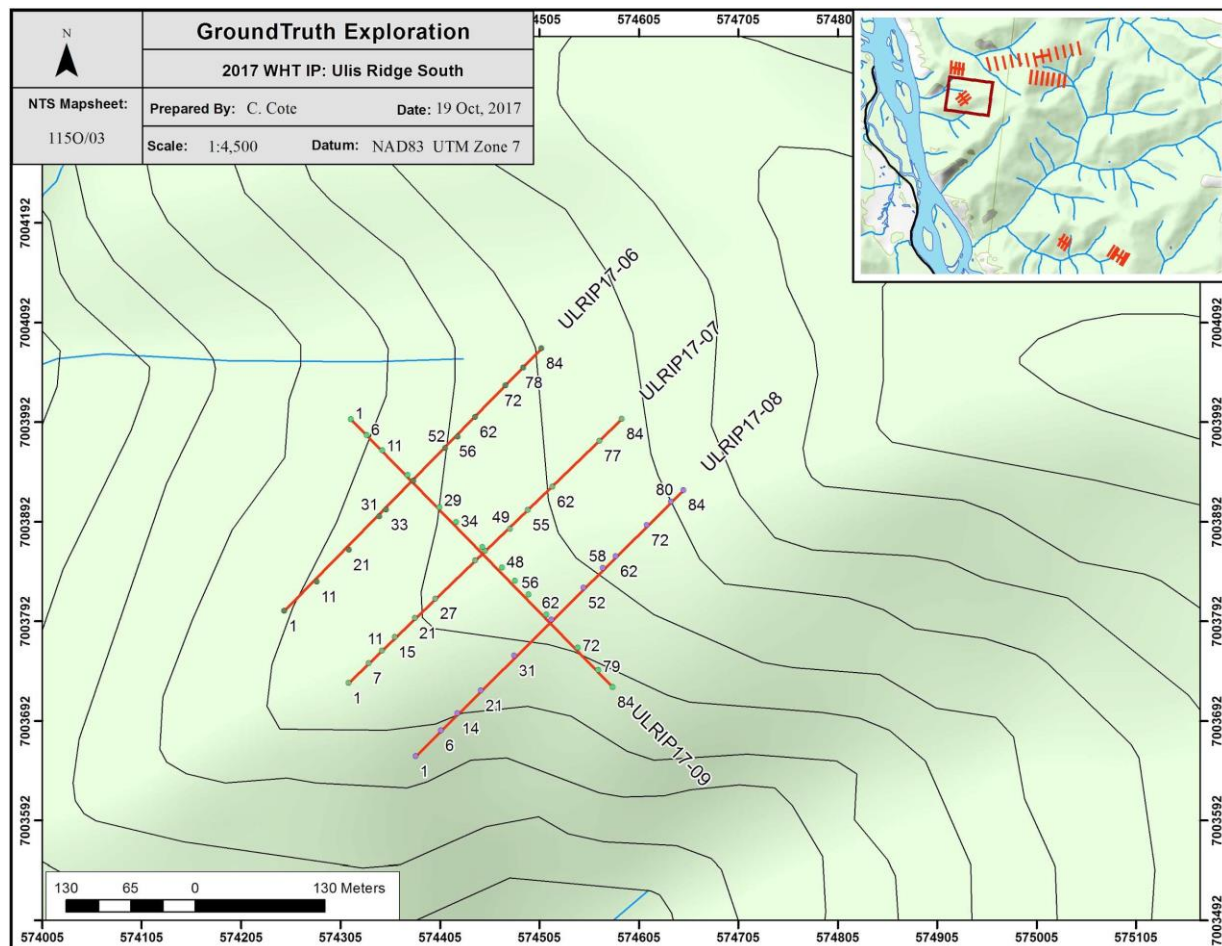


Figure 26: 2017 completed RES/IP southern grid on the Ullis Ridge zone.

## 6.2 Survey Results

The following figures display the inverted resistivity and induced polarization sections along each traverse in the Nine Mile NW zone. Note that the depth of penetration of the IP results can be notably less than the resistivity results.



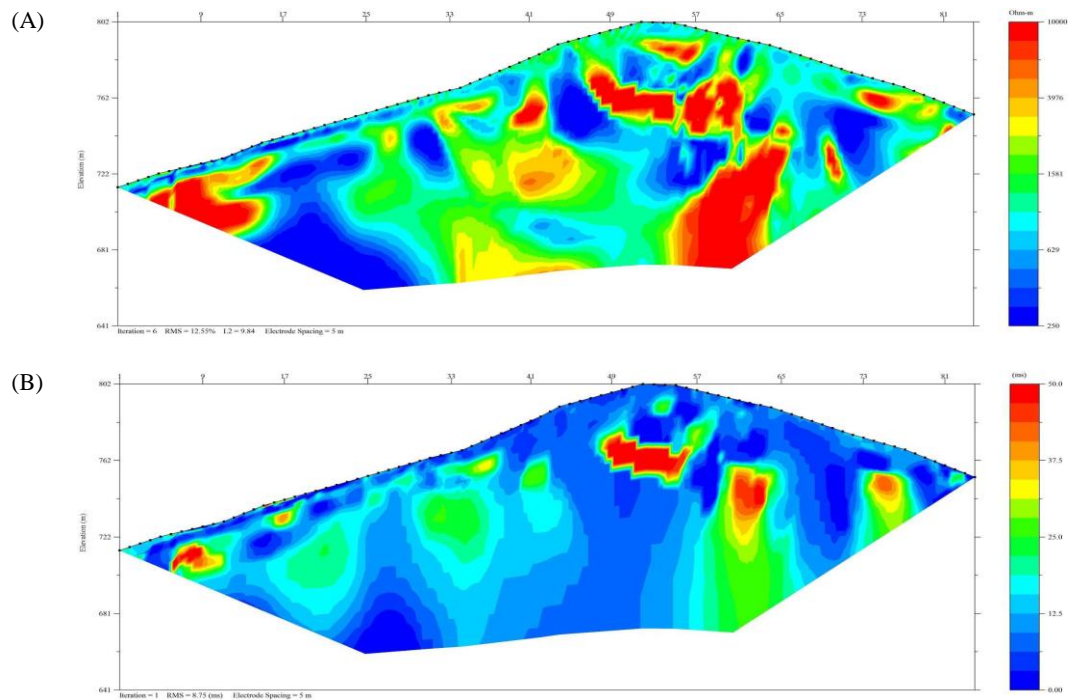


Figure 27: ULRIP17-01 sections. (A) Inverted resistivity (scale 250-10,000 Ohm-m). (B) Inverted IP (scale 0-50 ms).

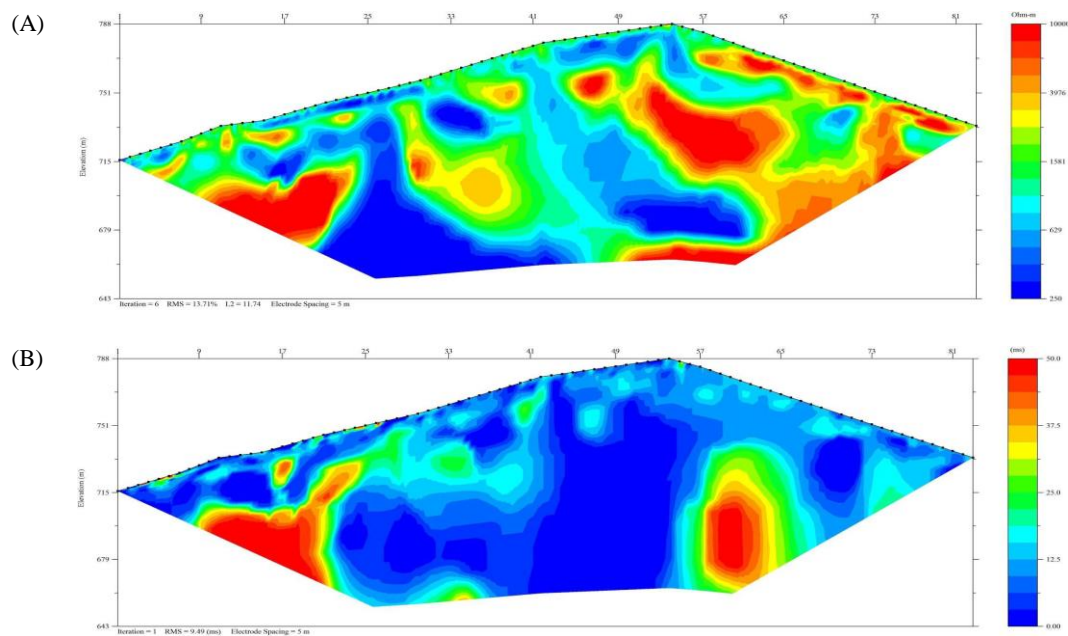


Figure 28: ULRIP17-02 sections. (A) Inverted resistivity (scale 250-10,000 Ohm-m). (B) Inverted IP (scale 0-50 ms).

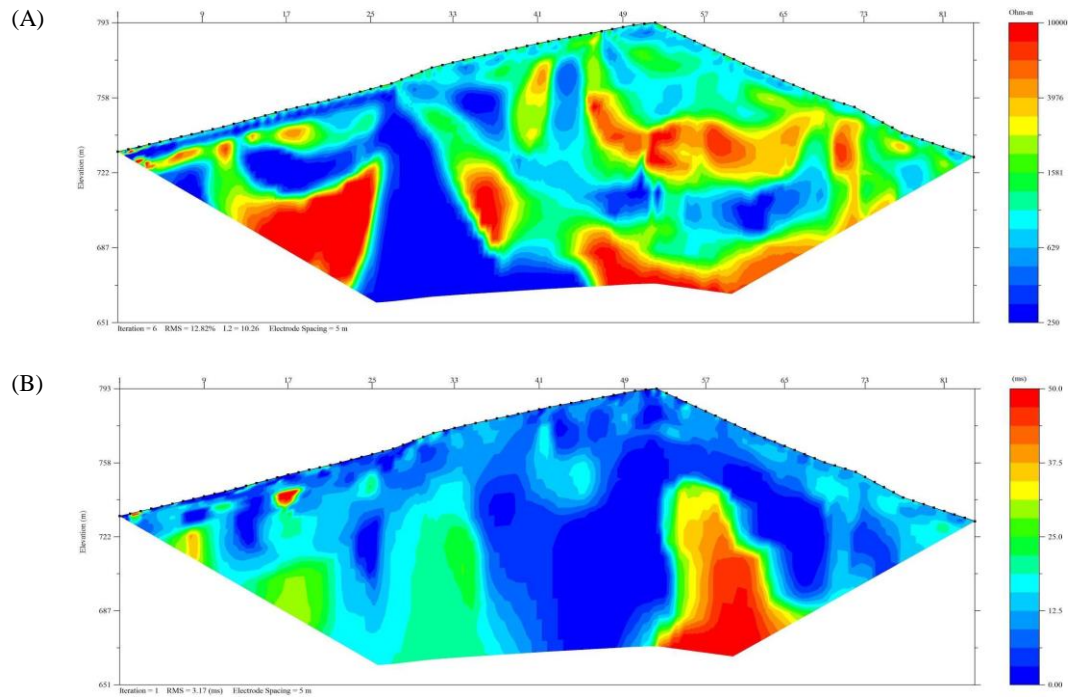
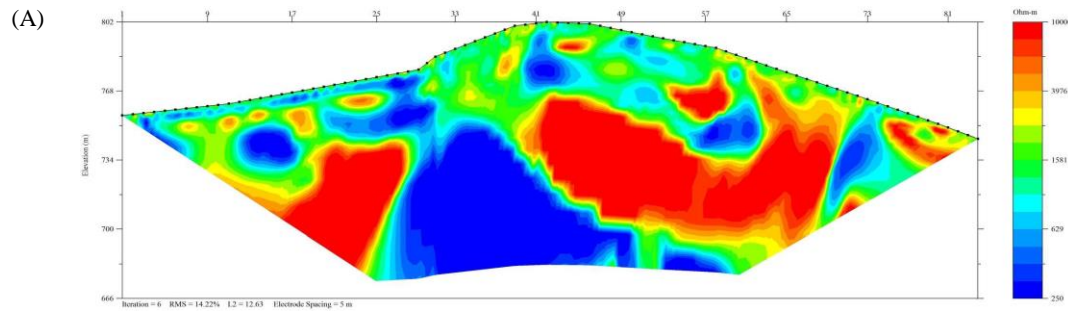


Figure 29: ULRIP17-03 sections. (A) Inverted resistivity (scale 250-10,000 Ohm-m). (B) Inverted IP (scale 0-50 ms).



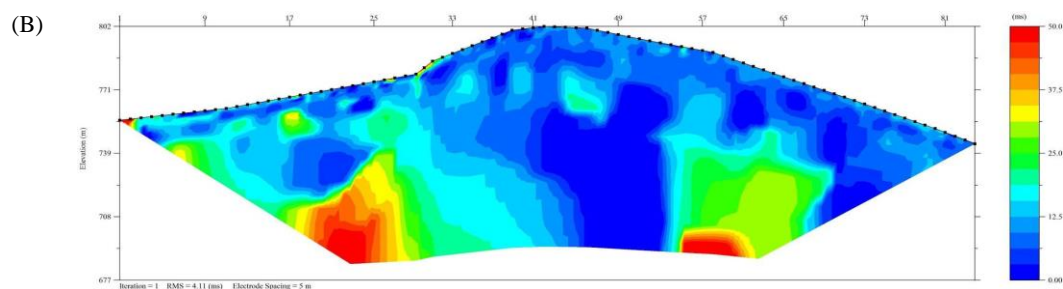


Figure 30: ULRIP17-04 sections. (A) Inverted resistivity (scale 250-10,000 Ohm-m). (B) Inverted IP (scale 0-50 ms).

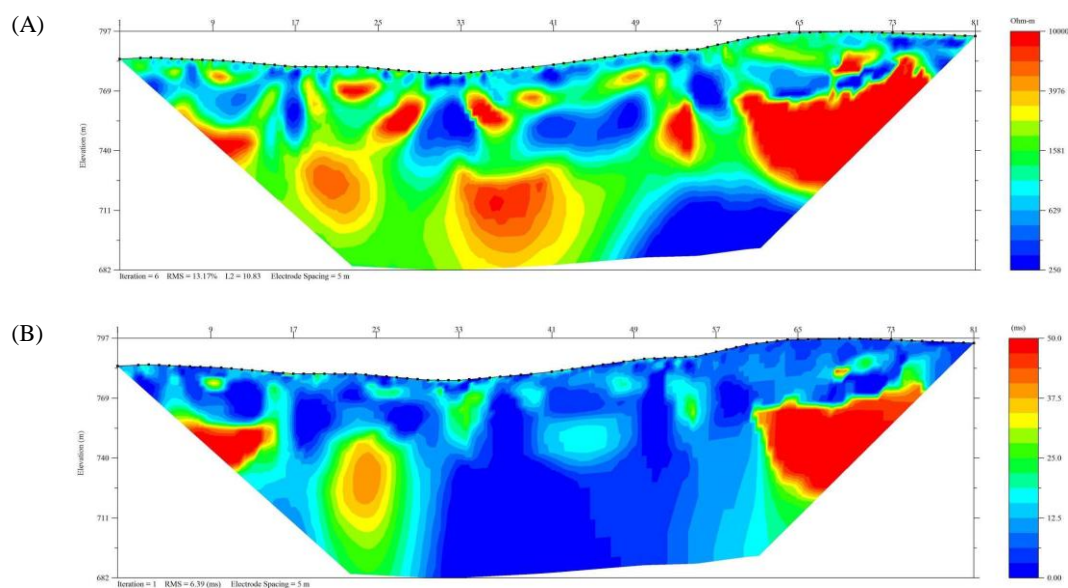
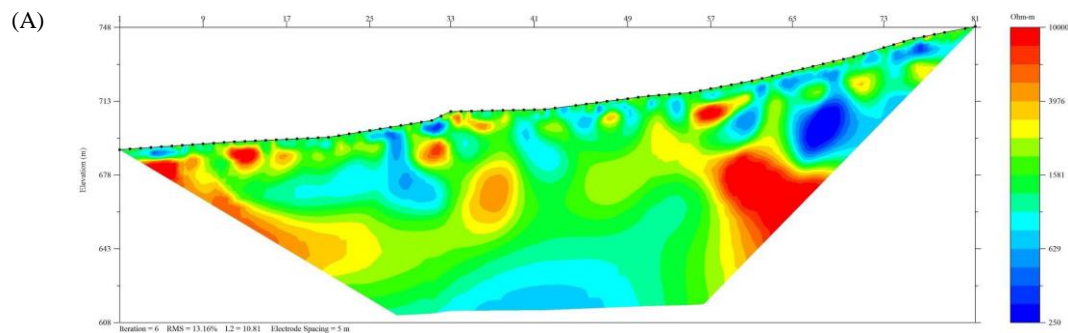


Figure 31: ULRIP17-05 sections. (A) Inverted resistivity (scale 250-10,000 Ohm-m). (B) Inverted IP (scale 0-50 ms).





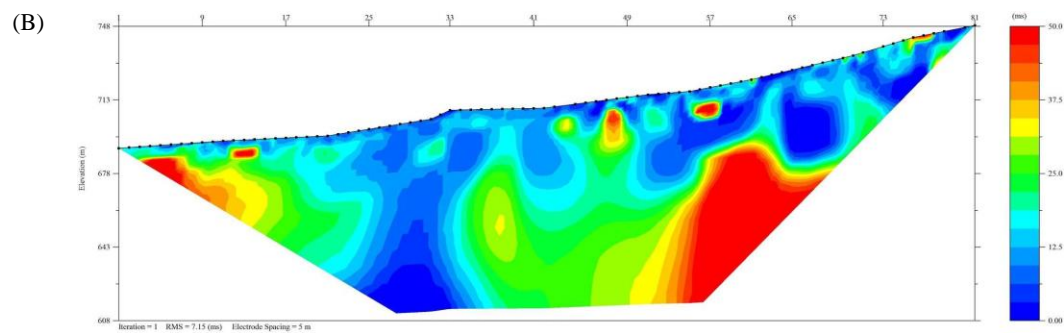


Figure 32: ULRIP17-06 sections. (A) Inverted resistivity (scale 250-10,000 Ohm-m). (B) Inverted IP (scale 0-50 ms).

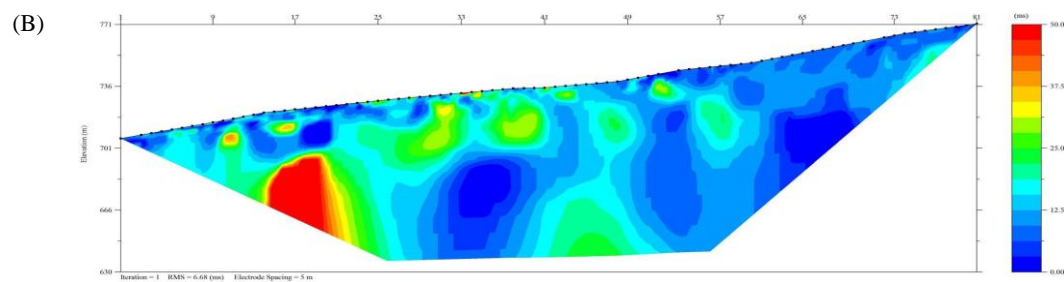
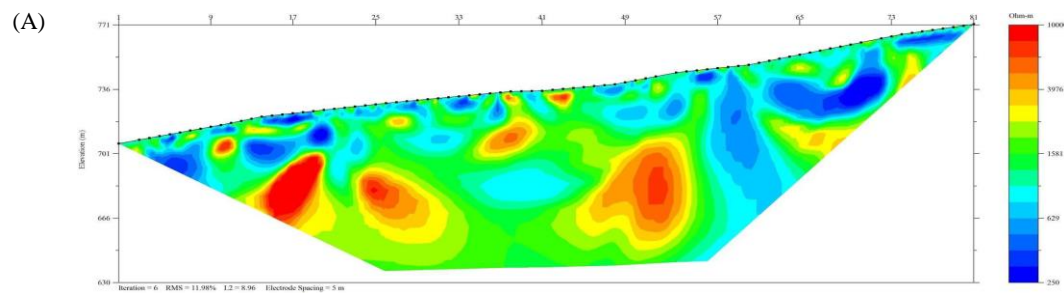


Figure 33: ULRIP17-07 sections. (A) Inverted resistivity (scale 250-10,000 Ohm-m). (B) Inverted IP (scale 0-50 ms).

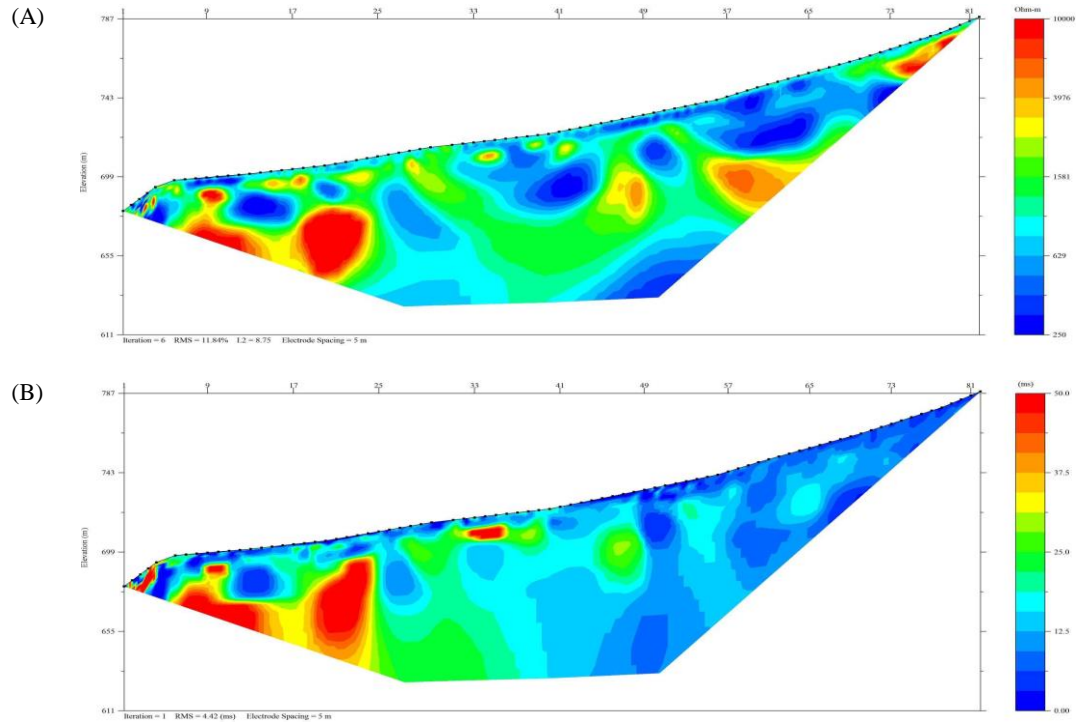
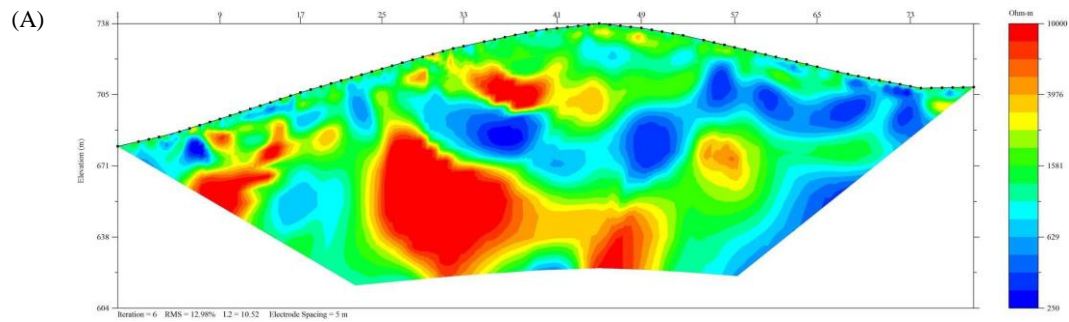


Figure 34: ULRIP17-08 sections. (A) Inverted resistivity (scale 250-10,000 Ohm-m). (B) Inverted IP (scale 0-50 ms).



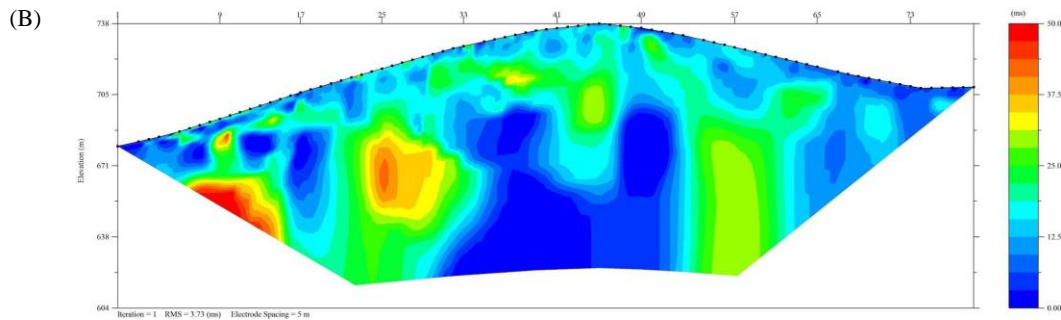


Figure 35: ULRIP17-09 sections. (A) Inverted resistivity (scale 250-10,000 Ohm-m). (B) Inverted IP (scale 0-50 ms).

### 6.3 Interpretation

The 2-D RES/IP surveys acquired in the Ulli Ridge zone show trending zones of resistivity and chargeability. In the northern grid, the resistivity profiles show a conductive zone that trends east-west just south of the saddle. This conductive zone is sandwiched by more resistive areas to the north and south. The corresponding IP shows higher chargeability in the north and south parts of the grid. Data from the crossline ULRIP17-05 shows good agreement with data from the corresponding inlines.

Resistivity profiles in the southern grid show that this area, overall, has a smaller range in resistivity than the northern grid. There are still trends between profiles showing subsurface resistivity and chargeability. To further constrain this interpretation, it is recommended that known geological and geochemical information is incorporated about the site. This will aid the interpreter to gain a better understanding of these anomalies and potentially aid them to identify geological structures and mineralized zones inherent to gold deposits.

## 7.0 McKinnon

### 7.1 Survey Summary

An overview of the two 2017 RES/IP grid on the McKinnon zone is shown in Figure 40. Brief specifications about the survey lines are outlined below.

Lines	MCKIP17-01 – MCKIP17-11
Number of Electrodes	84

---

Electrode Spacing	5m
Line Length	415m
Array	Extended dipole-dipole

The larger of the two grids (MCKIP17-01–MCKIP17-07) utilizes historical IP cut lines as well as acquires new IP data. The exact placement and number of these historical lines was unknown so the cut lines were utilized whenever the crew was able to locate them (i.e. lines MCKIP17-01, MCKIP17-02, and MCKIP17-04). This lead to inconsistent line spacing on this grid. Placement of the survey lines on both of the McKinnon grids maximize coverage of gold-in-soil anomalies and geological structures. Two crosslines (MCKIP17-07 and MCKIP17-11) are utilized to gain sufficient spatial insight to the distribution of subsurface structures.

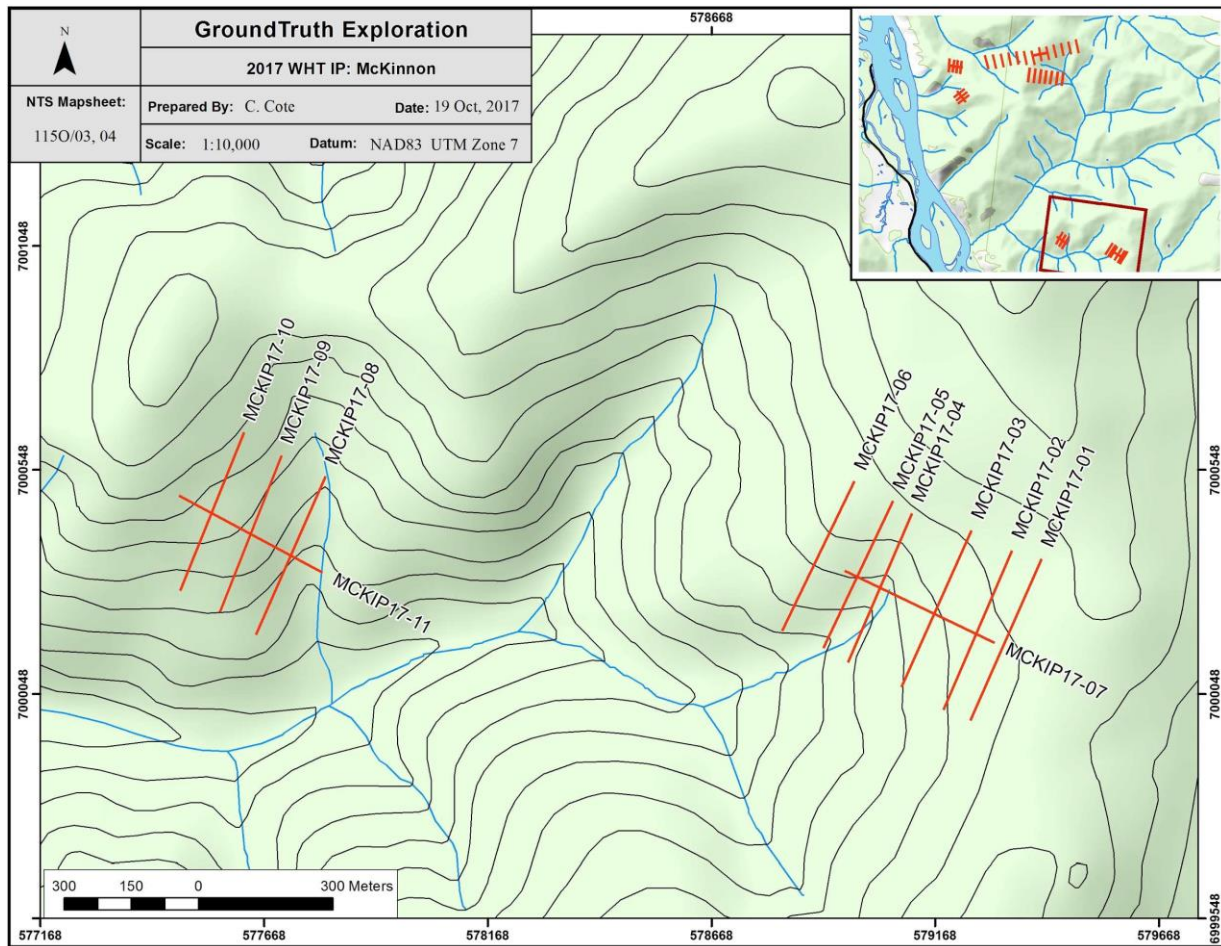


Figure 36: 2017 completed RES/IP grid on the McKinnon zone.

The larger McKinnon grid is covered by a variety of bulldozed areas, cut lines, and quad trails. The terrain is a combination of aspen and coniferous trees and the ground is covered by grasses, sandy soil, and clay. On each RES/IP traverse, the electrodes were carefully placed and saturated with calcium chloride solution to achieve the lowest possible contact resistance values. On both grids, most values ranged between 400–3,200 Ohms, and a handful of values reached upwards of 20,000 Ohms in particularly dry and rocky areas, where it is difficult to achieve consistent ground contact along the length of the electrode. In situations where one side of the traverse had better contacts than the other, the array measurement direction was chosen to read from low to high CR.



## 7.2 Survey Results

The following figures display the inverted resistivity and induced polarization sections along each traverse in the McKinnon zone. Note that the depth of penetration of the IP results can be notably less than the resistivity results.

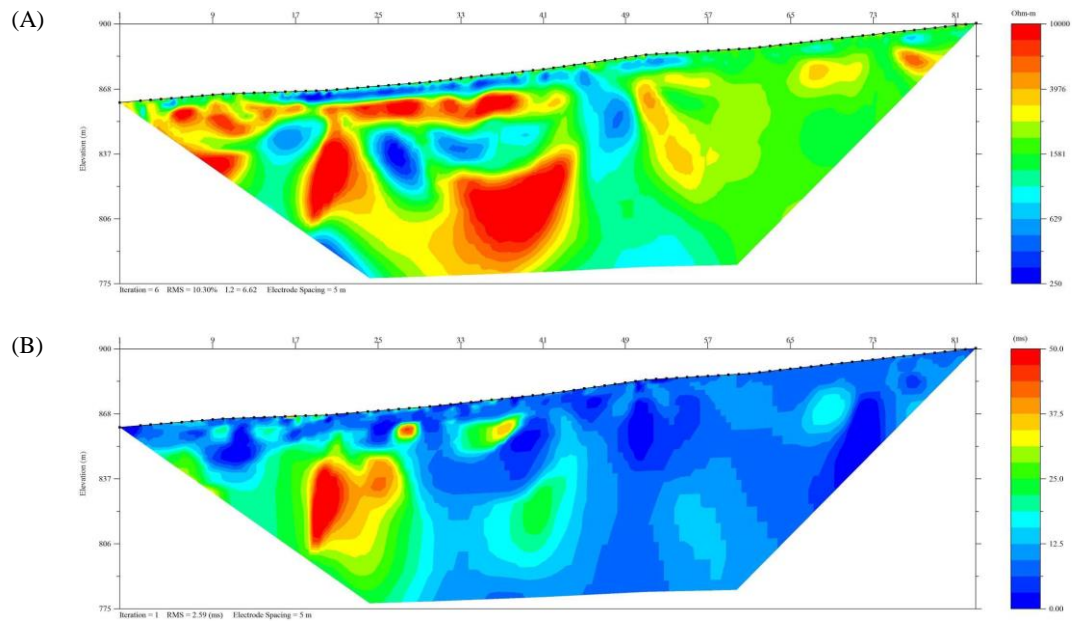


Figure 37: MCKIP17-01 sections. (A) Inverted resistivity (scale 250-10,000 Ohm-m). (B) Inverted IP (scale 0-50 ms).

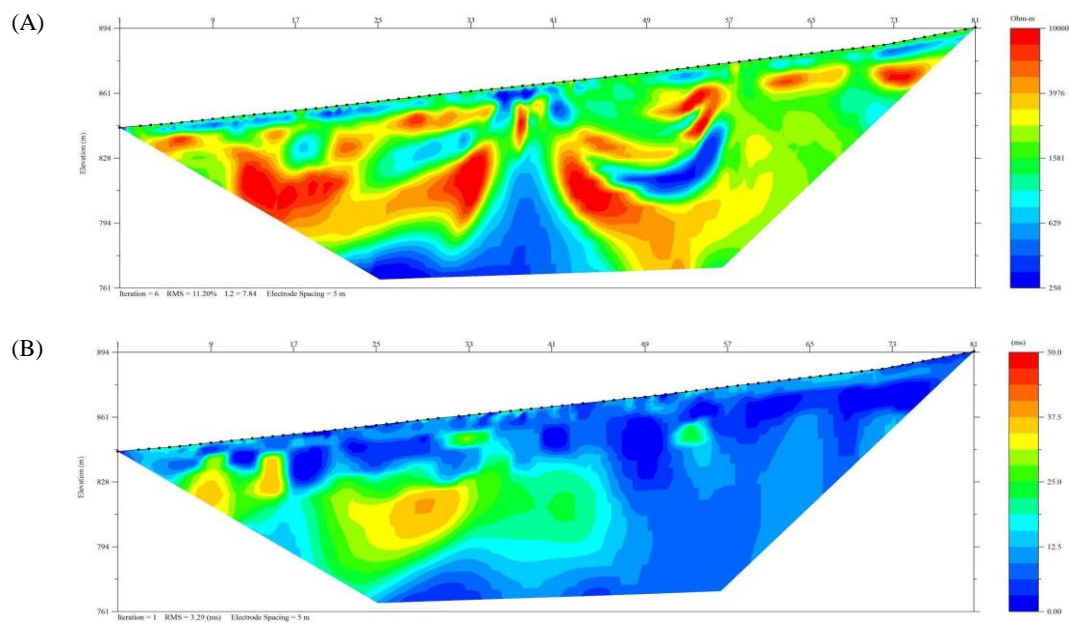


Figure 38: MCKIP17-02 sections. (A) Inverted resistivity (scale 250-10,000 Ohm-m). (B) Inverted IP (scale 0-50ms).

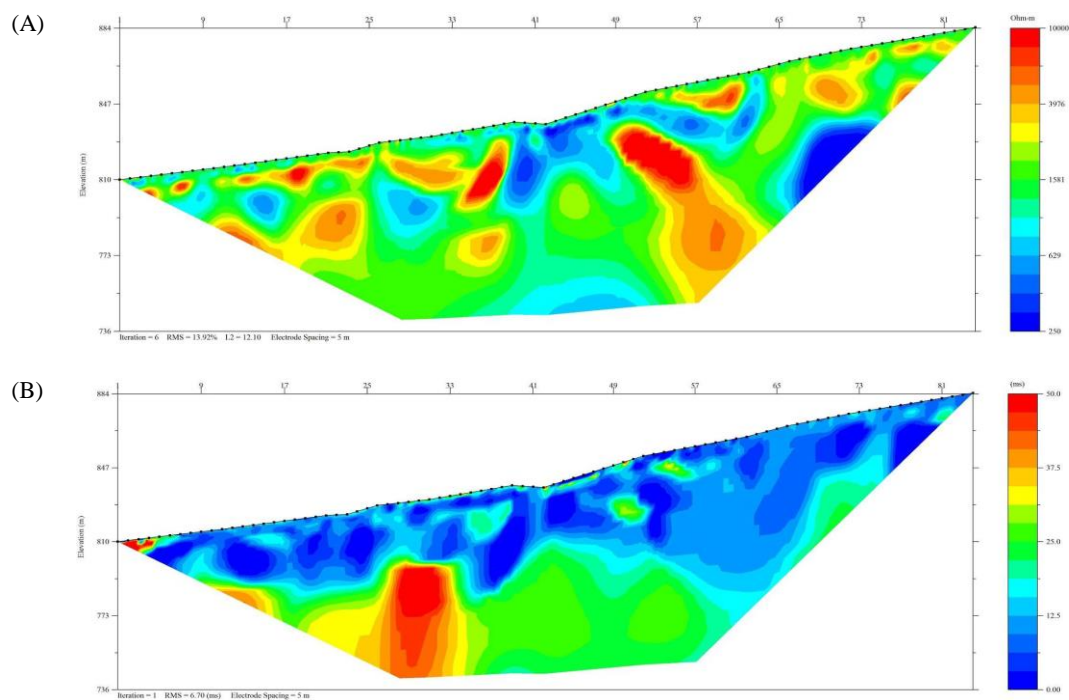


Figure 39: MCKIP17-03 sections. (A) Inverted resistivity (scale 250-10,000 Ohm-m). (B) Inverted IP (scale 0-50 ms).

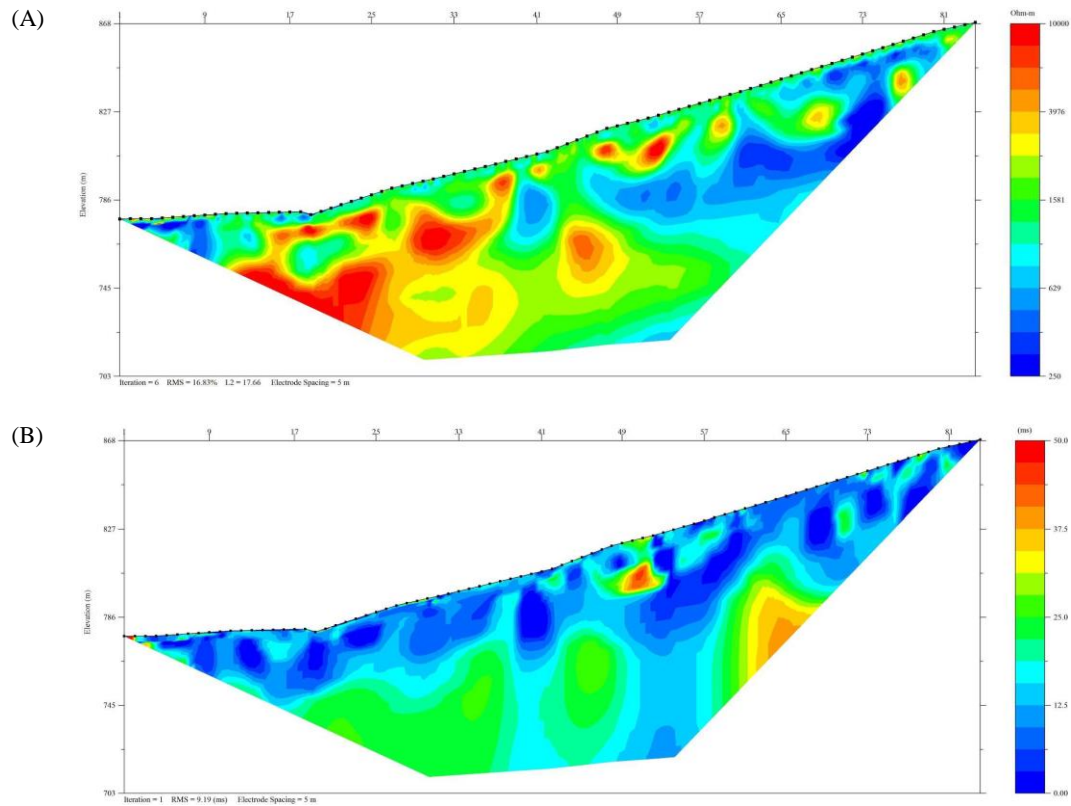


Figure 40: MCKIP17-04 sections. (A) Inverted resistivity (scale 250-10,000 Ohm-m). (B) Inverted IP (scale 0-50 ms).

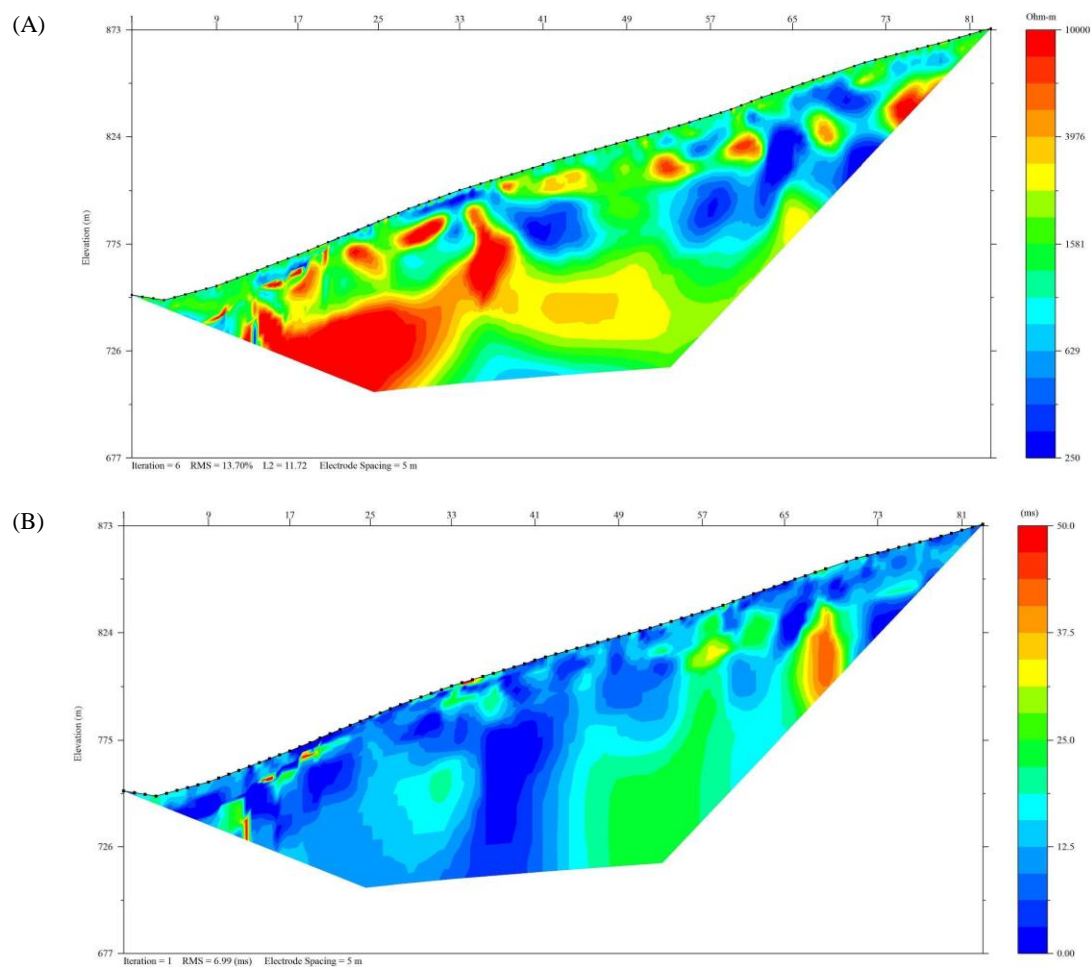


Figure 41: MCKIP17-05 sections. (A) Inverted resistivity (scale 250-10,000 Ohm-m). (B) Inverted IP (scale 0-50 ms).

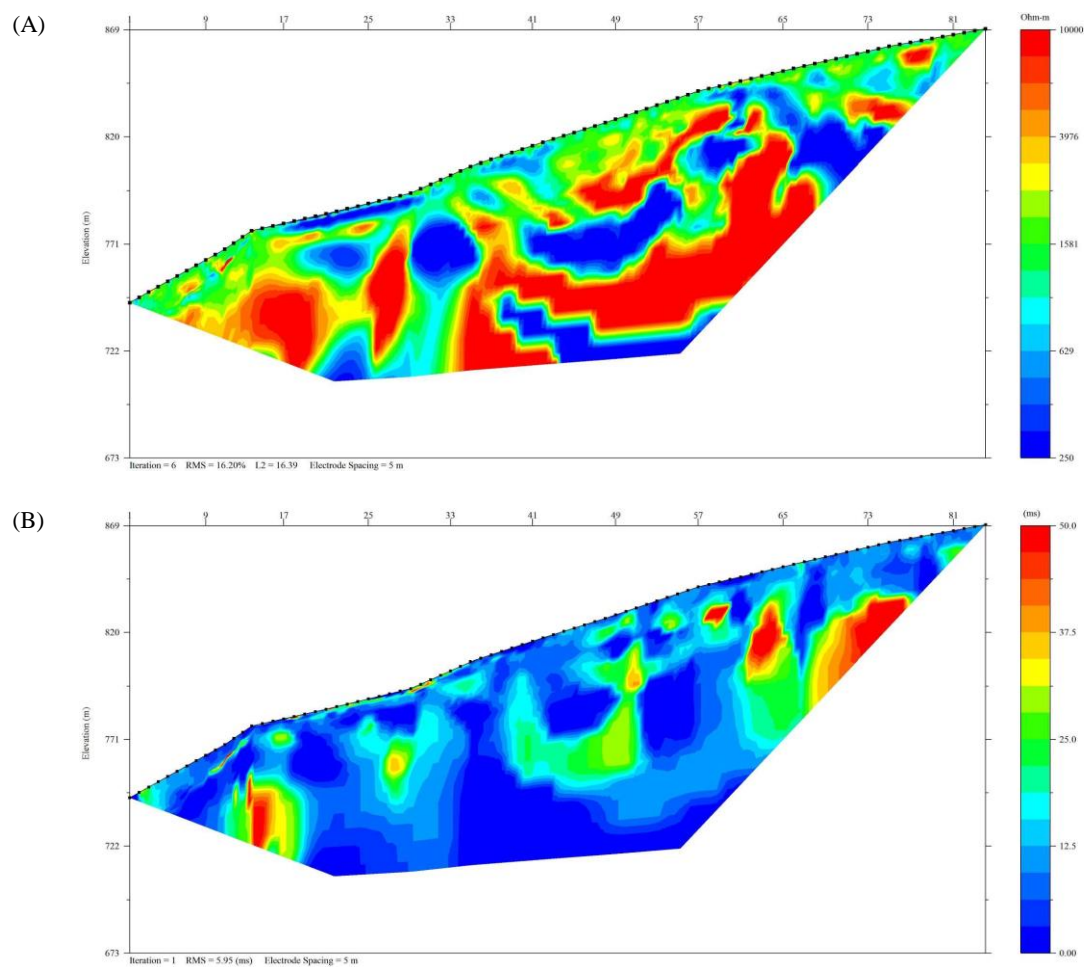


Figure 42: MCKIP17-06 sections. (A) Inverted resistivity (scale 250-10,000 Ohm-m). (B) Inverted IP (scale 0-50 ms).



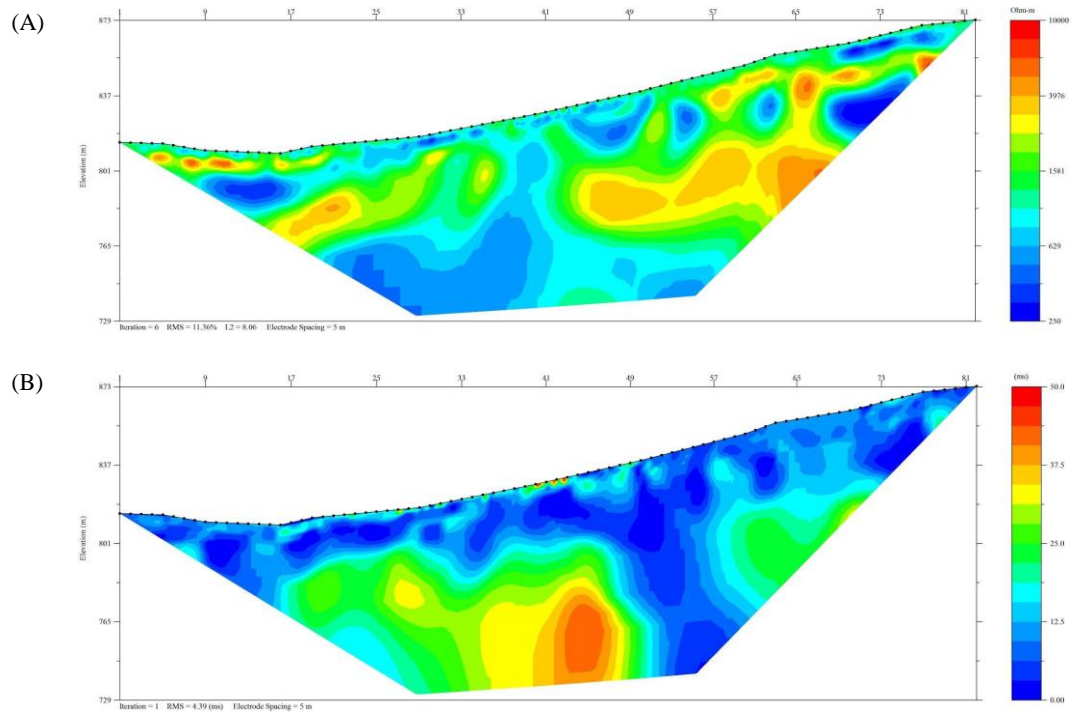


Figure 43: MCKIP17-07 sections. (A) Inverted resistivity (scale 250-10,000 Ohm-m). (B) Inverted IP (scale 0-50 ms).

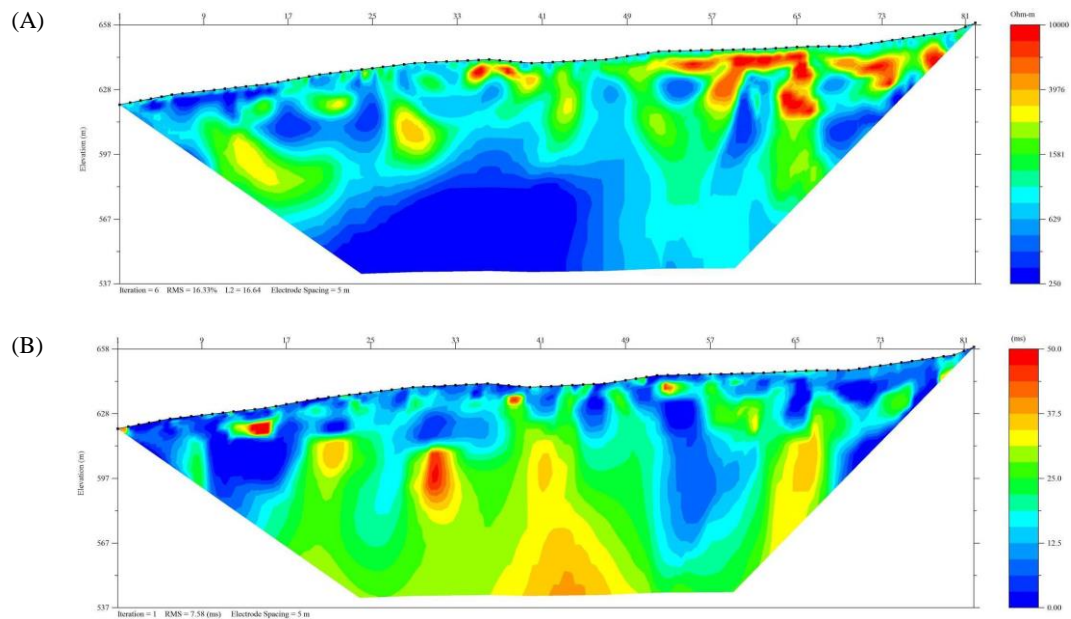


Figure 44: MCKIP17-08 sections. (A) Inverted resistivity (scale 250-10,000 Ohm-m). (B) Inverted IP (scale 0-50 ms).

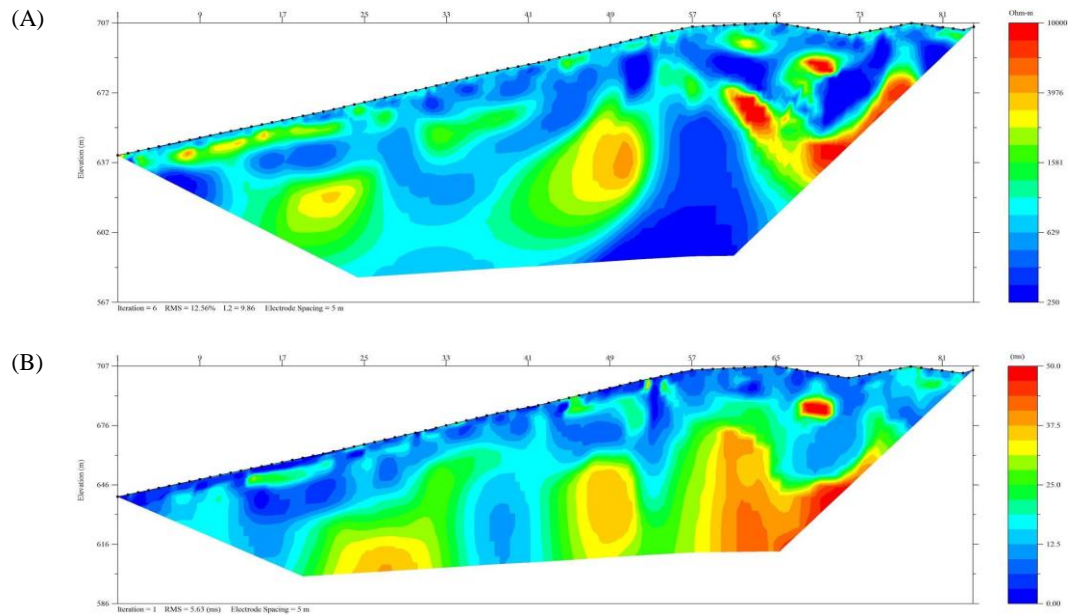
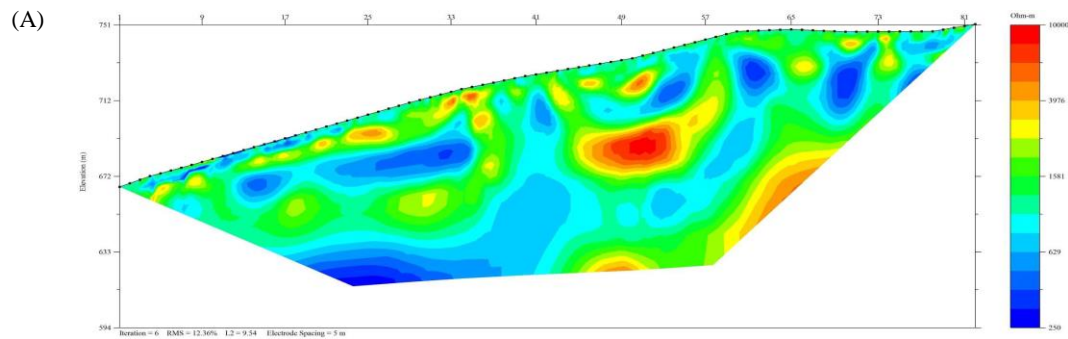


Figure 45: MCKIP17-09 sections. (A) Inverted resistivity (scale 250-10,000 Ohm-m). (B) Inverted IP (scale 0-50 ms).



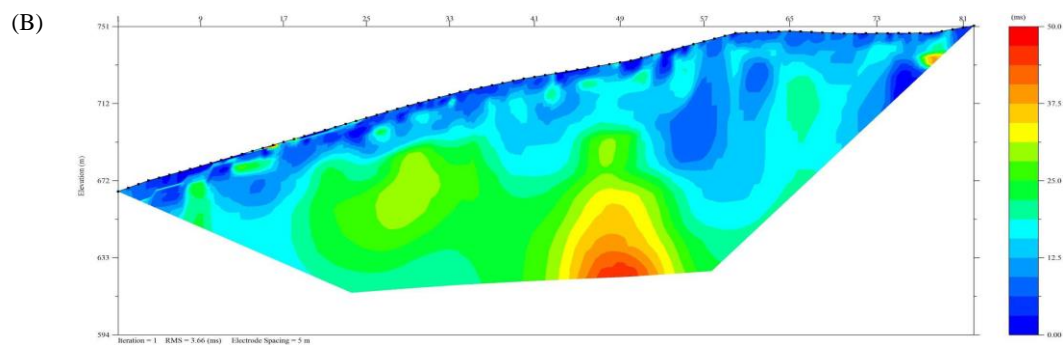
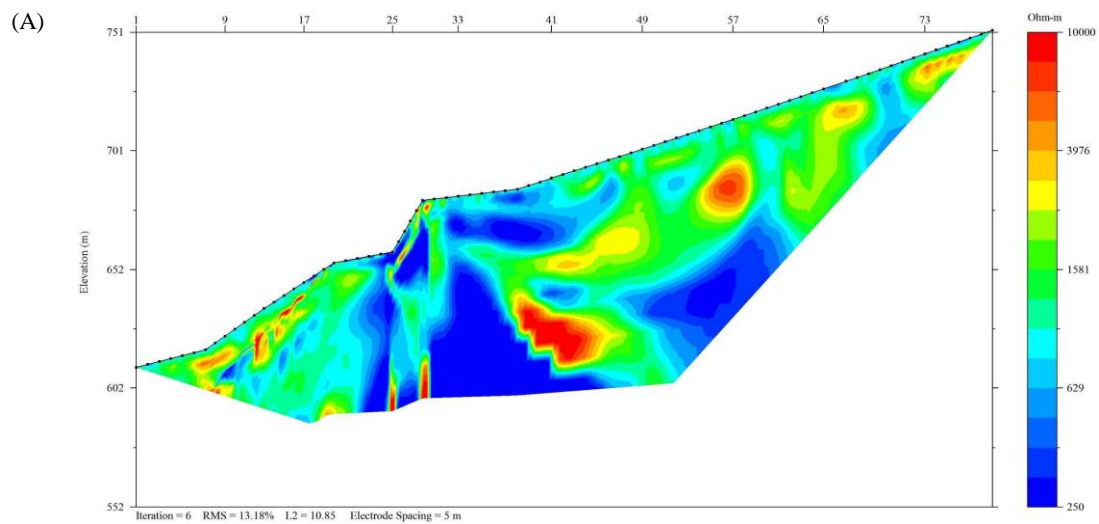


Figure 46: MCKIP17-10 sections. (A) Inverted resistivity (scale 250-10,000 Ohm-m). (B) Inverted IP (scale 0-50 ms).



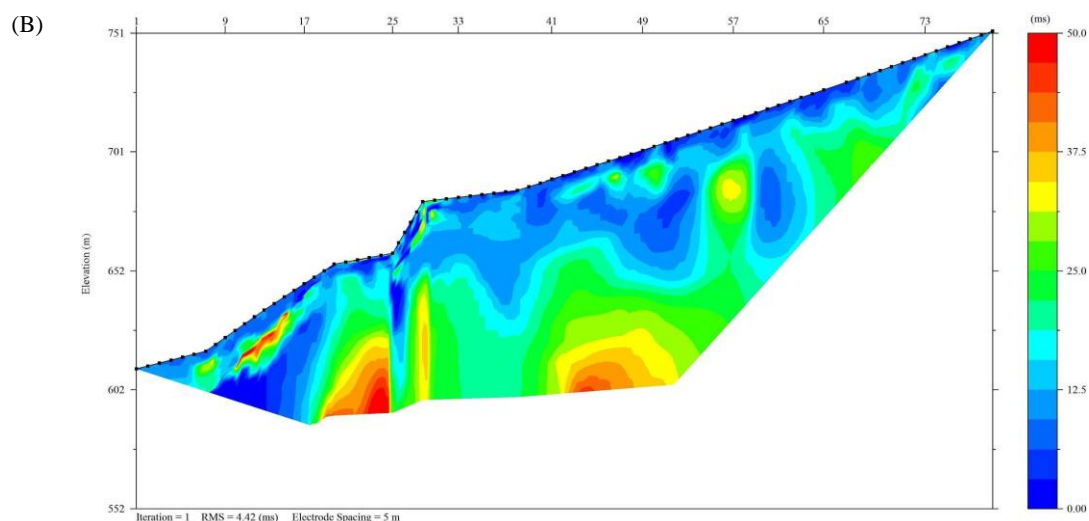


Figure 47: MCKIP17-11 sections. (A) Inverted resistivity (scale 250-10,000 Ohm-m). (B) Inverted IP (scale 0-50 ms).

### 7.3 Interpretation

The 2-D RES/IP surveys acquired in the McKinnon area show good qualitative correlation between anomalous resistivity and chargeability zones. The anomalies are sufficiently massive and smooth to give an indication of structure and mineralization within the grid area. In both grids, the crossline inversions show good correlation with the inline inversions. In the larger grid, it appears that there is a unit of higher chargeability that trends approximately northwest-southeast. In the smaller grid, there is a conductive subsurface unit that corresponds with an area that has higher chargeability. To further constrain this interpretation, it is recommended that known geological and geochemical information is incorporated about the site. This will aid the interpreter to gain a better understanding of these anomalies and potentially aid them to identify geological structures and mineralized zones inherent to gold deposits.

## Appendix A: Description of Files and File Structure

This section explains the file naming structure and data content for each project.

Each RES/IP traverse has a unique Line ID created by combining: (1) the three letter project code for the property or zone, (2) an IP or RES data designation, (3) the last two digits of the year the survey was read, and (4) an identifying number for the traverse within each property or zone.

Example: ALBIP17-01, where ALB is the project code, IP is the type of data collected, 17 represents the year 2017, and 01 means that this is the first RES/IP dataset acquired on this property.

Each array dataset has a unique Data File ID. This ID is comprised by the date (yy-mm-dd), the first letter of the array type used (e.g. D for dipole-dipole or W for Wenner), and the number of times this array has been used that day.



Example: 170813D1

File Structure and Content:

- DATA
  - └ Line ID
    - Figures
      - figures of merged data pseudosections and inversions
    - GPS
      - Contains the DGPS raw data
    - Pictures
      - Pictures along the line
    - RAW
      - IP (data with IP data-misfits removed)
      - RES (data with RES data-misfits removed)
      - unprocessed data from SuperSting unit
    - XYZ
      - Inverted data for RES and IP saved in XYZ format

## Appendix B: SuperSting R1/IP technical specification

Measurement modes	Apparent resistivity, resistance, self potential (SP), induced polarization (IP), battery voltage
Measurement range	+/- 10V
Measuring resolution	Max 30 nV, depends on voltage level
Screen resolution	4 digits in engineering notation
Output current	1mA – 2 A continuous, measured to high accuracy
Output voltage	800 Vp-p, actual electrode voltage depends on transmitted current and ground resistivity
Output power	200 W
Input gain ranging	Automatic, always uses full dynamic range of receiver
Input impedance	>20 M $\Omega$
SP compensation	Automatic cancellation of SP voltages during resistivity measurement. Constant and linearly varying SP cancels completely.
Type of IP measurement	Time domain chargeability (M), six time slots measured and stored in memory
IP current transmission	ON+, OFF, ON-, OFF
IP time cycles	0.5, 1 , 2 , 4 and 8 seconds (combined resistivity/IP mode)
Measure cycles	Running average of measurement displayed after each cycle. Automatic cycle stop when reading errors fall below user set limit or user set max cycles are done.
Resistivity time cycles	Basic measure time is 0.4, 0.8, 1.2, 3.6, 7.2 or 14.4 seconds as selected by user via keyboard, autoranging and commutation adds about 1.4 s.
Signal processing	Continuous averaging after each complete cycle. Noise errors calculated and displayed as percentage of reading. Reading displayed as resistance ( $\Delta V/I$ ) and apparent resistivity ( $\Omega m$ ). Resistivity is calculated using user entered electrode array coordinates.
Noise suppression	Better than 100 dB at $f > 20$ Hz Better than 120 dB at power line frequencies (16 2/3, 20, 50 and 60 Hz) for measure cycles of 1.2 s and above
Total accuracy	Better than 1% of reading in most cases (lab measurements). Field measurement accuracy depends on ground noise and resistivity. Instrument will calculate and display running estimate of measuring accuracy.
System calibration	Calibration is done digitally by the microprocessor based on correction values stored in memory.
Supported manual	Resistance, Schlumberger, Wenner, dipole-dipole, pole-dipole, pole-pole, SP-absolute, SP-gradient
Operating system	Stored in re-programmable flash memory. New version can be downloaded from our web site and stored in the flash memory.

Data storage	Full resolution reading average and error are stored along with user entered coordinates and time of day for each measurement. Storage is effected automatically in a job oriented file system
Data display	Apparent resistivity (Ohmmeter), injected current (mAmp) and measured voltage (mVolt) are displayed and stored in memory for each measurement
Memory capacity	The memory can store 24,468 measurements in Resistivity Mode and 14,966 measurements in combined Resistivity/IP Mode
Data transmission	RS-232C channel available to dump data from the instrument to a Windows type computer on user command.
Automatic multi-electrodes	The SuperSting is designed to run dipole-dipole, pole-dipole, pole-pole, Wenner and Schlumberger surveys including roll-along surveys completely automatic with the Swift Dual Mode Automatic Multi-electrode system (patent 6,404,203) or with switch box and passive cables. The SuperSting can run any other array by using user programmed command files. These files are ASCII files and can be created using a regular text editor. The command files are downloaded to the SuperSting RAM memory and can at any time be recalled and run. Therefore there is no need for a fragile computer in the field.
Manual measurements	The instrument has four banana pole screws for connecting current and potential electrodes during manual measurments
User controls	20 key tactile, weather proof keyboard with alpha numeric entry keys and function keys. On/off switch. Measure button. LCD night light switch (push to light).
Display	Graphics LCD display (16 lines x 30 characters) with night light.
Power supply, field	12V or 2x12 V DC external power (one or two 12 V batteries), connector on front panel.
Power supply, office	DC power supply
Operating time	Depends on survey conditions and size of battery used. Internal circuitry in auto mode adjusts current to save energy
Operating temperature	-5 to +50°C
Weight	10.9 kg (24 lb.)
Dimensions	Width 184 mm (7.25"), length 406 mm (16") and height 273 mm (10.75")

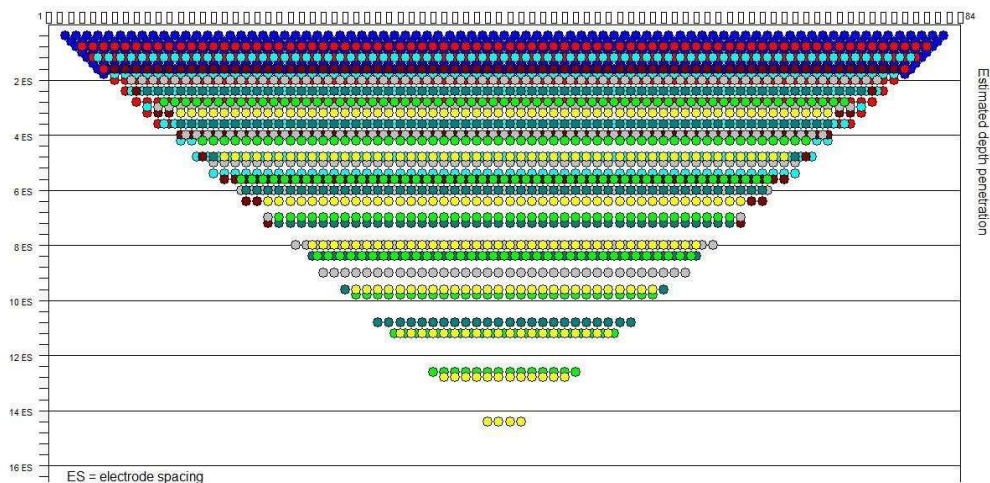
## Appendix C: Extended Dipole-Dipole Array

The extended dipole-dipole array provides extended data coverage of the standard dipole-dipole array. The electrode configuration for dipole-dipole is shown below, where the current electrodes (A and B) and potential electrodes (M and N) are equivalently spaced by “a”, and separated by a factor “n” times the spacing “a”. A measurement of apparent resistivity can be calculated using the equation below the figure, where V = potential difference (V), I = current (Amp), and  $\rho_A$  = apparent resistivity (Ohm-m).

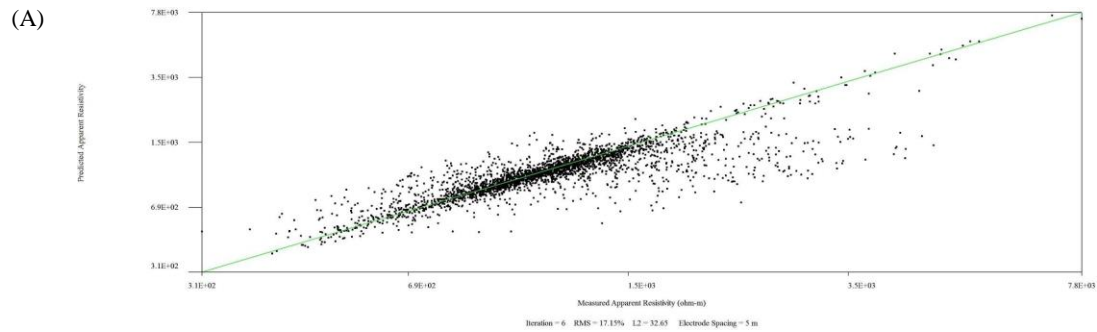


$$\rho_A = \frac{V}{I} \pi a n(n+1)(n+2).$$

Penetration depth of the extended dipole-dipole array (measurement locations shown below) is approximately 14 times the electrode spacing, which is equivalent to 70m using 5m electrode spacing, but is also dependent on: (1) the actual distribution of subsurface resistivity, and (2) the best achievable contact resistance values between the electrodes and the ground. The figure below shows the measurement locations (in pseudo depth) for an extended dipole-dipole array using 84 surface electrodes.



## Appendix D: Data Misfit Crossplots



(B)

Figure D-1: WHTIP17-01 data misfit crossplots. (A) Measured vs. predicted apparent resistivity (Ohm-m). (B) Measured vs. predicted chargeability (ms).



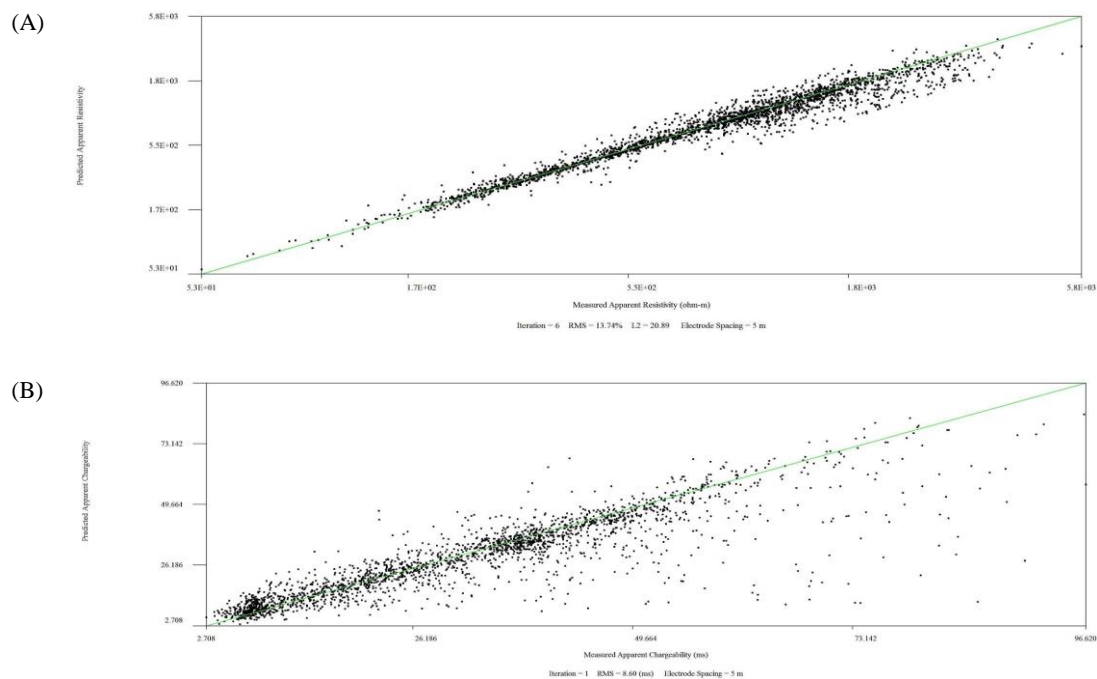


Figure D-2: WHTIP17-02 data misfit crossplots. (A) Measured vs. predicted apparent resistivity (Ohm-m). (B) Measured vs. predicted chargeability (ms).

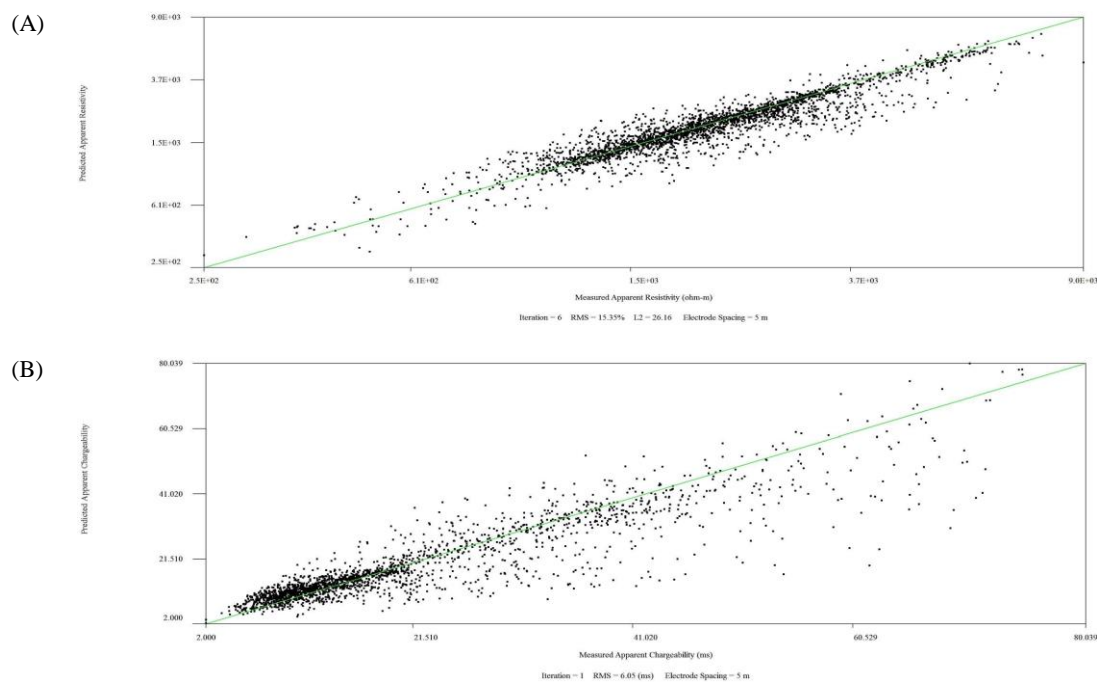


Figure D-3: WHTIP17-03 data misfit crossplots. (A) Measured vs. predicted apparent resistivity (Ohm-m). (B) Measured vs. predicted chargeability (ms).

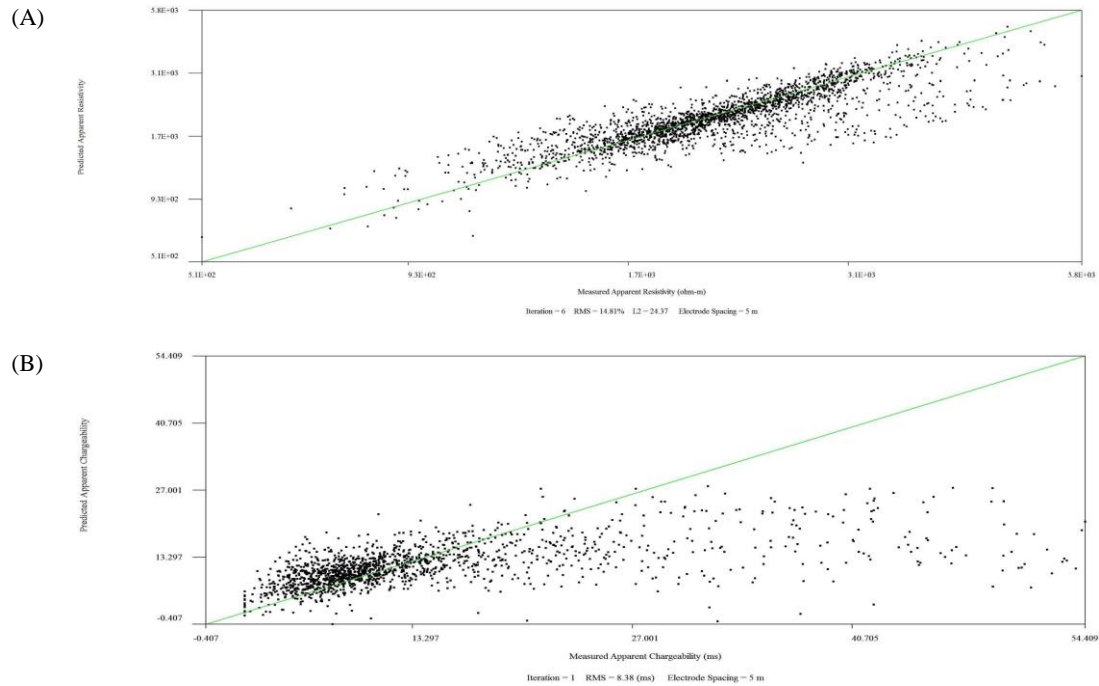
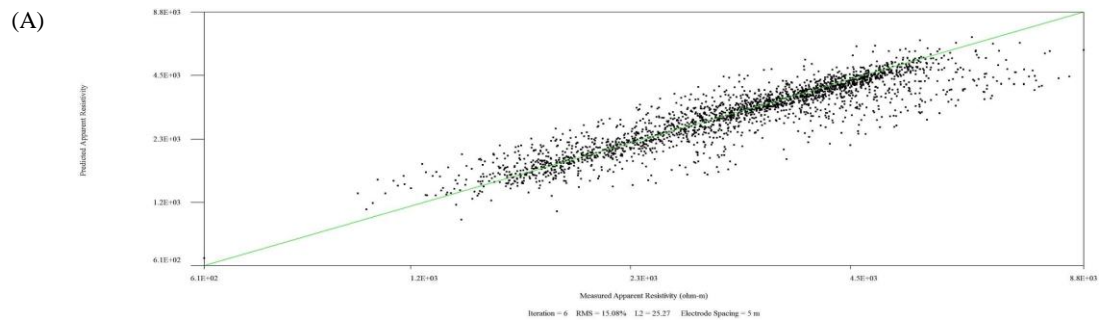


Figure D-4: WHTIP17-04 data misfit crossplots. (A) Measured vs. predicted apparent resistivity (Ohm-m). (B) Measured vs. predicted chargeability (ms).



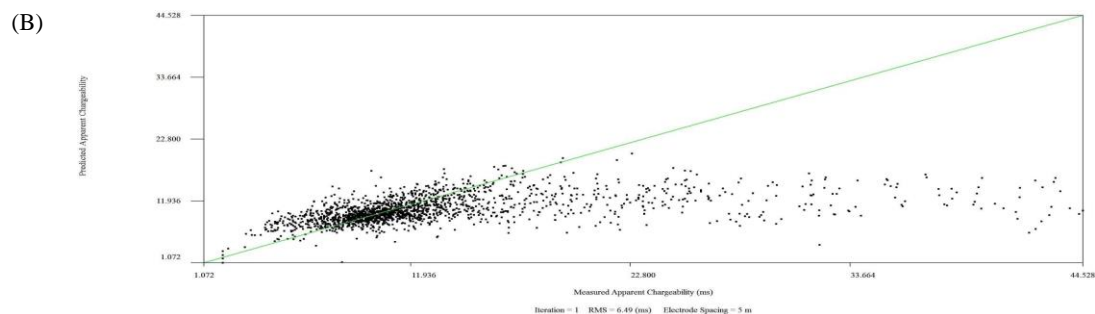


Figure D-5: WHTIP17-05 data misfit crossplots. (A) Measured vs. predicted apparent resistivity (Ohm-m). (B) Measured vs. predicted chargeability (ms).

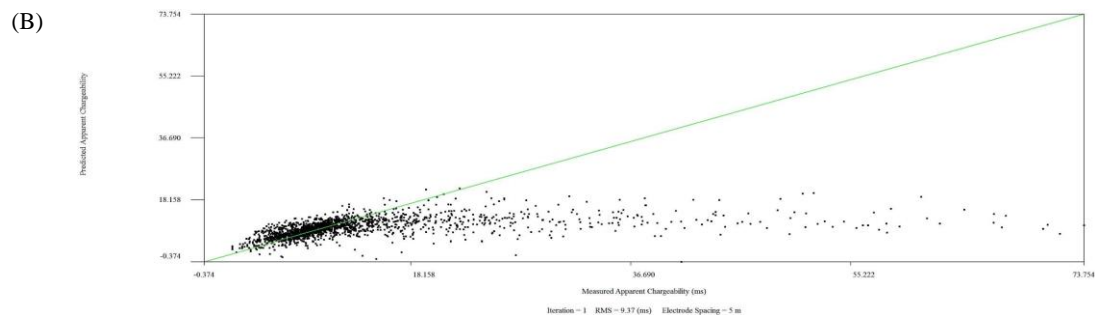
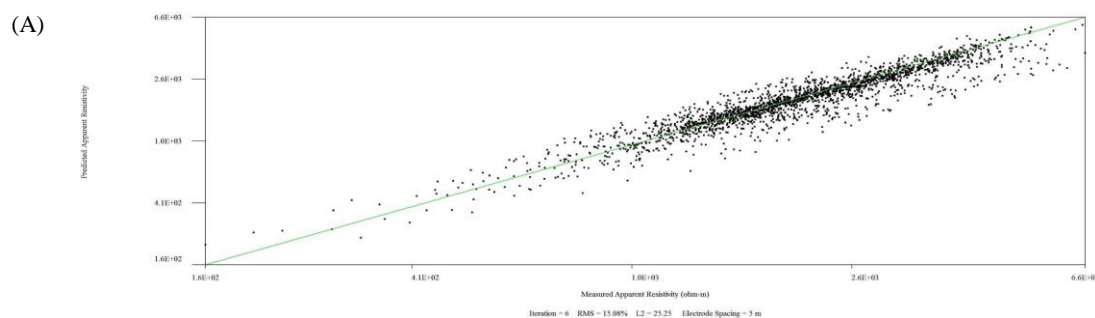


Figure D-6: WHTIP17-06 data misfit crossplots. (A) Measured vs. predicted apparent resistivity (Ohm-m). (B) Measured vs. predicted chargeability (ms).

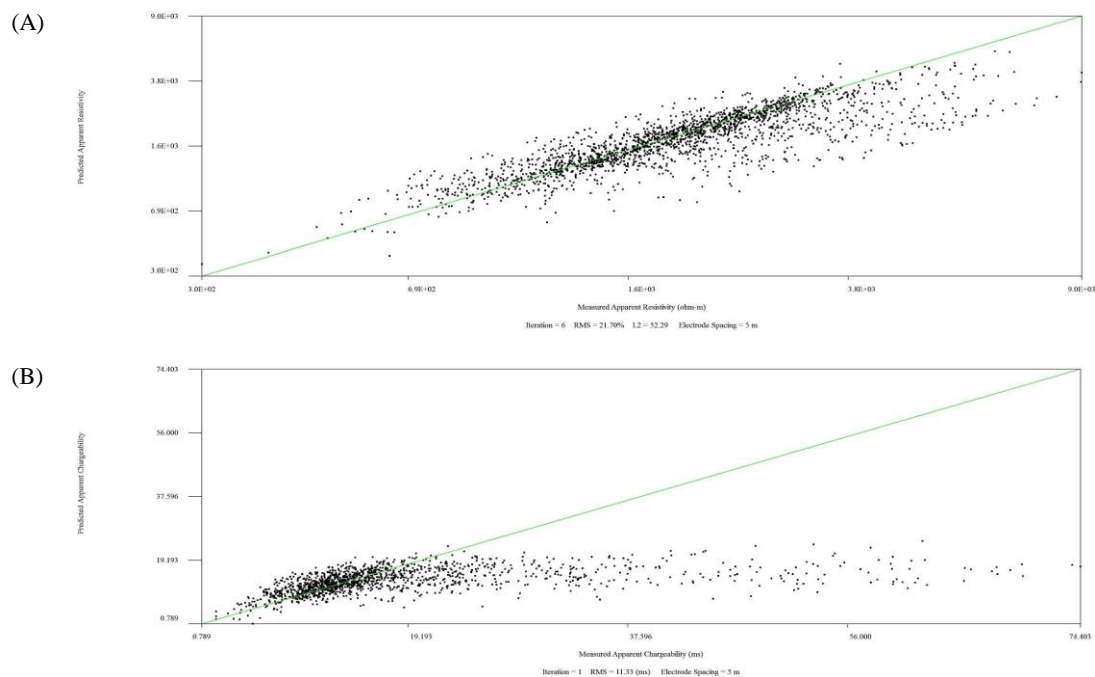


Figure D-7: WHTIP17-07 data misfit crossplots. (A) Measured vs. predicted apparent resistivity (Ohm-m). (B) Measured vs. predicted chargeability (ms).

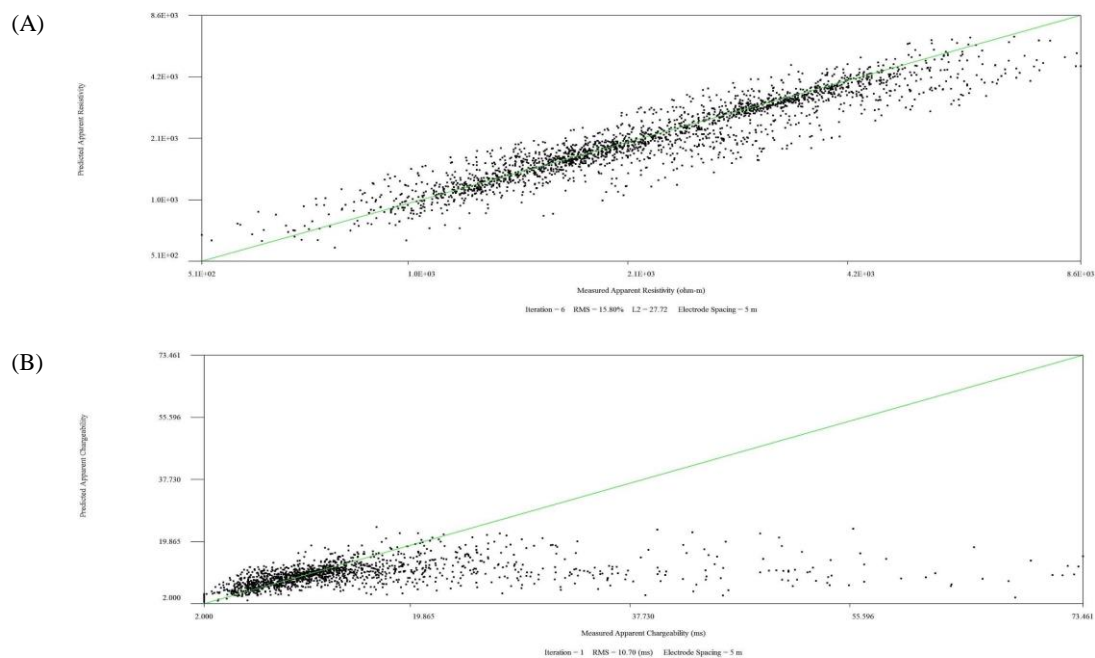


Figure D-8: WHTIP17-08 data misfit crossplots. (A) Measured vs. predicted apparent resistivity (Ohm-m). (B) Measured vs. predicted chargeability (ms).

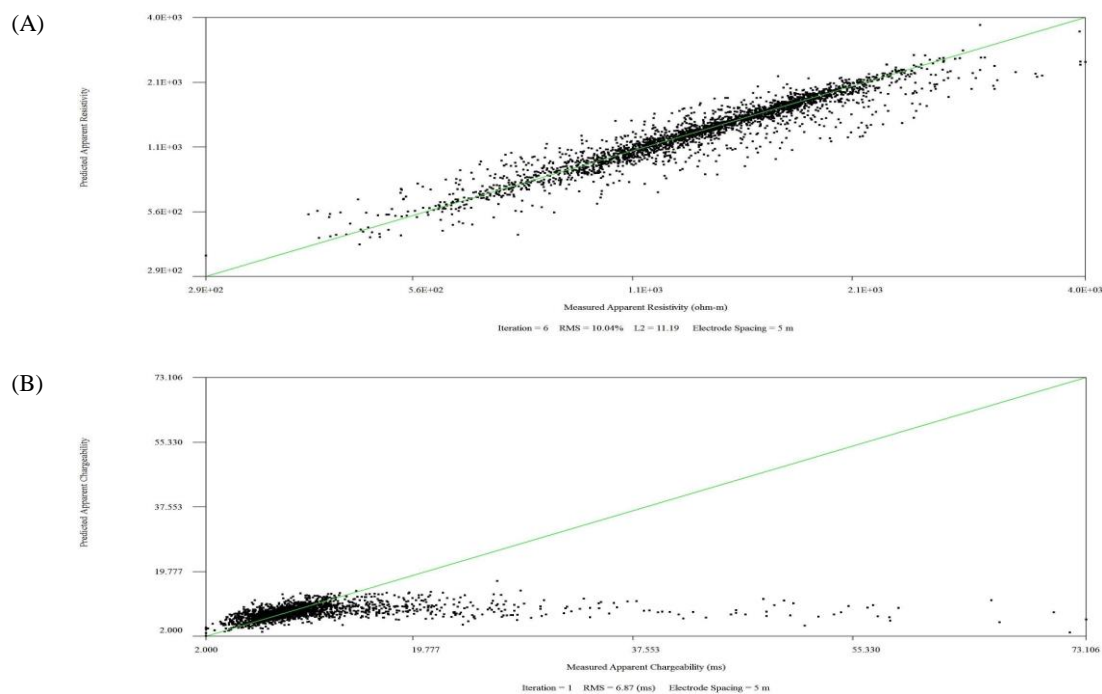


Figure D-9: WHTIP17-09 data misfit crossplots. (A) Measured vs. predicted apparent resistivity (Ohm-m). (B) Measured vs. predicted chargeability (ms).

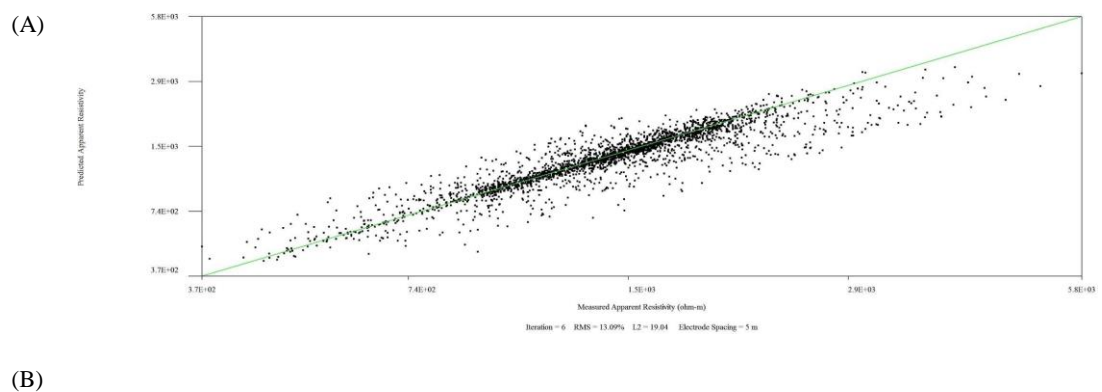
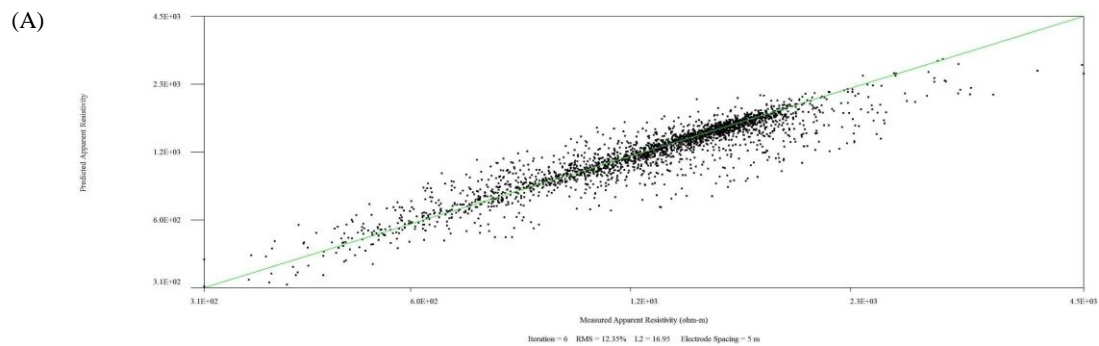
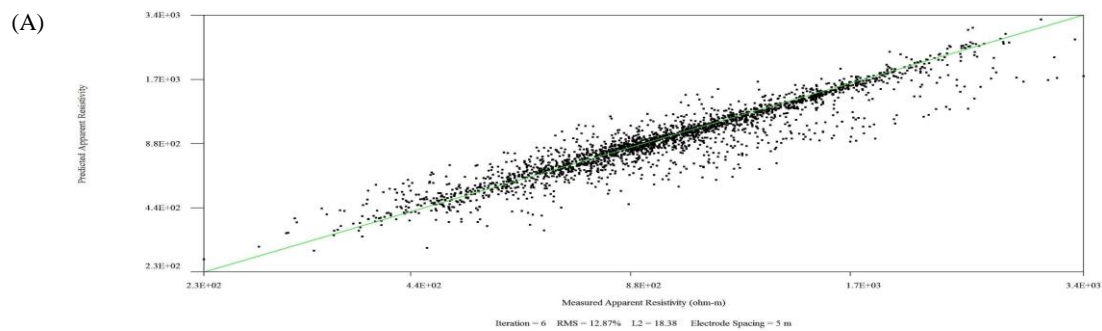


Figure D-10: WHTIP17-10 data misfit crossplots. (A) Measured vs. predicted apparent resistivity (Ohm-m). (B) Measured vs. predicted chargeability (ms).



(B)

Figure D-11: WHTIP17-11 data misfit crossplots. (A) Measured vs. predicted apparent resistivity (Ohm-m). (B) Measured vs. predicted chargeability (ms).





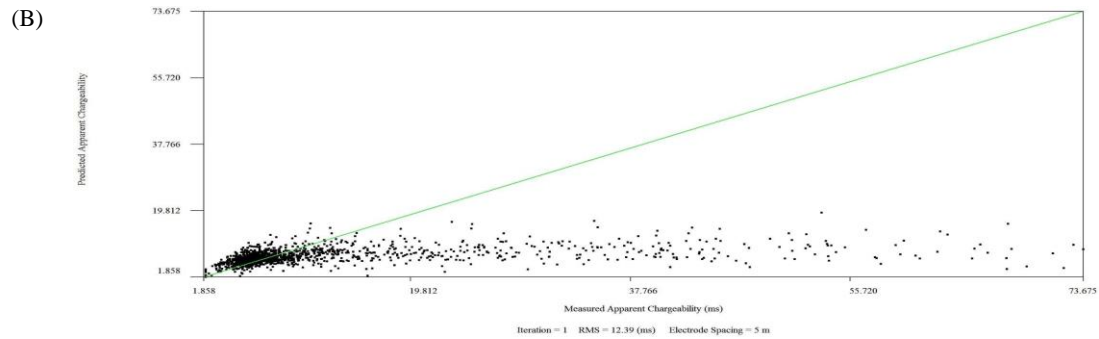


Figure D-12: WHTIP17-12 data misfit crossplots. (A) Measured vs. predicted apparent resistivity (Ohm-m). (B) Measured vs. predicted chargeability (ms).

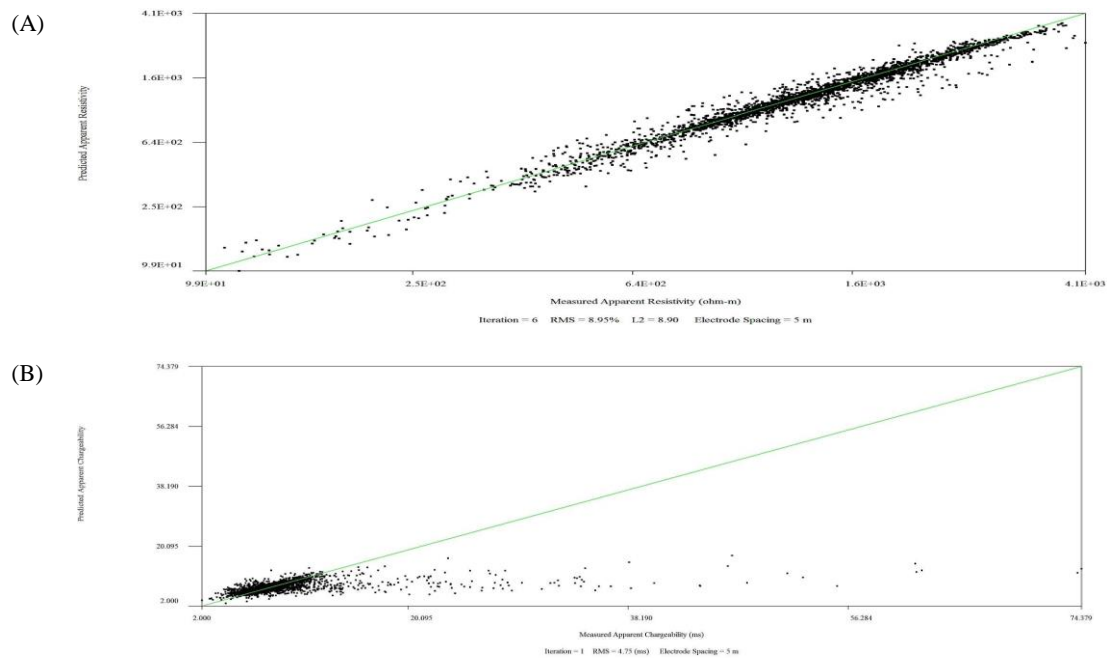


Figure D-13: WHTIP17-13 data misfit crossplots. (A) Measured vs. predicted apparent resistivity (Ohm-m). (B) Measured vs. predicted chargeability (ms).

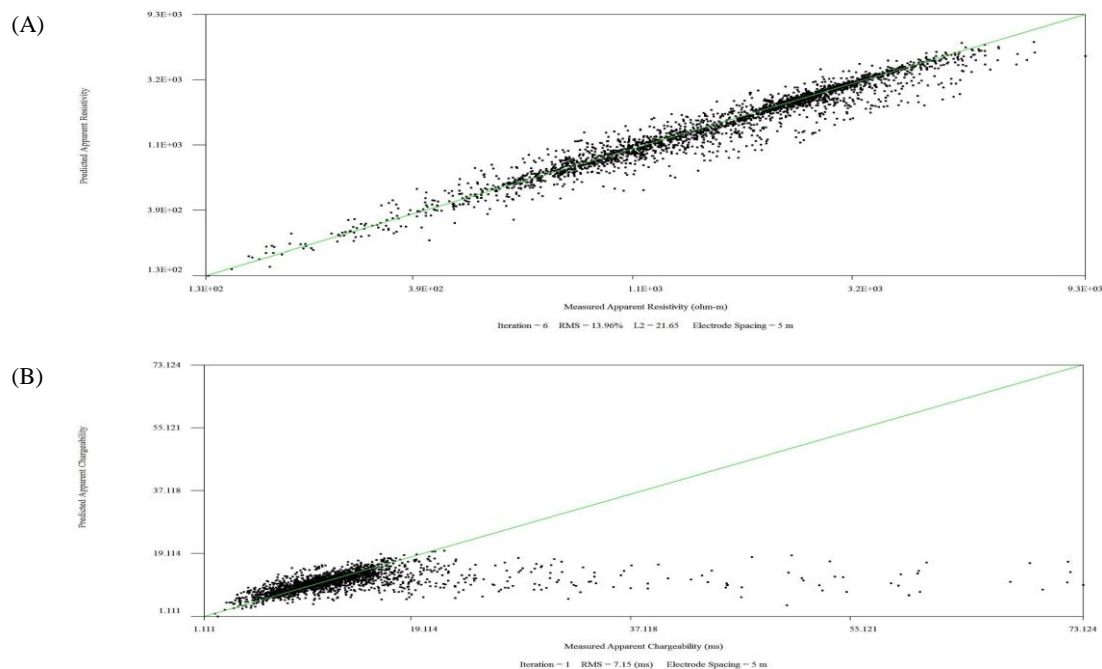


Figure D-14: WHTIP17-14 data misfit crossplots. (A) Measured vs. predicted apparent resistivity (Ohm-m). (B) Measured vs. predicted chargeability (ms).

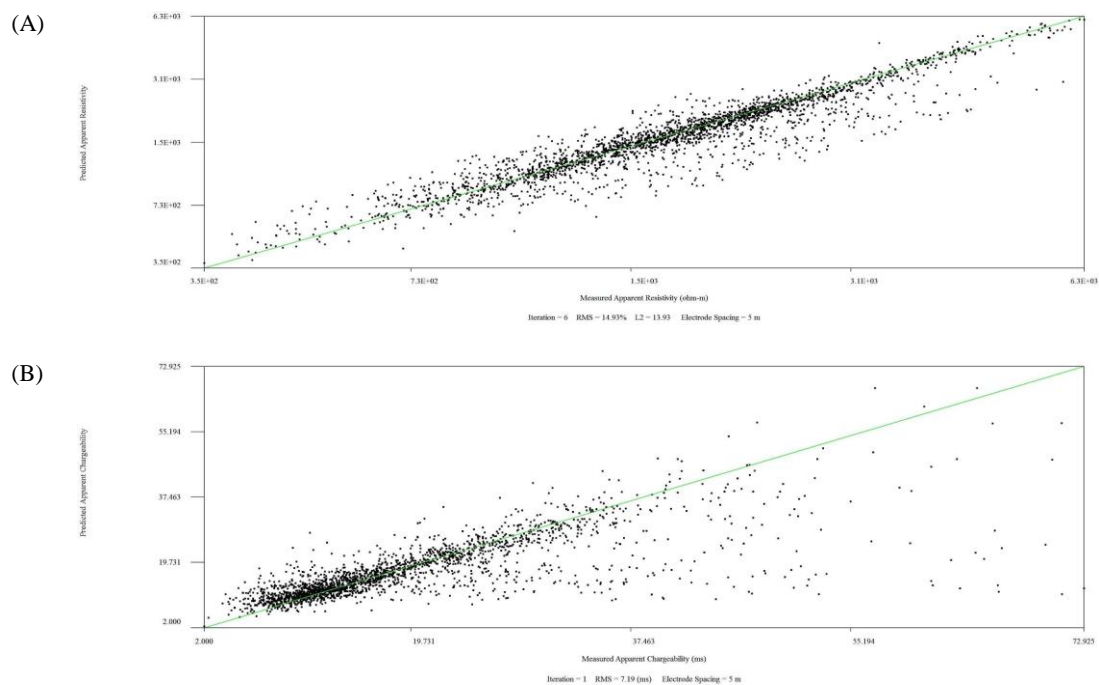


Figure D-15: ARCIP17-01 data misfit crossplots. (A) Measured vs. predicted apparent resistivity (Ohm-m). (B) Measured vs. predicted chargeability (ms).

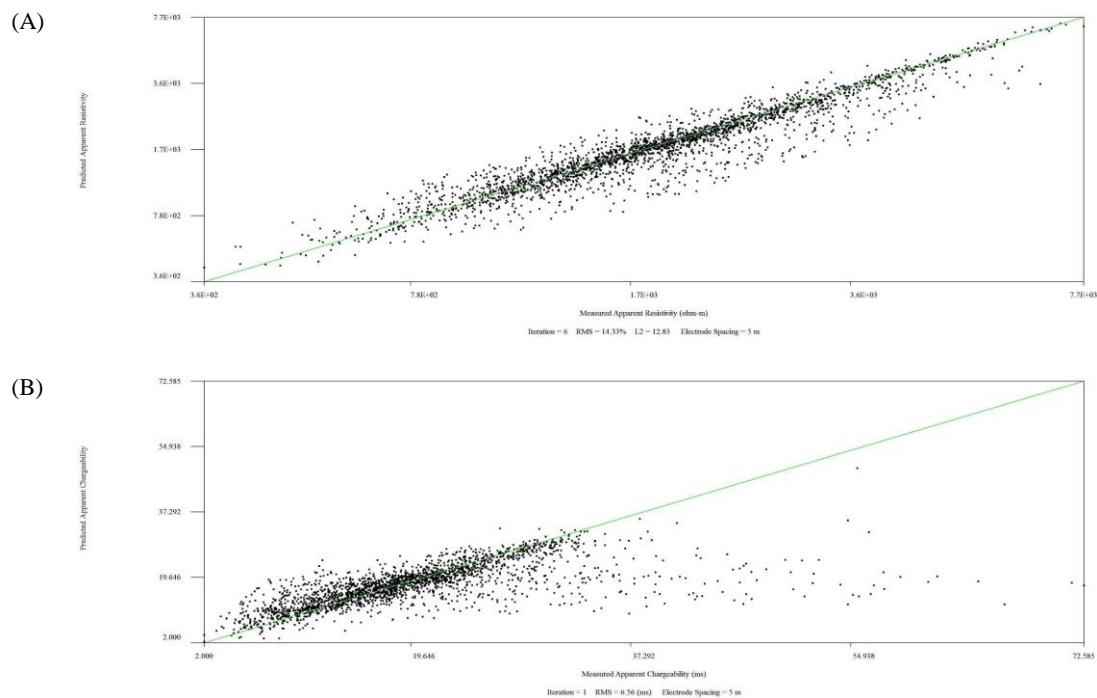
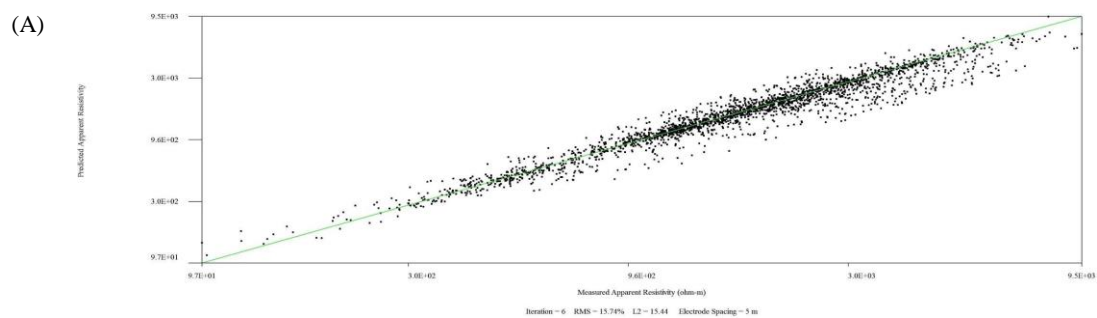


Figure D-16: ARCIP17-02 data misfit crossplots. (A) Measured vs. predicted apparent resistivity (Ohm-m). (B) Measured vs. predicted chargeability (ms).



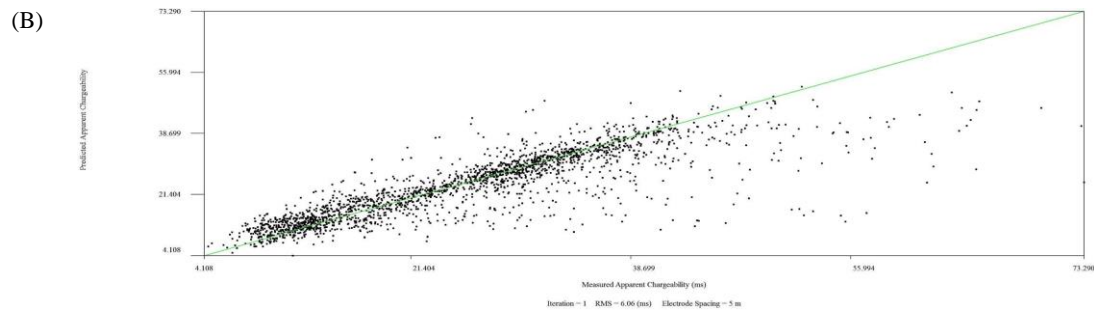


Figure D-17: ARCIP17-03 data misfit crossplots. (A) Measured vs. predicted apparent resistivity (Ohm-m). (B) Measured vs. predicted chargeability (ms).

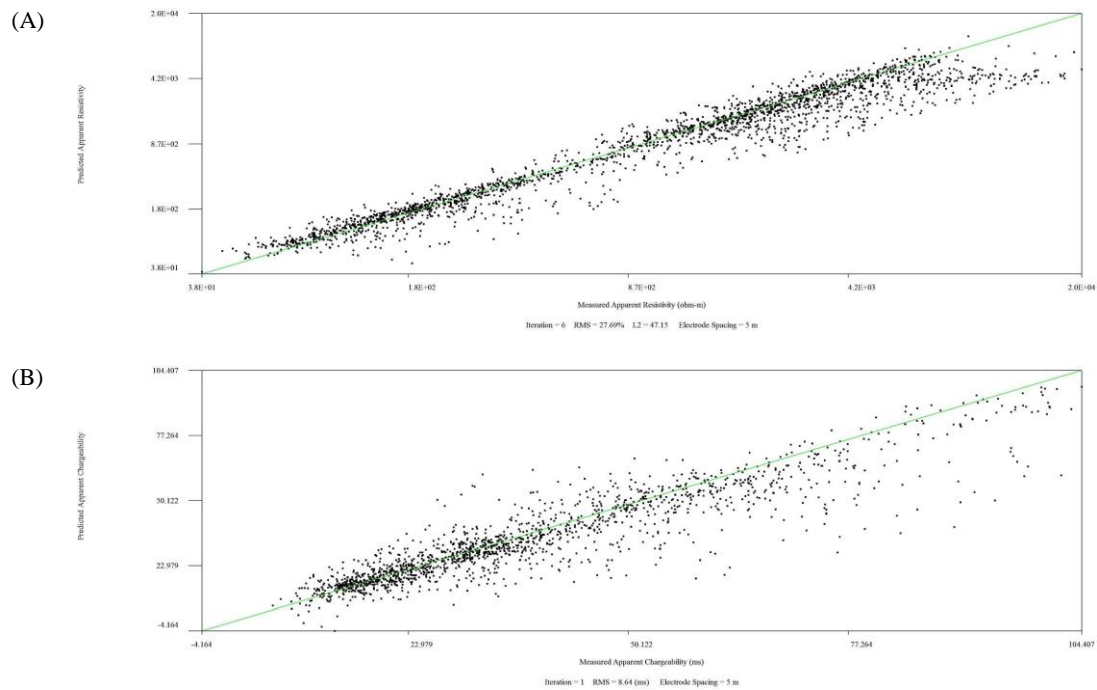
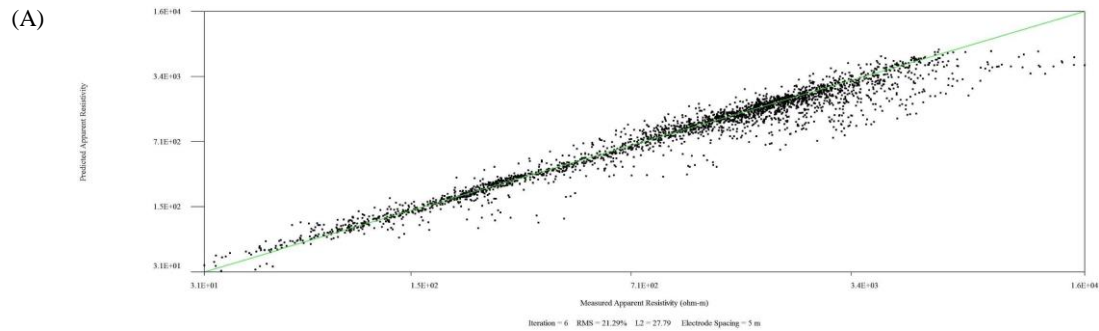
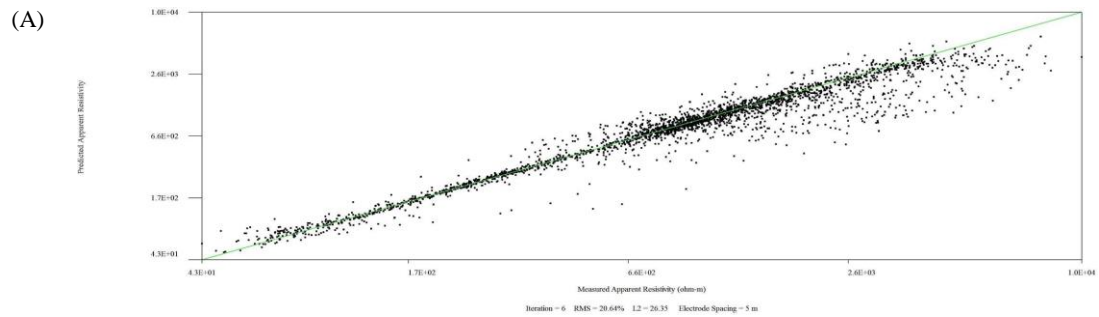


Figure D-18: ARCIP17-04 data misfit crossplots. (A) Measured vs. predicted apparent resistivity (Ohm-m). (B) Measured vs. predicted chargeability (ms).



(B)

Figure D-19: ARCIP17-05 data misfit crossplots. (A) Measured vs. predicted apparent resistivity (Ohm-m). (B) Measured vs. predicted chargeability (ms).



(B)

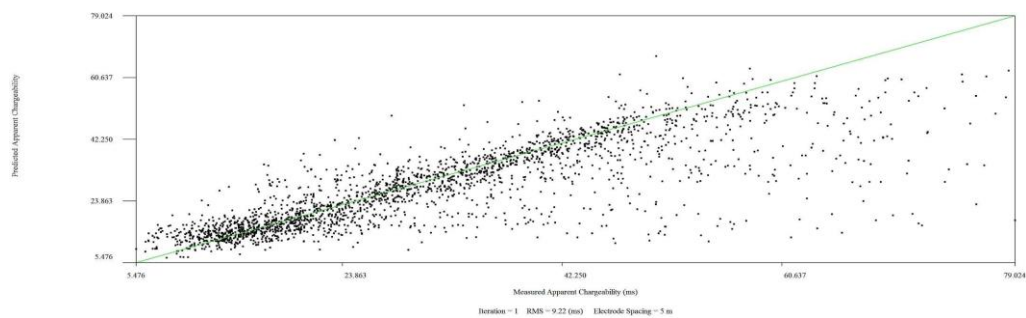


Figure D-20: ARCIP17-06 data misfit crossplots. (A) Measured vs. predicted apparent resistivity (Ohm-m). (B) Measured vs. predicted chargeability (ms).

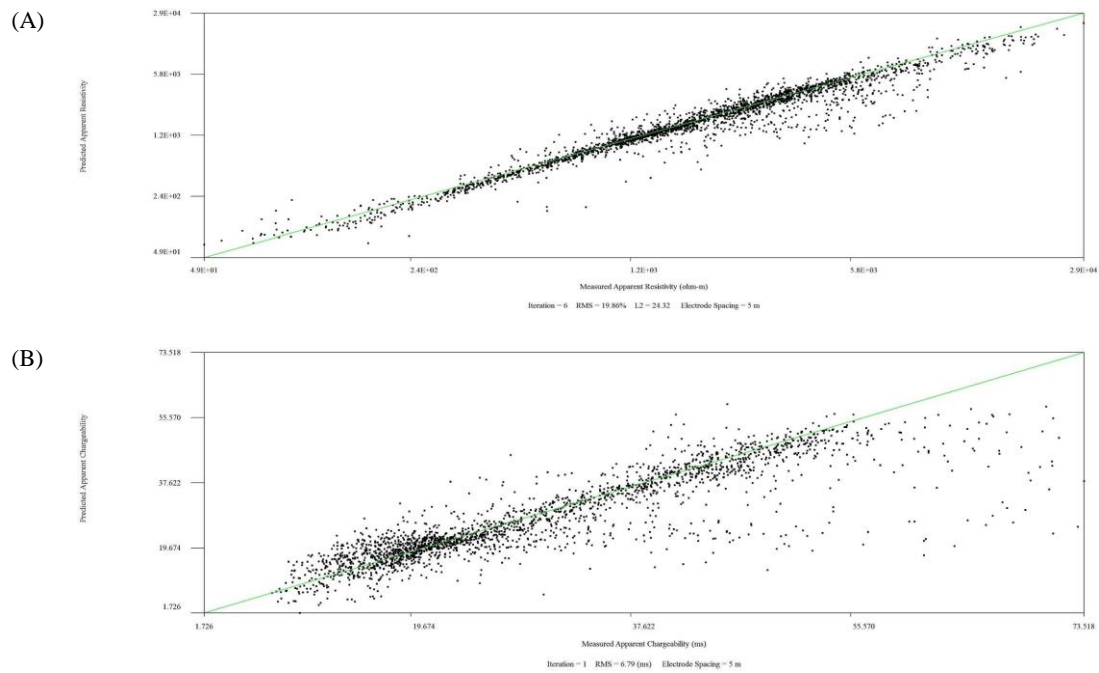


Figure D-21: ARCIP17-07 data misfit crossplots. (A) Measured vs. predicted apparent resistivity (Ohm-m). (B) Measured vs. predicted chargeability (ms).

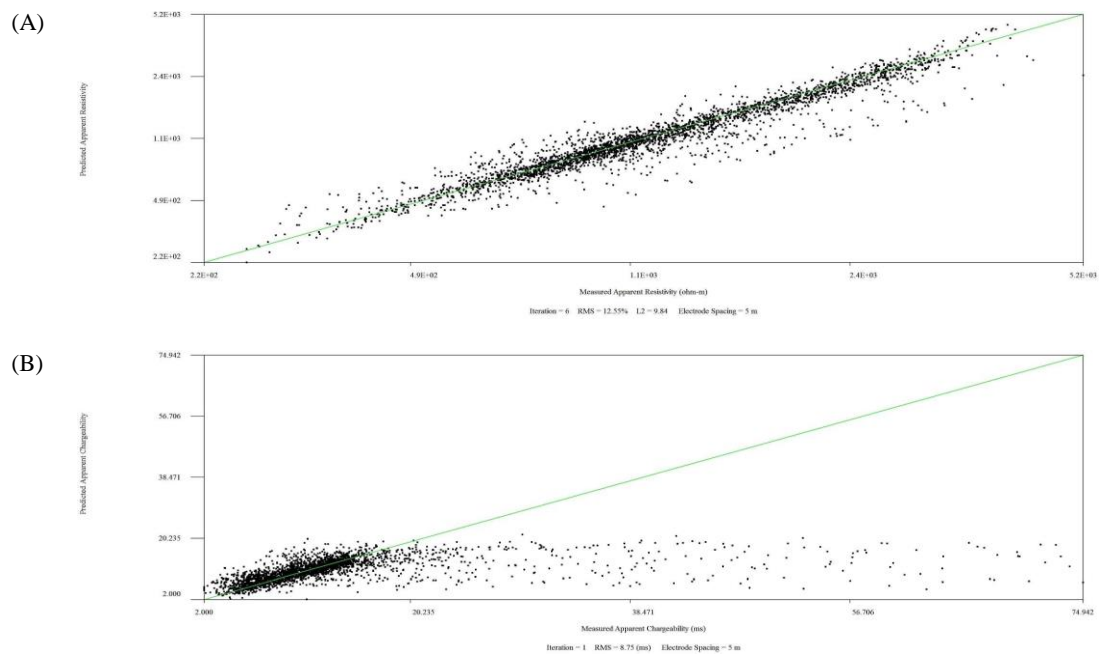




Figure D-22: ULRIP17-01 data misfit crossplots. (A) Measured vs. predicted apparent resistivity (Ohm-m). (B) Measured vs. predicted chargeability (ms).

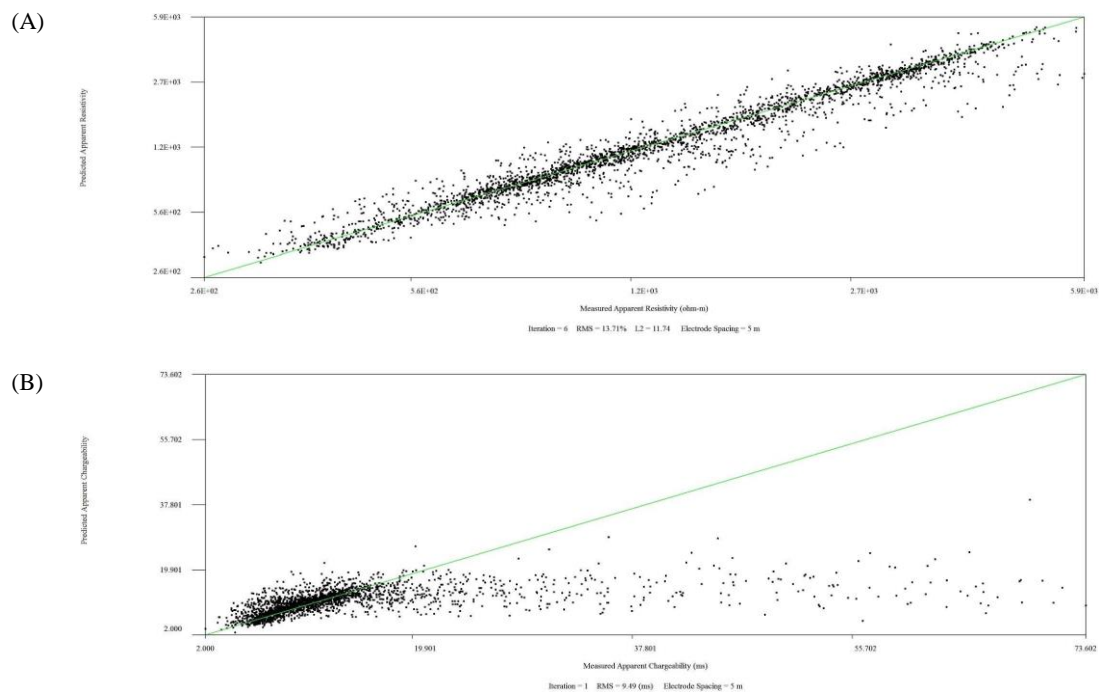
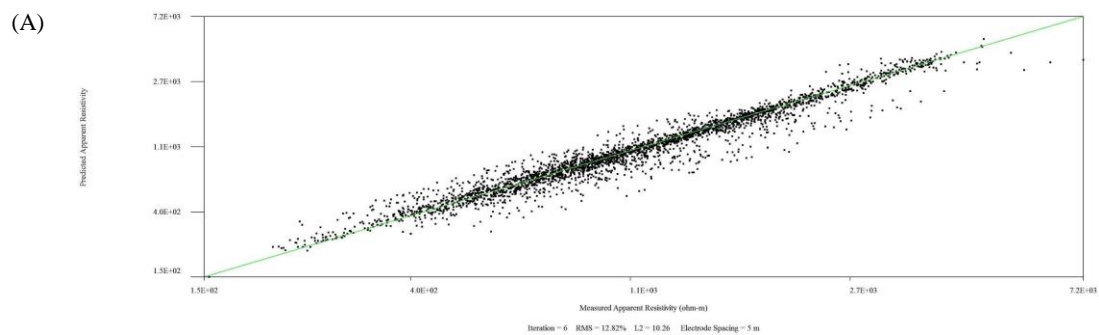


Figure D-23: ULRIP17-02 data misfit crossplot. (A) Measured vs. predicted apparent resistivity (Ohm-m). (B) Measured vs. predicted chargeability (ms).



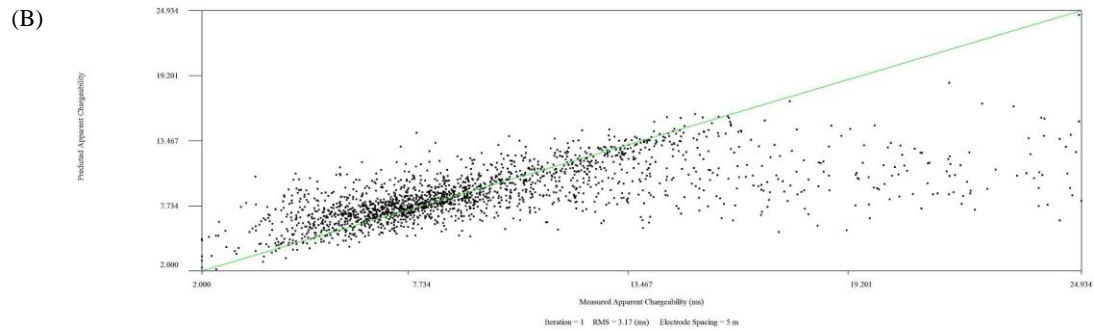


Figure D-24: ULRIP17-03 data misfit crossplot. (A) Measured vs. predicted apparent resistivity (Ohm-m). (B) Measured vs. predicted chargeability (ms).

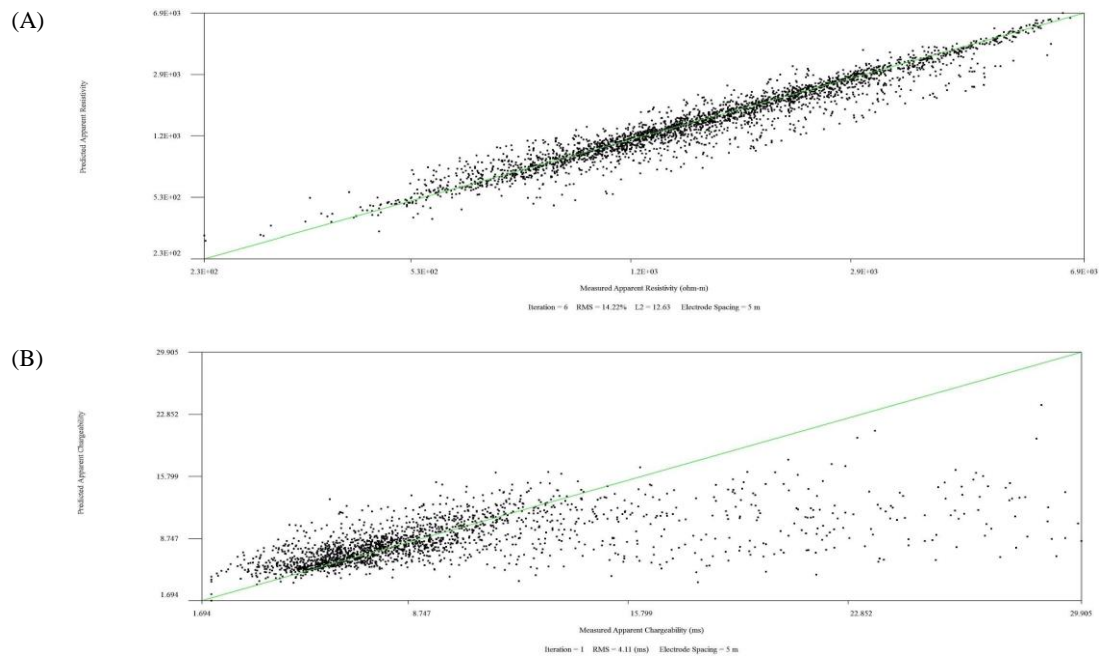


Figure D-25: ULRIP17-04 data misfit crossplots. (A) Measured vs. predicted apparent resistivity (Ohm-m). (B) Measured vs. predicted chargeability (ms).

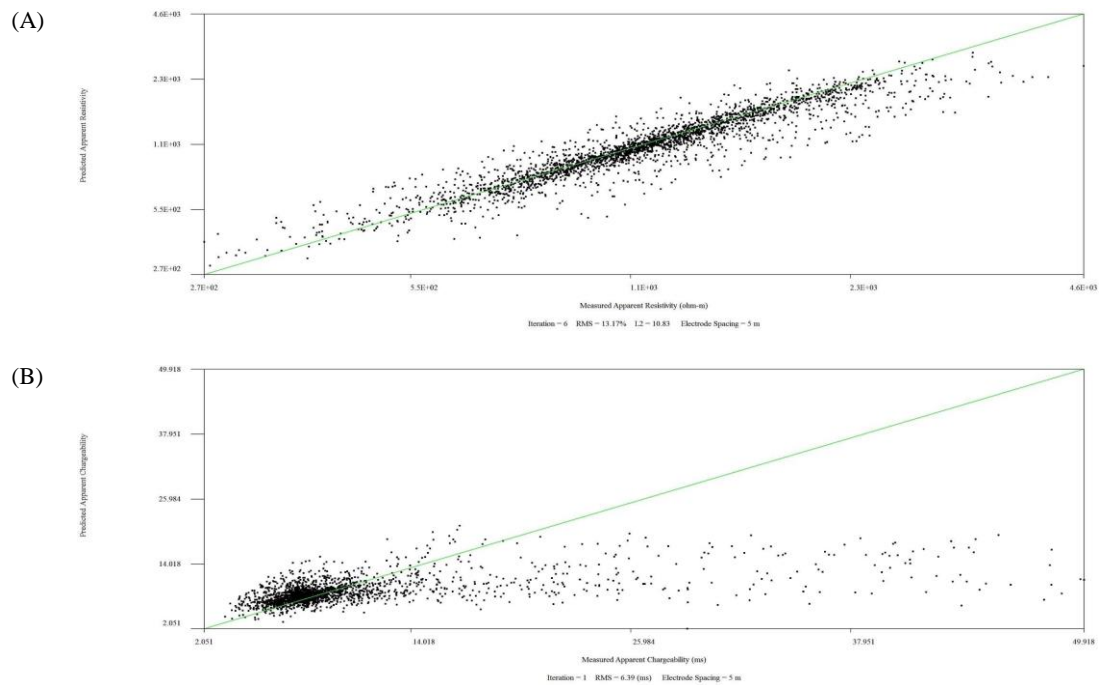


Figure D-26: ULRIP17-05 data misfit crossplots. (A) Measured vs. predicted apparent resistivity (Ohm-m). (B) Measured vs. predicted chargeability (ms).

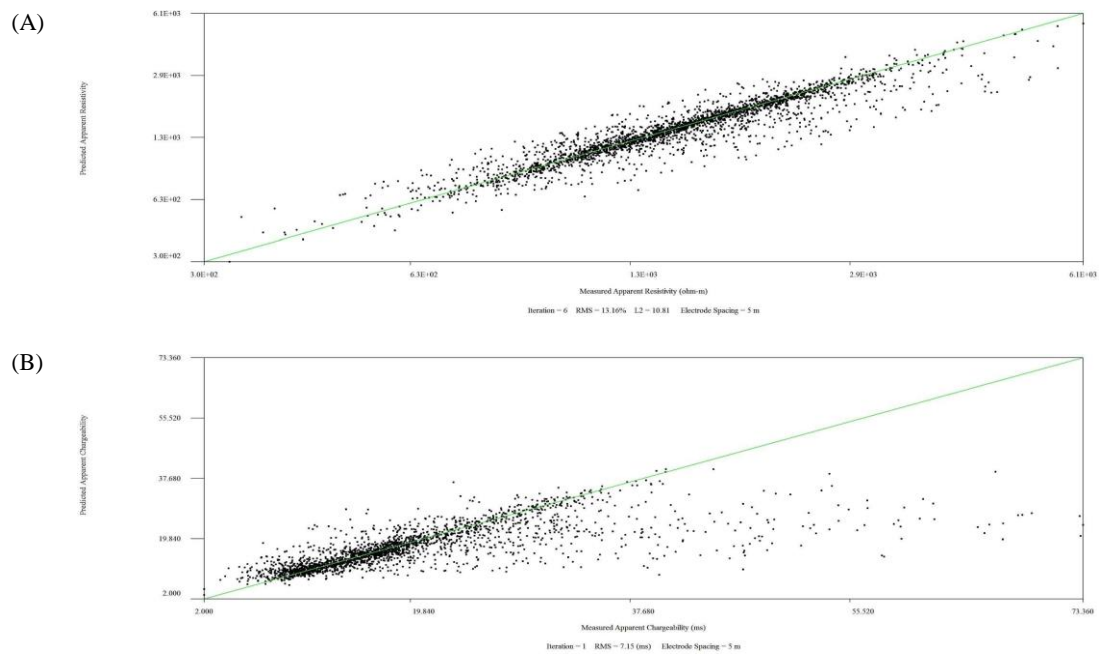


Figure D-27: ULRIP17-06 data misfit crossplots. (A) Measured vs. predicted apparent resistivity (Ohm-m). (B) Measured vs. predicted chargeability (ms).

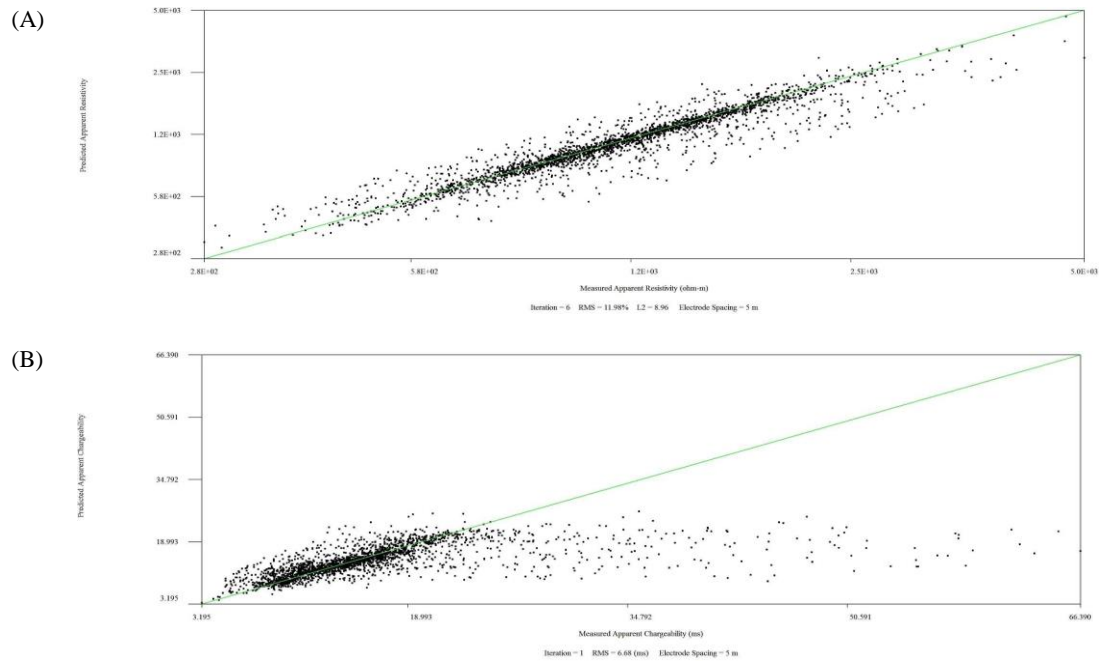
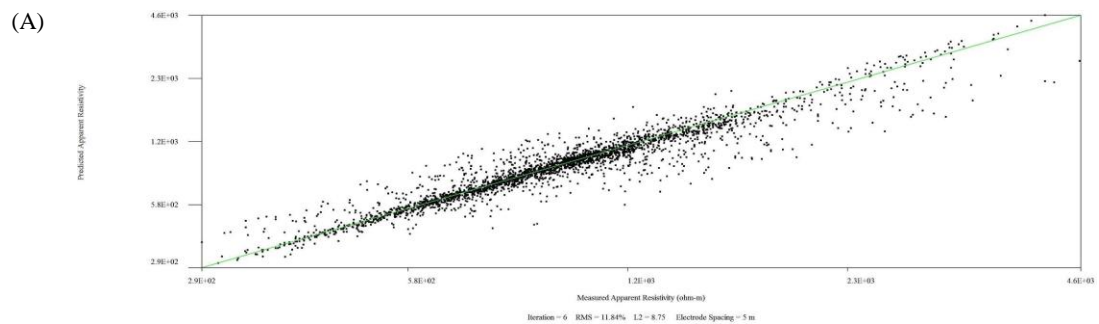


Figure D-28: ULRIP17-07 data misfit crossplots. (A) Measured vs. predicted apparent resistivity (Ohm-m). (B) Measured vs. predicted chargeability (ms).



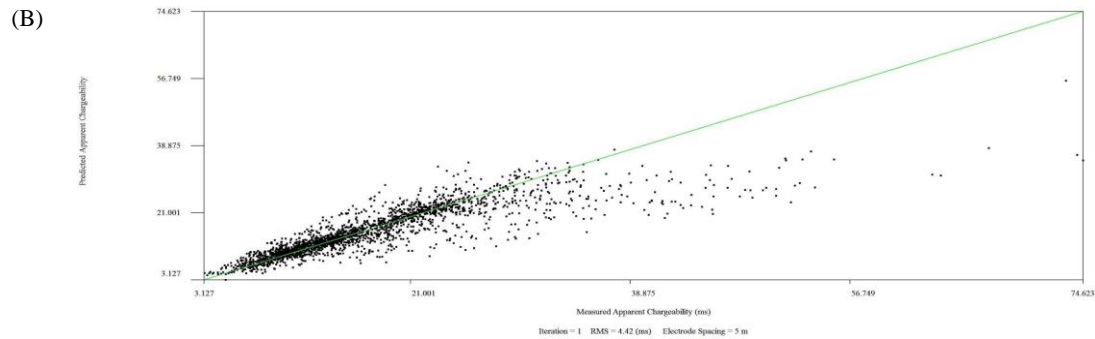


Figure D-29: ULRIP17-08 data misfit crossplots. (A) Measured vs. predicted apparent resistivity (Ohm-m). (B) Measured vs. predicted chargeability (ms).

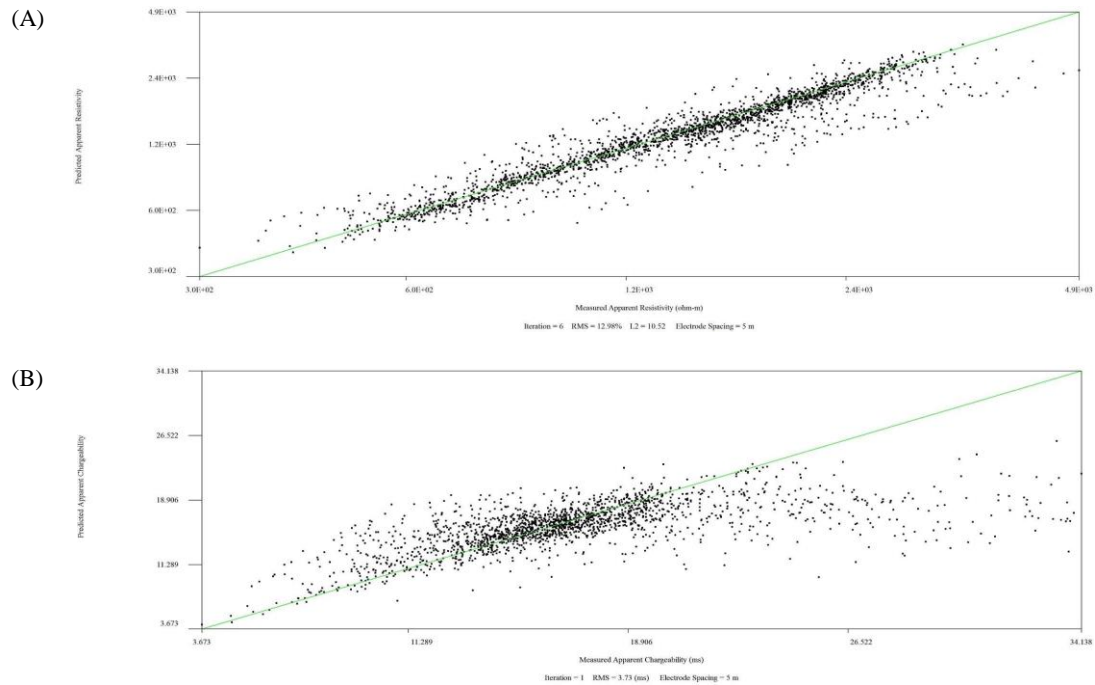


Figure D-30: ULRIP17-09 data misfit crossplots. (A) Measured vs. predicted apparent resistivity (Ohm-m). (B) Measured vs. predicted chargeability (ms).

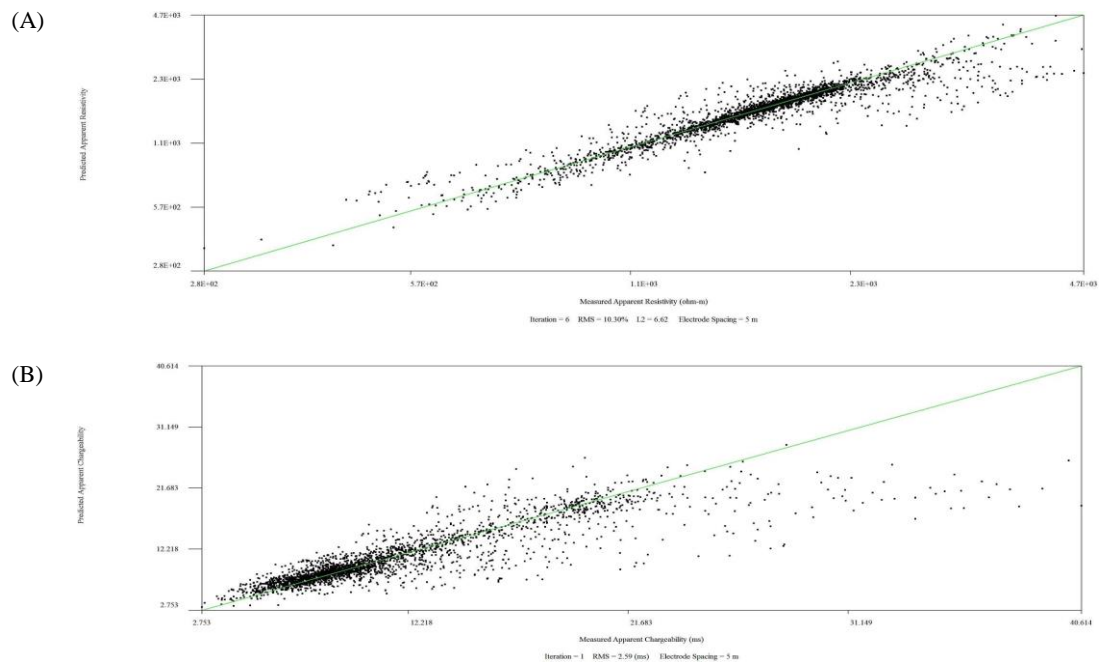


Figure D-31: MCKIP17-01 data misfit crossplots. (A) Measured vs. predicted apparent resistivity (Ohm-m). (B) Measured vs. predicted chargeability (ms).

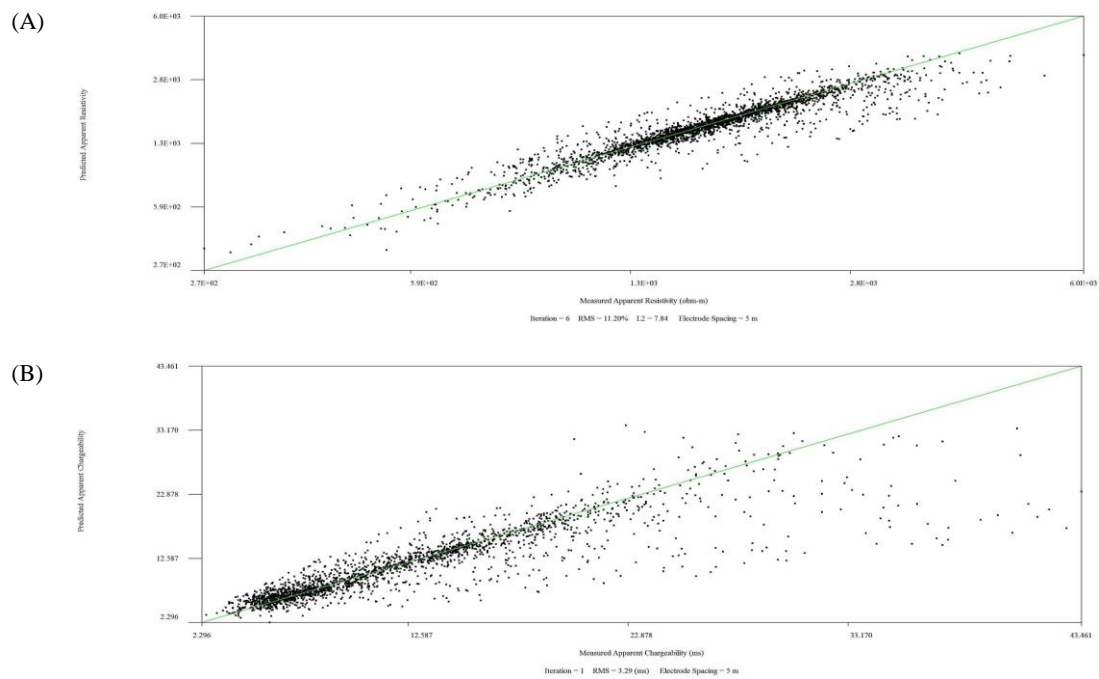




Figure D-32: MCKIP17-02 data misfit crossplots. (A) Measured vs. predicted apparent resistivity (Ohm-m). (B) Measured vs. predicted chargeability (ms).

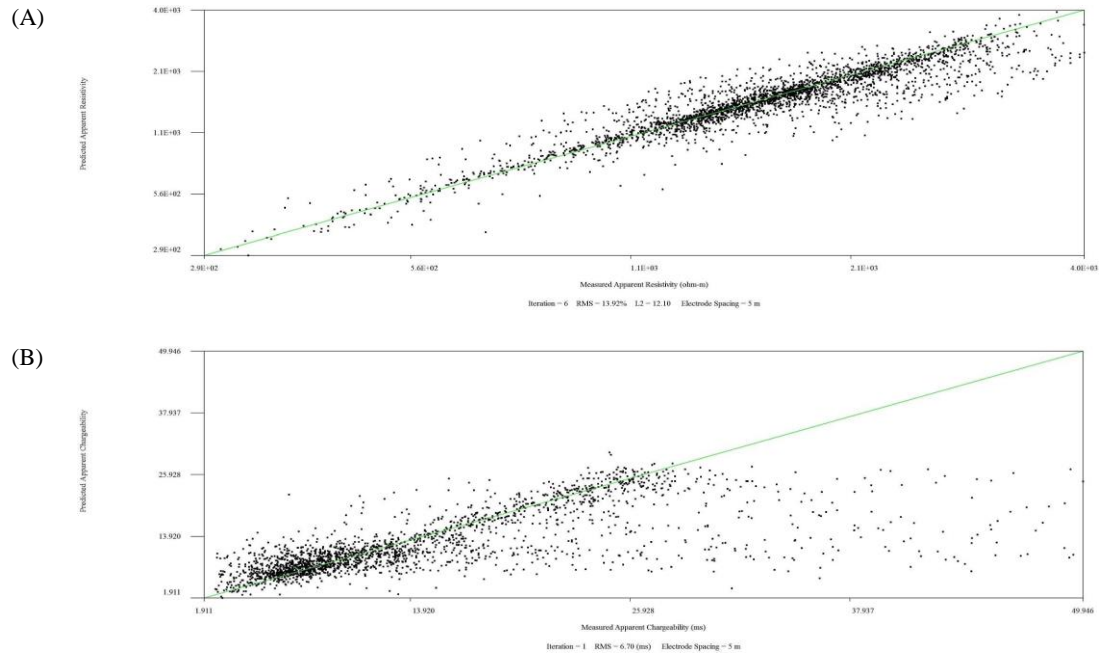
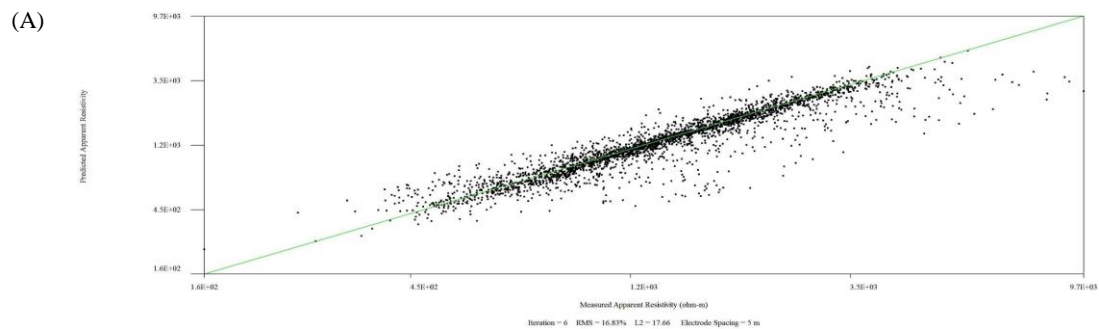


Figure D-33: MCKIP17-03 data misfit crossplots. (A) Measured vs. predicted apparent resistivity (Ohm-m). (B) Measured vs. predicted chargeability (ms).



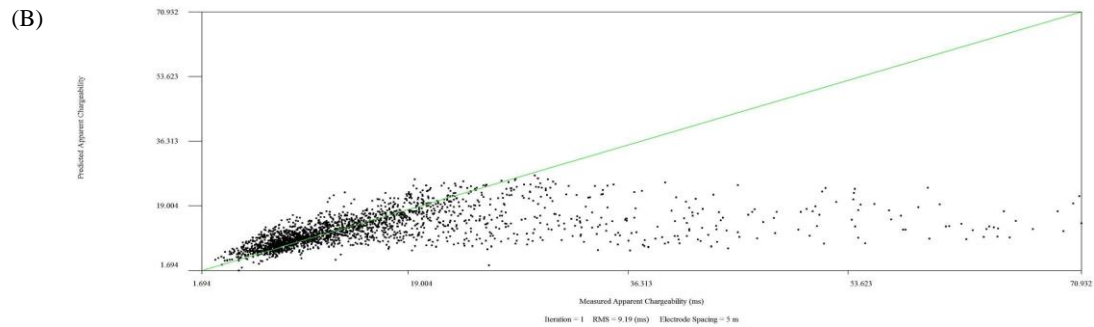


Figure D-34: MCKIP17-04 data misfit crossplots. (A) Measured vs. predicted apparent resistivity (Ohm-m). (B) Measured vs. predicted chargeability (ms).

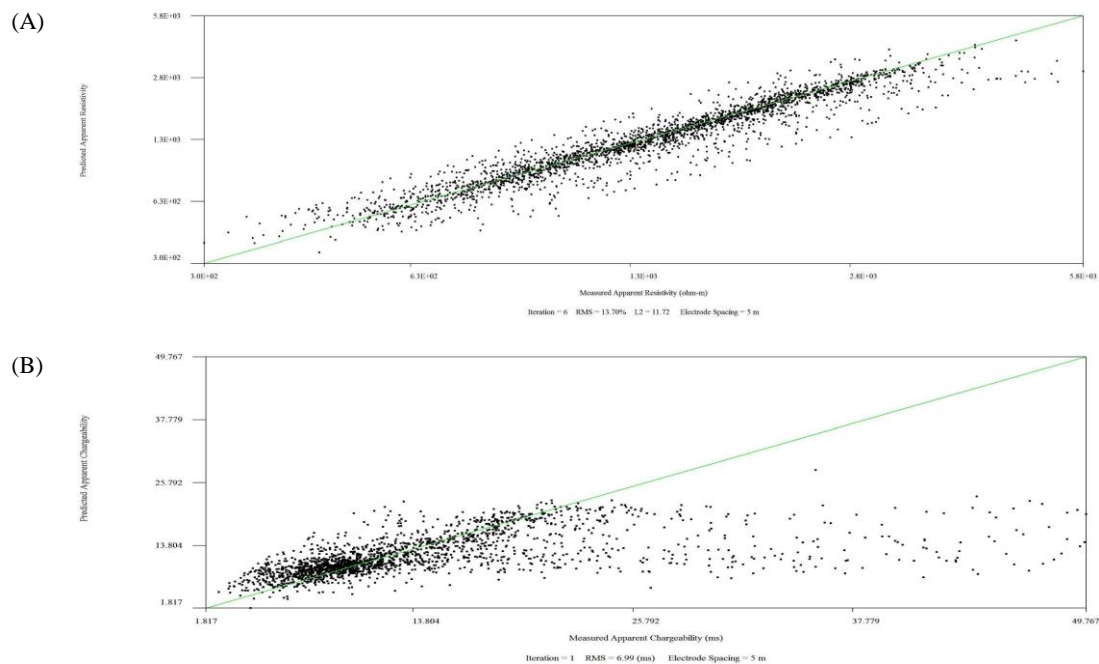


Figure D-35: MCKIP17-05 data misfit crossplots. (A) Measured vs. predicted apparent resistivity (Ohm-m). (B) Measured vs. predicted chargeability (ms).

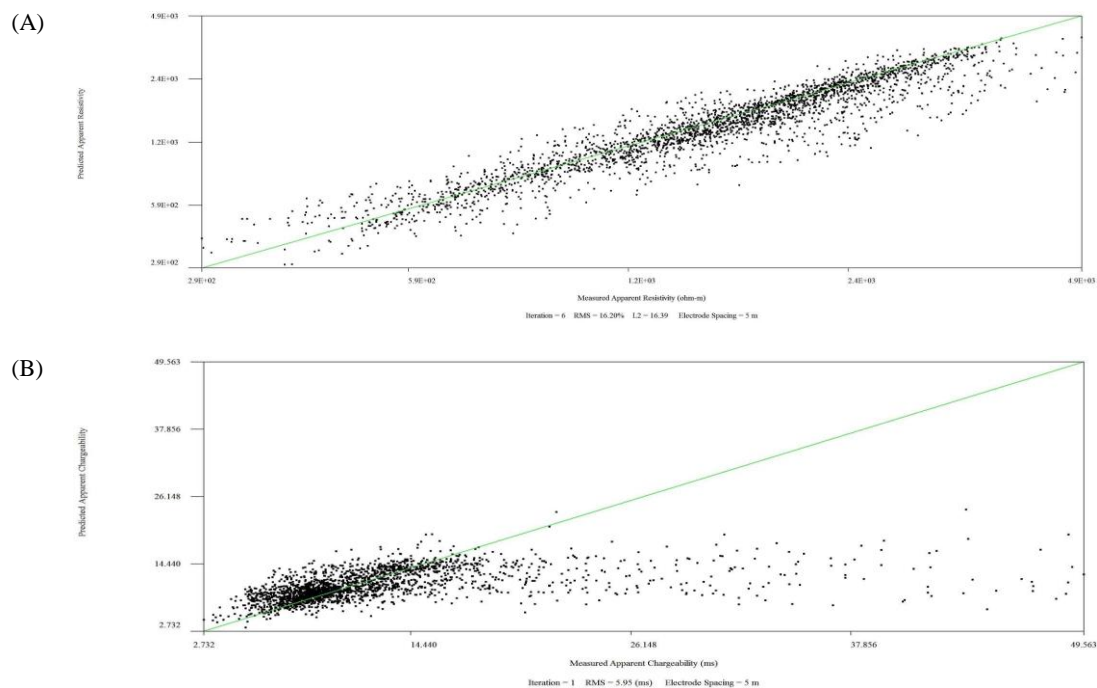


Figure D-36: MCKIP17-06 data misfit crossplots. (A) Measured vs. predicted apparent resistivity (Ohm-m). (B) Measured vs. predicted chargeability (ms).

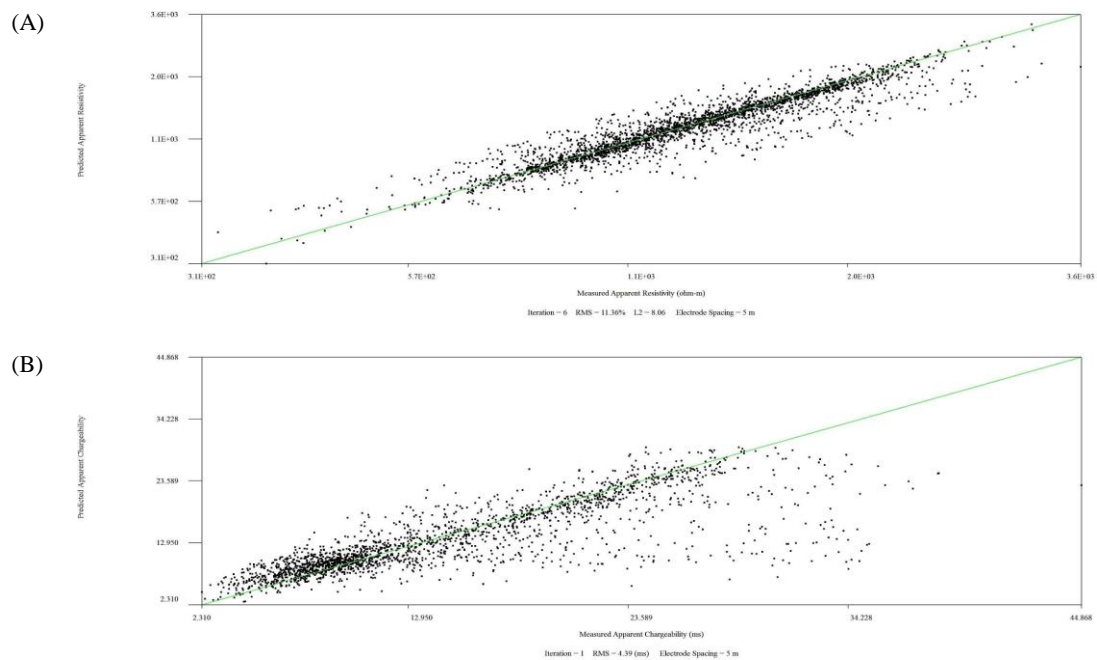


Figure D-37: MCKIP17-07 data misfit crossplots. (A) Measured vs. predicted apparent resistivity (Ohm-m). (B) Measured vs. predicted chargeability (ms).

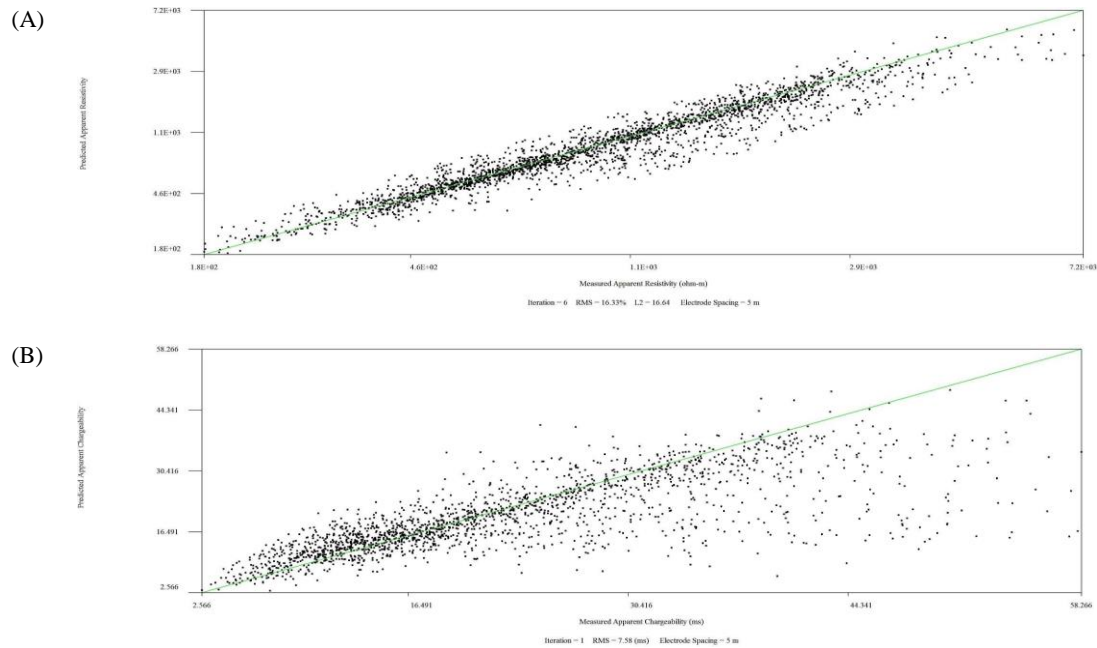
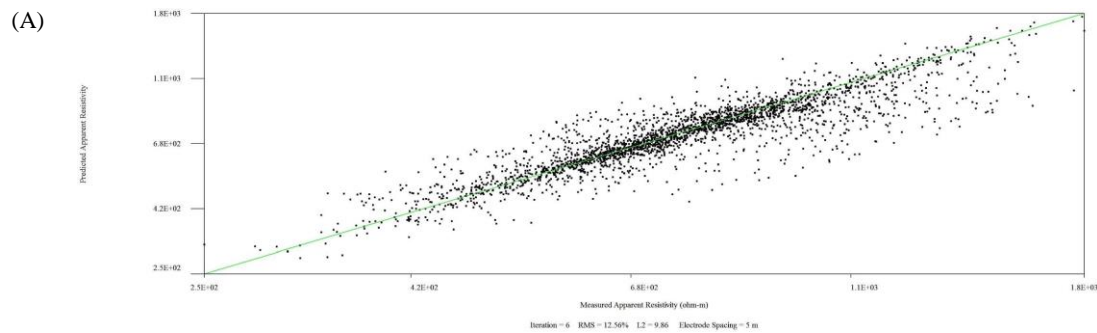


Figure D-38: MCKIP17-08 data misfit crossplots. (A) Measured vs. predicted apparent resistivity (Ohm-m). (B) Measured vs. predicted chargeability (ms).



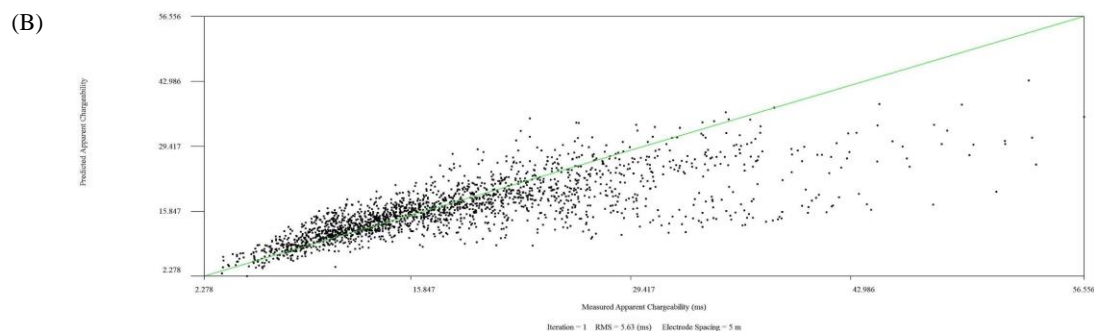


Figure D-39: MCKIP17-09 data misfit crossplots. (A) Measured vs. predicted apparent resistivity (Ohm-m). (B) Measured vs. predicted chargeability (ms).

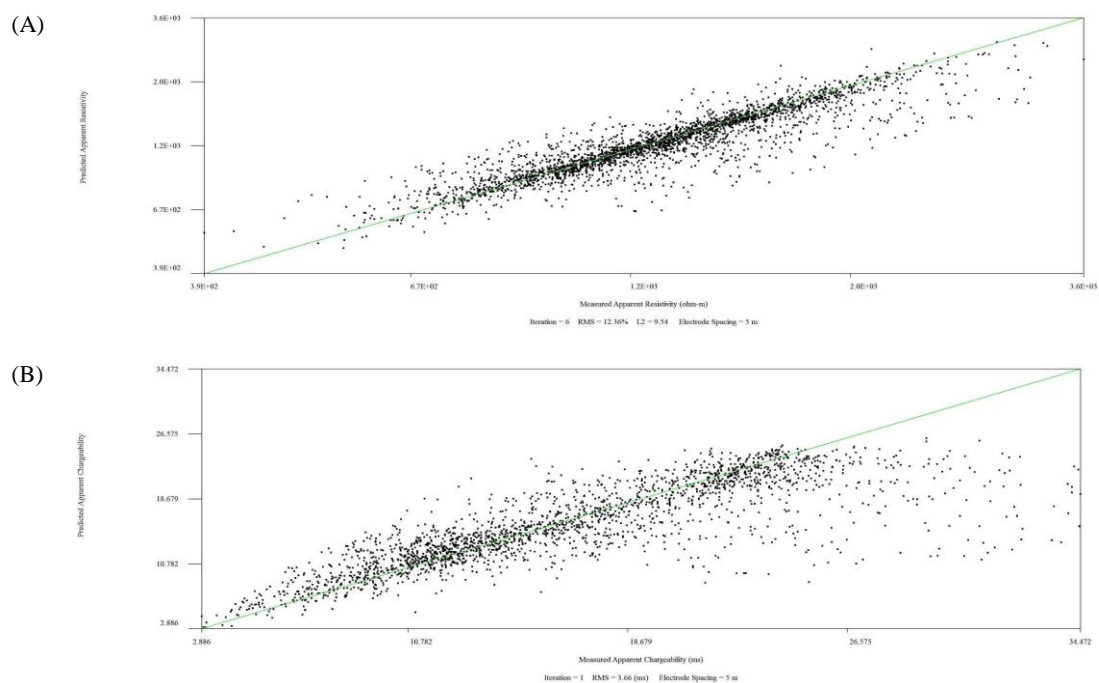


Figure D-40: MCKIP17-10 data misfit crossplots. (A) Measured vs. predicted apparent resistivity (Ohm-m). (B) Measured vs. predicted chargeability (ms).

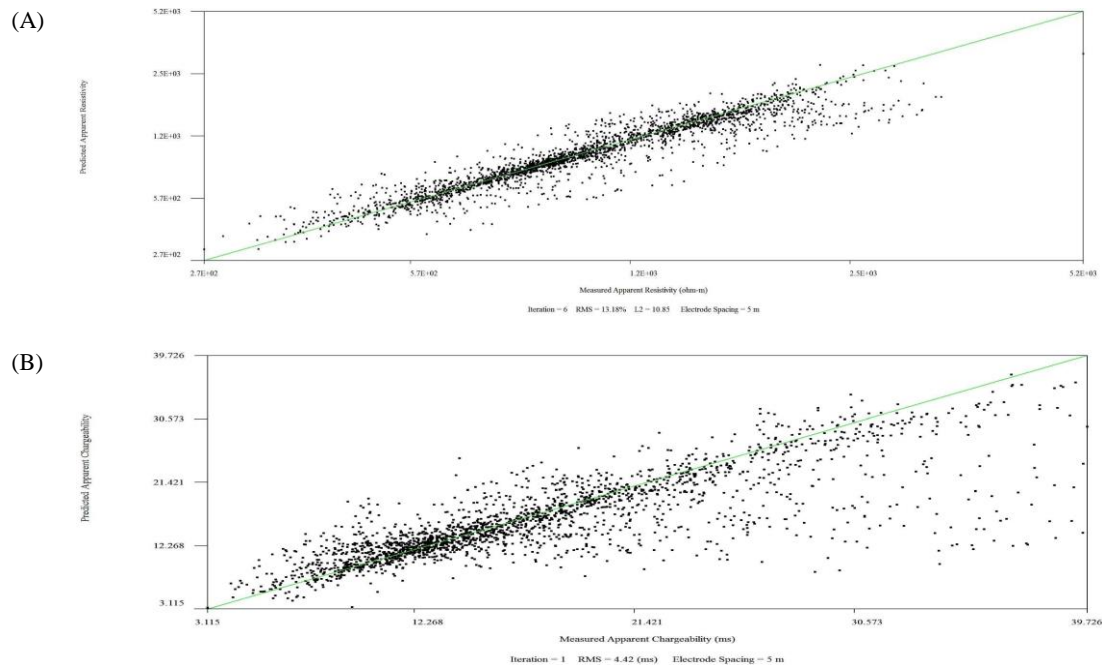


Figure D-41: MCKIP17-11 data misfit crossplots. (A) Measured vs. predicted apparent resistivity (Ohm-m). (B) Measured vs. predicted chargeability (ms).